DIRECTLY MODULATED LASERS FOR OPTICAL ACCESS NETWORKS

ZAINEB AL-QAZWINI

B. Sc. (1^{st} Hons.), University of Tripoli, Libya, M. Sc., UPM, Malaysia

A THESIS SUBMITTED FOR THE DEGREE OF
DOCTOR OF PHILOSOPHY

DEPARTMENT OF ELECTRICAL & COMPUTER ENGINEERING
NATIONAL UNIVERSITY OF SINGAPORE

2012

Declaration

I hereby declare that the thesis is my original work and it has been written by me in its entirety. I have duly acknowledged all the sources of information which have been used in the thesis.

This thesis has also not been submitted for any degree in any university previously.

Zaineb Al-Qazwini
20 August 2012

Acknowledgments

The work described in this thesis was conducted with the kind help and support of many people to whom I would like to express my thanks.

Firstly, I would like to express my great appreciation and sincere gratitude to my supervisor, Dr. Kim Hoon, for his continuous guidance, high-quality advice, and generous support throughout my PhD research.

I also feel grateful for the support I have received from the National University of Singapore through NUS Research Scholarship. Many thanks also go to my colleagues and the staff of Communications and Lightwave Systems labs at the National University of Singapore for providing a friendly work environment.

On a personal level, I would like to acknowledge my parents, Prof. Ali Al-Qazwini and Dr. Sawsan A. Dhia, for their sacrifices, support, patience, encouragement, and help throughout my entire life. Special thanks also to my sister Yusser Al-Qazwini for her unfailing support and help. Last but not least, I would like to thank my friends for their love and support all the while, which gives me the strength to carry on.

Table of Contents

Summary

Directly-modulated lasers (DMLs) have been the transmitter of choice for low-speed (≤2.5 Gb/s) cost-sensitive access networks, thanks to their cost-effectiveness, small footprint, high output power, and low driving voltage. The use of these attractive devices for the transmission of 10-Gb/s signals is challenging since their performance is mainly limited by the frequency chirp. The current modulation of DMLs is always accompanied by frequency modulation (FM), and consequently induces large frequency chirp, which limits the transmission distance over standard single-mode fiber (SSMF) to less than 10 km at 1550-nm window at 10 Gb/s and beyond. The limited transmission distance can be remarkably improved by making good use of the chirp-induced frequency modulation through the frequency-shift keying modulation of DMLs. The main problem in this scheme is, however, that DMLs exhibit highly non-uniform FM response at low frequencies (i.e., <10 MHz) which degrades the system performance.

In this thesis, we employ DC-balanced line coding to deplete the low-frequency contents of the signal residing in the non-uniform FM response of the DML, such that only the flat region of the FM response at higher frequencies is utilized. In Chapter 3 of this thesis, we investigate a variety of DC-balanced line codes, including 5B/6B, 7B/8B, 8B/10B, 9B/10B, and 64B/66B, in a 10-Gb/s DML-based transmission system. Among the examined codes, 9B/10B exhibits the best performance. This is because it can greatly deplete the low-frequency contents of the signals, yet it expands the bandwidth by 11.11% only. Using 9B/10B line coding, we are able to achieve 65-km

transmission of directly modulated 10-Gb/s signals over SSMF (dispersion-induced penalty was 2.5 dB) without any dispersion compensation.

In Chapter 4, we demonstrate the generation of 10-Gb/s non-return-to-zero signals using a DML driven by 3.5-GHz-bandwidth electrical duobinary signals. This scheme greatly relieves the modulation bandwidth requirements of the DML. For example, it is expected that 40-Gb/s signals can be accommodated with a 14-GHz-bandwidth DML using this approach. We utilize 9B/10B line coding to overcome the non-uniform FM response of the DML. Using the proposed transmitter, the generated 10-Gb/s signals can travel up to ~20 km over SSMF at 1550 nm (2-dB dispersion penalty) without any dispersion compensation.

In Chapter 5, we employ DC-balanced line coding, including 9B/10B and 8B/10B, to avoid the non-uniform FM response of the DML in the dual modulation-based electro-absorption modulated laser composed of a DML and an electro-absorption modulator. The DC-balanced line coding is effective in eliminating the performance degradation caused by the non-uniform FM-response of the DML in this system. However, the low overhead is essential to gain benefit from the line coding. Using 9B/10B line coding, we are able to achieve 171 km transmission over SSMF without dispersion compensation.

Finally, in Chapter 6, we apply DC-balanced line coding, including 8B/10B, 5B/6B, 7B/8B, and 9B/10B, for the downstream modulation in a wavelength-shared wavelength-division-multiplexed passive optical network, which employs a 10-Gb/s DML and 2.5-Gb/s reflective semiconductor optical amplifier for downlink and uplink, respectively. The use of DC-balanced line coding has two purposes. First, it ameliorates the performance degradation of the downstream signal caused by the non-uniform FM response of the DML. Second, it greatly suppresses the interference between the downstream and upstream data, which in turn, remarkably improves the upstream performance. Among the tested line codes, 9B/10B line coding exhibits the best downlink performance providing sufficient power margins for downlink and uplink.

The findings of this thesis will help in implementing 10-Gb/s optical access networks in a cost-effective manner by utilizing DMLs with suitable DC-balanced line coding. The use of line coding is beneficial for cost-sensitive access applications since it is a digital solution and can be applied to commercially available DMLs without the need to replace the deployed fiber links or the existing devices at the transmitter or receiver sides.

List of Tables

List of Figures

List of Acronyms

Acronyms	**Description**
AM	Amplitude Modulation
AMI	Alternate Mark Inversion
ASK	Amplitude-Shift Keying
BER	Bit-Error Ratio
CML	Chirp Managed Laser
CO	Central Office
CPFSK	Continuous Phase Frequency-Shift Keying
CW	Continuous Wave
DC	Direct Current
DCF	Dispersion-Compensating Fiber
DCM	Dispersion-Compensation Module
DFB	Distributed Feedback
DFE	Decision-Feedback Equalizer
DI	Delay Interferometer
DML	Directly Modulated Laser
DeMUX	Demultiplexer
DPSK	Differential phase-shift keying
EAM	Electro-Absorption Modulator
EDC	Electronic Dispersion Compensation
EDFA	Erbium-Doped Fiber Amplifier
EML	Electro-Absorption Laser
ER	Extinction Ratio

FEC	Forward Error Correction
FFE	Feed-Forward Equalizer
FM	Frequency Modulation
FSK	Frequency-Shift Keying
FSR	Free Spectral Range
HDTV	High-Definition Television
HPF	High-Pass Filter
IM	Intensity Modulation
IRZ	Inverse Return-to-Zero
ISI	Inter-Symbol Interference
ITU-T	International Telecommunication Union-Telecommunication Standardization Sector
$LiNbO_3$	Lithium Niobate
LPF	Low-Pass Filter
LSB	Least Significant Bit
MQW	Multi-Quantum Well
MSB	Most Significant Bit
MUX	Multiplexer
MZM	Mach-Zehnder Modulator
NDF	Negative Dispersion Fiber
NRZ	Non-Return-to-Zero
NZDSF	Non-Zero Dispersion-Shifted Fiber
OBPF	Optical Band-Pass Filter
OLT	Optical Line Terminal
ONU	Optical Network Unit
OOK	On-Off Keying

OPEX	Operation Expenditure
OSR	Optical Spectrum Reshaper
PC	Polarization Controller
PD	Photodiode
PON	Passive Optical Network
PRBS	Pseudo-Random Binary Sequence
PSK	Phase-Shift Keying
QW	Quantum Well
RF	Radio Frequency
RMS	Root Mean Square
RSOA	Reflective Semiconductor Optical Amplifier
RZ	Return-to-Zero
SI-BH	Semi-Insulated Semiconductor Buried Heterostructure
SNR	Signal-to-Noise Ratio
SSMF	Standard Single-Mode Fiber
TE	Transverse Electric
TM	Transverse Magnetic
TO	Transistor Outline
VCSEL	Vertical-Cavity Surface-Emitting Laser
VOA	Variable Optical Attenuator
WDM	Wavelength Division Multiplexing
WGR	Wavelength Grating Router

Chapter 1

Introduction

1.1 Overview

Over the last decade, the tremendous growth in Internet traffic driven by high bandwidth applications such as video streaming, Internet telephony, high-definition television (HDTV), social networking and online gaming have greatly increased the bandwidth demands on optical access networks. These networks, which serve numerous residential and business users have not scaled up commensurately and have therefore become the major bottleneck for broadband services [1, 2]. Unlike long-haul and metro networks where higher cost can be tolerated by the service and volume, optical access networks require low implementation and operation costs to make the transmission technology viable. High-speed optical transmission systems (10 Gb/s and beyond) for cost-sensitive access applications have thereby attracted extensive research interest and great development efforts. A key enabler for these systems is the use of cost-effective transmitters able to meet the low-cost requirements of access networks. In this concept, directly modulated laser (DML)-based optical transmitters offer many advantages compared with other transmitter options using external modulators, such as electro-absorption modulators (EAMs) or Mach-Zehnder modulators (MZMs). Not only DMLs reduce component complexity and implementation cost by eliminating the need for external modulators, but they also offer small footprint, cost-effectiveness, and ease of integration, thanks to their semiconductor-based structure [3, 4]. DMLs also provide high output power and require low driving voltage, compared to their external modulator-based counterparts [3, 5]. Therefore, they obviate the need for costly optical amplifiers and allow the use of low-cost drivers.

DML merits notwithstanding, the modulation bandwidth of DMLs is typically limited to less than 20 GHz by the nonlinear gain effects and the carrier transport lifetime [5]. More importantly, the current modulation of DMLs always gives rise to a large *frequency chirp*, which in turn severely limits the transmission distance over widely deployed standard single-mode fiber (SSMF) at 1550 nm [4, 6]. Therefore, DMLs have mainly been used for low-speed (≤2.5 Gb/s), cost-sensitive applications.

The remaining sections in this chapter address the motivation, objectives, and organization of this thesis.

1.2 Research Motivation

The operation of DMLs at 10 Gb/s and higher is challenging and faces two major problems: small extinction ratio (ER) and large frequency chirp. The intensity modulation (IM) in DMLs is always accompanied by phase modulation which in turn induces large frequency chirp [4, 6]. As a result, the pulse width is considerably broadened when propagating through SSMF at the 1550-nm window due to the fiber dispersion, leading to severe performance degradation under high-speed modulation [6, 7]. When the intensity-modulation-based DML is biased with a high bias current to minimize the transient chirp and to increase the modulation bandwidth, the ER should be reduced, otherwise the large current modulation required to achieve high ER would lead to a large frequency chirp [8]. Nevertheless, even with a limited ER, the adverse effects of the frequency chirp severely limit the transmission distance over SSMF at 1550 nm. For example, at 10 Gb/s, the transmission distance that can be achieved with DMLs is typically limited to below 10 km without dispersion compensation [6].

Although several techniques have been proposed to combat the chirp effects, most of them require complex electrical or optical implementations [9-13] and some others require either replacing the installed fiber links with new types of optical fiber [8, 14-16] or modifying the structure of the laser diode in order to exhibit low frequency chirp [17-19].

In this thesis, we utilize frequency-shift keying (FSK) modulation of DMLs to make good use of the frequency chirp at 10 Gb/s [20]. The major issue in this scheme is that the frequency modulation (FM) response of the laser diode is non-uniform at low frequency range (typically below 10 MHz), which results in a severe performance degradation [21, 22]. Most of the previously reported approaches to mitigate this problem require modifying the laser structure in order to exhibit highly flat FM response [23-25] or, otherwise, using either electrical or optical implementations that increase the system cost and complexity [26-29]. The use of DC-balanced line coding[*] has also been proposed to overcome the non-uniform FM response of the DML by depleting the low-frequency spectral contents of the signal falling in the non-uniform region of the DML FM response, and thereby only the flat region of the FM response at higher frequencies will be utilized [21, 30-33]. Not only the use of line coding offers a fully digital solution, but also it is also compatible with the device approaches, which require modifying the laser structure to achieve a flat FM response. In addition, line coding can alleviate the performance degradation induced by the non-

---

[*] DC-balanced line coding encodes data vectors to be free of DC or have a low DC component regardless of data patterns.

uniform FM response without the need to replace the existing transmitters, fiber links, or receivers. In the previous studies, however, the proposed line codes induce large coding overheads, which in turn increase the bandwidth requirements for the transmission devices (e.g., drivers, DMLs, receivers) and make the system more susceptible to chromatic dispersion. In this thesis, we will investigate and evaluate various DC-balanced line coding formats for 10-Gb/s DML-based transmission systems.

1.3 Research Objectives

The objectives of this thesis are to:

- Investigate the use of various DC-balanced line coding schemes to find a suitable code for 10-Gb/s directly modulated systems. The code should be able to alleviate the performance degradation associated with the non-uniform FM response of the directly frequency-modulated laser, yet it should not impose a large overhead on the data in order to maintain the bandwidth efficiency.
- Utilize DC-balanced line coding to improve the performance of two DML-based optical transmitters: (1) DML-based transmitter driven by highly band-limited electrical duobinary signals aiming to alleviate the modulation bandwidth limitation of the DML, and (2) dually modulated electro-absorption modulated laser composed of a DML and an EAM.
- Apply DC-balanced line coding to the downstream modulation in a single-fiber, wavelength-shared, loop-back wavelength-division-multiplexed (WDM) passive optical network (PON) which employs a 10-Gb/s DML and 2.5-Gb/s reflective semiconductor optical amplifier (RSOA) for downlink and uplink, respectively. The use of DC-balanced line coding should be capable of improving the

performance of the downstream signals as well as suppressing the interference between the downstream and upstream signals.

1.4 Thesis Organization

This thesis consists of eight chapters organized as follows:

Chapter 1: Introduction provides an overview of the thesis followed by the research motivation and objectives.

Chapter 2: Literature Review reviews the relevant literature on DML-based transmission systems. First, Section 2.1 presents the key features and basic characteristics of DMLs. Second, the direct intensity modulation of DMLs is discussed in Section 2.2. In this section, we also review several schemes that have been proposed to mitigate the chirp problem associated with the intensity modulation of DMLs. Next, the FSK modulation of DMLs is covered in Section 2.3. This Section discusses several approaches reported to combat the performance degradation associated with the non-uniform FM response of the DML in these systems.

Chapter 3: DC-Balanced Line Coding for 10-Gb/s Directly Modulated Lasers experimentally investigates the use of line coding to suppress the low-frequency contents of the signal in order to exploit only the uniform FM-response region of the DML. In this chapter, we examine various line codes to propose a code most suitable for 10-Gb/s directly modulated systems, such that it can maintain sufficiently low DC characteristics, yet it induces relatively small overhead.

Chapter 4: Directly-Modulated Laser Driven by Low-Bandwidth Duobinary Signals introduces and experimentally demonstrates a DML-based transmitter driven by highly band-limited electrical duobinary signals to alleviate the modulation bandwidth limitation of DMLs. In the proposed scheme, we employ DC-balanced line coding to avoid the performance degradation caused by the non-uniform FM response of the DML.

Chapter 5: DC-Balanced Line Coding for the Dual Modulation of Directly Modulated Lasers and Electro-absorption Modulators proposes and experimentally demonstrates the use of DC-balanced line coding to enhance the performance of the dually modulated electro-absorption modulated laser (EML) which is composed of a DML and an EAM.

Chapter 6: DC-Balanced Line Coding for Downlink Modulation using DMLs in Bidirectional WDM PONs Using Remodulation proposes and demonstrates through experiment the use of DC-balanced line coding for a cost-effective implementation of wavelength-shared, single-fiber 10-Gb/s downlink, 2.5-Gb/s uplink WDM PON. We use DMLs and RSOAs for the downstream and upstream transmission, respectively. In this Chapter, we examine the use of simple and bandwidth-efficient DC-balanced line codes for downstream modulation to ameliorate the performance of both the downlink and uplink.

Chapter 7: Conclusions and Future Works summarizes the research findings of this thesis and suggests future works.

1.5 Contributions of the Thesis

The contributions of the thesis are listed as follows.

Chapter 3

- We investigated the use of various DC-balanced line coding schemes for 10-Gb/s DML-based transmission systems to alleviate the performance degradation associated with the non-uniform FM response of the DML.

- We demonstrated the transmission of directly modulated 10-Gb/s signals over 65 km of SSMF using 9B/10B line coding without any dispersion compensation.
- We proposed a system setup to apply the proposed scheme for WDM systems.

Chapter 4

- We proposed a 10-Gb/s optical transmitter using a DML driven by highly band-limited (3.5 GHz) electrical duobinary signals to relieve the modulation bandwidth requirements of the DML.
- We demonstrated the proposed transmitter using two configurations: destructive-port and constructive-port. Both configurations exhibited good receiver sensitivities and dispersion tolerance large enough to be used for optical access networks.
- We achieved 20-km transmission over SSMF using the proposed transmitter with 9B/10B line coding without any dispersion compensation.
- We proposed a system setup to apply the proposed transmitter for WDM systems.

Chapter 5

- We employed DC-balanced line coding to eliminate the performance degradation caused by the non-uniform FM-response of the DML in the dual modulation-based EML composed of a DML and an EAM.
- We demonstrated the proposed transmitter using two configurations: push-pull and push-push.
- Using the proposed scheme, we achieved 171-km transmission over SSMF with a long pseudo-random binary sequence (PRBS) length of 2^{20}-1 by utilizing 9B/10B line coding without any dispersion compensation.

Chapter 6

- We demonstrated a cost-effective single-fiber single-wavelength 10-Gb/s downlink and 2.5-Gb/s uplink WDM-PON system using DMLs and RSOAs for downlink and uplink, respectively.
- We applied DC-balanced line coding for the downstream modulation to alleviate the performance degradation associated with the non-uniform FM response of the DML and also to suppress the remodulation-induced crosstalk between the downstream and upstream data.

Chapter 2

Literature Review

2.1 Directly Modulated Lasers

There are two common ways to superimpose a data stream onto a light beam: direct modulation, as shown in Figure 2.1 (a), and external modulation, as illustrated in Figure 2.1 (b). In direct modulation, the electrical current is directly driven into the laser diode resulting in a series of optical pulses. The laser diode switches between ON and OFF states for a logical 1 and 0, respectively. In an externally modulated system, on the other hand, an external modulator (e.g., MZM) modulates a continuous-wave (CW) light into the desired optical bit pattern as illustrated in Figure 2.1 (b) [34, 35].

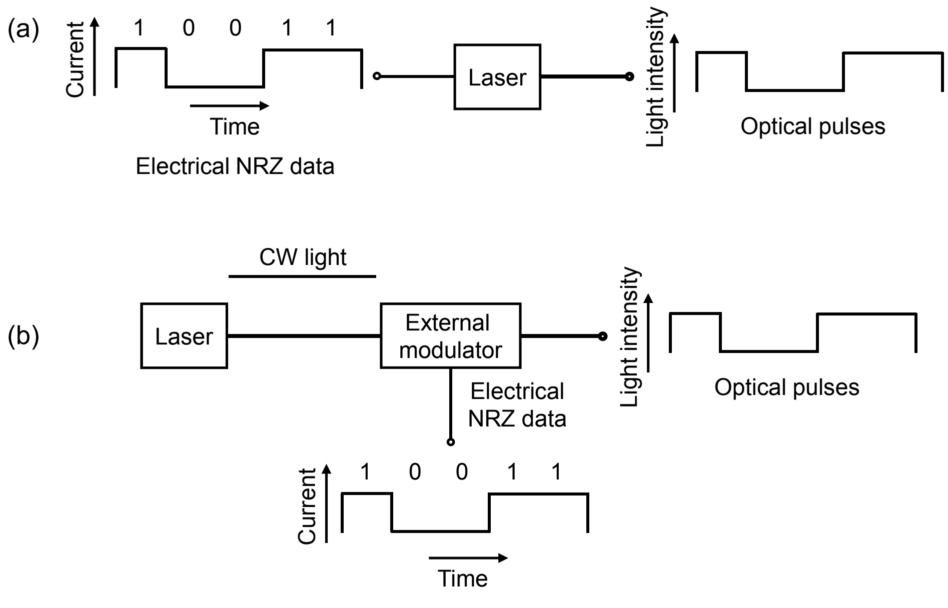

Figure 2.1: Illustration of (a) direct modulation, and (b) external modulation of a laser source.

DML-based optical transmitters offer many advantages over external modulator-based counterparts. Not only they reduce the system complexity and cost by eliminating the need for external modulators, but they also offer compactness, cost-effectiveness, and ease of integration due to their semiconductor-based structure [3, 4]. DMLs also provide high output power and require low driving voltage, compared to their external modulator-based counterparts [3, 5]. Therefore, they obviate the need for costly optical amplifiers and allow the use of low-cost drivers.

However, directly intensity-modulated lasers tend to have wider spectral width under high-speed modulation due to the frequency chirp [36]. The current modulation of the DML is always accompanied by FM and consequently induces a large frequency chirp [4, 6]. The interaction of the DML chirp with the dispersion of the conventional SSMF (e.g., Corning SMF-28 fiber) at 1550 nm severely limits the transmission distance at 10 Gb/s [6]. In addition, the modulation bandwidth of the DML is typically limited by the nonlinear gain effect and the carrier transport lifetime to less than 20 GHz [37].

The intensity modulation in DMLs is accompanied by phase modulation due to the carrier-induced change in the refractive index governed by the linewidth enhancement factor α [6]. The phase modulation, in turn, causes a shift in the instantaneous frequency from the steady-state value (ν_0). This time-dependent shift in frequency $(\Delta\nu)$ is called frequency chirp and can be expressed by [38, 39]

$$\Delta\nu(t) = \frac{\alpha}{4\pi}\left(\frac{d}{dt}[\ln\{P(t)\} + \kappa P(t)]\right) \tag{2.1}$$

where $P(t)$ is the output power of the laser diode and κ is the adiabatic chirp coefficient directly related to the nonlinear gain compression coefficient ε and given by [4]

$$\kappa = \frac{2\Gamma}{\eta h \nu V}\varepsilon \tag{2.2}$$

where Γ is the optical confinement factor, η is the differential quantum efficiency, h is Planck's constant, ν is the optical frequency, and V is the volume of the active layer.

The first term on the right-hand side of Eq. (2.1) characterizes the *transient chirp* (also called dynamic chirp) caused by the dynamics of electron-photon resonance [40]. The transient chirp represents the wavelength shift associated with the ON and OFF states. It dominates when the laser OFF state is close to the threshold, or if dP/dt is large due to either a large output power swing or fast rise-time current pulses [4]. On the other hand, when the laser operates at far beyond the threshold current, its FM characteristics are mainly determined by the *adiabatic chirp*, which is described by the second term of Eq. (2.1). The adiabatic chirp corresponds to the steady-state emission frequency difference between the ON and OFF states and is linearly proportional to the output power difference between both states as observed from Eq. (2.1) [41]. The adiabatic chirp is caused by the nonlinear gain effects, such as carrier heating [42] and spectral hole burning [38, 43, 44].

As a result of frequency chirping, the leading edge of the pulse undergoes a shift towards higher frequencies (i.e., blue shift), while the trailing edge shifts towards lower frequencies (i.e., red shift) [6]. Therefore, the pulse width is considerably broadened when propagating through 1550-nm SSMF due to fiber dispersion and the pulse may spread over few bit periods by the time it reaches the receiver which severely degrades the performance of the optical transmission system [6, 7, 36]. The interaction between the laser chirp and fiber dispersion is illustrated in Figure 2.2.

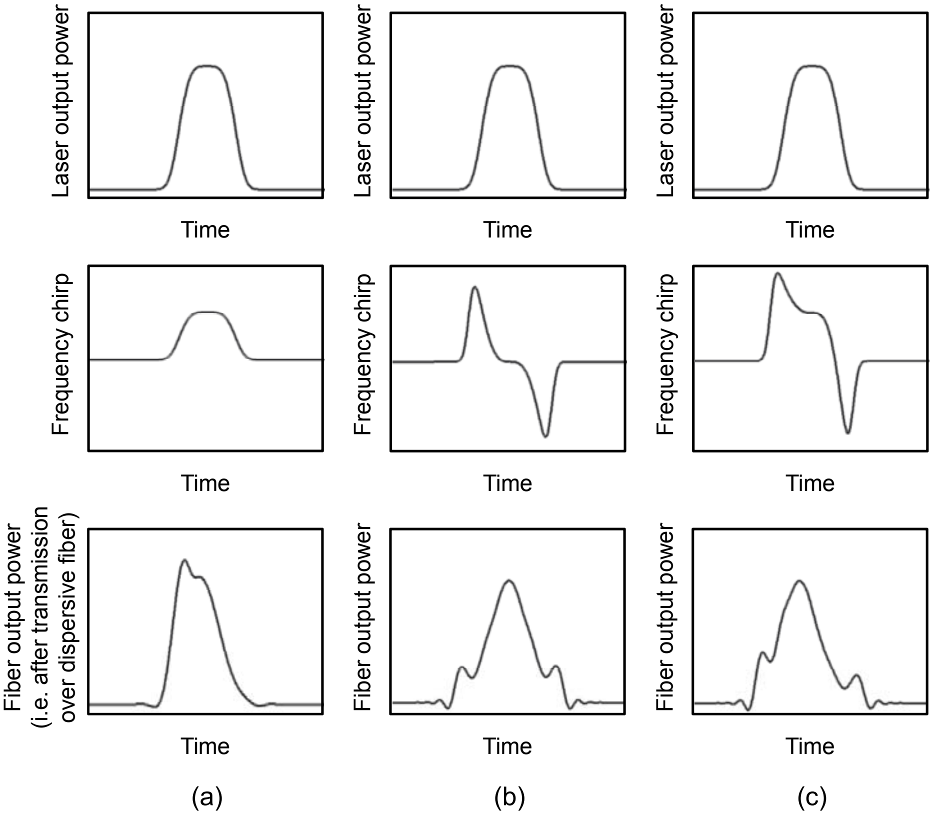

Figure 2.2: Illustration of pulse distortion induced by the interaction between the fiber dispersion and (a) adiabatic chirp, (b) transient chirp, and (c) combined adiabatic and transient chirp, based on [45].

Due to the adiabatic chirp, the laser frequency increases with the optical power as shown in Figure 2.2 (a). When the dispersion coefficient of the fiber is positive, which is the case in SSMF at the 1550-nm window, the rising edge travels faster than the falling edge. Therefore, in the output pulse, the rising time is decreased resulting in an overshoot, while the falling time is increased as illustrated in Figure 2.2 (a). In Figure 2.2 (b), only the transient chirp is considered, and thus, frequency deviations occur at the rising and falling edges. The rising edge propagates faster than the flat part of the pulse while the falling edge propagates slower, and consequently, the pulse is broadened. It is worth noting that because the transient chirp is proportional to the derivative of the natural logarithm of the pulse power as shown in Eq. (2.1), it is thereby strongly sensitive to the pulse slopes. As a result, the distorted output waveforms may be considerably different for supposedly similar input waveforms [45]. Figure 2.2 (c) shows the combined effects of transient and adiabatic chirp.

An important measure of the performance of optical transmission systems is the bit rate-distance (BL) product, which describes the maximum fiber length (L) that can be used at a given bit rate B. For a directly modulated distributed-feedback (DFB) laser, the maximum transmission distance is limited by [6]

$$L < |4BDs_\lambda|^{-1} \tag{2.3}$$

where D is the dispersion parameter and s_λ is the root mean square (RMS) width of the pulse spectrum broadened by the frequency chirp. Assuming D = 16 ps/nm/km and s_λ = 0.15 nm, DML-based optical transmission systems operating at 10 Gb/s are limited to a transmission distance of ~10 km over SSMF at 1550 nm without any dispersion compensation.

2.2 Directly Intensity-Modulated Lasers

As aforementioned in Chapter 1, directly intensity-modulated lasers at 10 Gb/s and beyond suffer from two major problems: small ER and large frequency chirp. The current modulation of the DML is always accompanied by FM and consequently induces large frequency chirp. When the DML is biased with a high bias current to minimize the transient chirp and increase the modulation bandwidth, the ER should be reduced, otherwise the large current modulation required to achieve high ER would lead to a large frequency chirp [8]. Nevertheless, even with a limited ER, the adverse effects of the frequency chirp severely limit the transmission distance over SSMF at 1550 nm. As mentioned in Section 2.1, at 10 Gb/s, the transmission distance that can be achieved with DMLs is typically limited to ~10 km without dispersion compensation.

The remaining parts of Section 2.2 provide an overview of various methods reported to combat the frequency chirping in DMLs. We categorize these approaches as either device-based or system-based approaches. The latter category includes precompensation at the transmitter, postcompensation at the receiver, and optical compensation approaches.

2.2.1 Device Approaches

As stated in Section 2.1, the origin of chirp in semiconductor lasers is originated from the carrier-induced index changes governed by the linewidth enhancement factor, α [6]. Unfortunately, this factor cannot be eliminated in semiconductor lasers, although it can be reduced by a factor of about 2 by employing a multiquantum-well (MQW) structure [17-19]. For example, α value for MQW DFB lasers is about 3 at 1550 nm compared to approximately 5-6 for conventional DFB lasers resulting in a nearly twofold improvement in the transmission distance for MQW DFB lasers [4]. A further reduction in α can be achieved using strained MQW lasers [46]. These lasers exhibit low frequency chirp under direct modulation even at bit rates as high as 10 Gb/s [6].

Nevertheless, such device approaches require modifying the laser structure in order to exhibit low chirp, and yet the chirp effects cannot be fully eliminated.

Alternatively, several other system approaches have been proposed to alleviate the chirp effects which are covered in Section 2.2.2.

2.2.2 System Approaches

2.2.2.1 Precompensation at the Transmitter

In these approaches, the characteristics of the input pulses are modified in the electrical domain at the transmitter side to combat the chirp effects before the pulses are launched into the fiber link [6, 47, 48].

The interplay between the positive chirp of DMLs and the positive dispersion of conventional SSMF deteriorates the optical signal and limits the maximum achievable transmission distance [49]. This is because when a pulse with a positive chirp travels through an SSMF, the blue-shifted leading edge of the pulse advances relative to the main portion of the pulse, resulting in a considerable pulse broadening and significant chirp-induced power penalty due to inter-symbol interference (ISI) [6, 49]. Electronic precompensation (also called prechirping) techniques thereby take advantage of the linearity of the fiber dispersion in the optical domain in order to delay the spreading of the bit into adjacent slots by arranging for the light in the leading edge of the pulse to have lower frequency than that in the trailing edge of the pulse as shown in Figure 2.3.

By prechirping the pulse in this manner, low-frequency light in the leading edge propagates slower resulting in pulse-width compression. In other words, the low-frequency light in the leading edge should pass through the entire pulse slot before it starts impinging on the trailing pulse and causing errors [50].

In [11], the concept of electronic prechirping was adopted for 10-Gb/s DML systems by the use of artificial neural networks, which act as a nonlinear signal-processing unit. Even though transmission over 190-km SSMF was demonstrated using this scheme, it considerably increases the implementation complexity and cost. A major difficulty with this method is that each transmitter has to be adjusted depending on the span length.

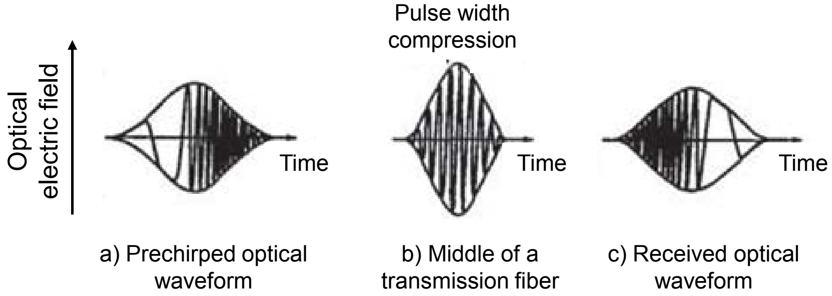

Figure 2.3: Principle of electronic precompensation (or prechirping) at the tranmitter [51].

2.2.2.2 Postcompensation at the Receiver

Another way to alleviate the chirp effects is to include electronic dispersion compensation (EDC) at the receiver to mitigate the dispersion without foreknowledge of the fiber length or other span characteristics. This makes EDC especially attractive for networks with dynamic wavelength routing, in which the optical path length may change when wavelengths are rerouted [10]. Therefore, EDC can provide an adaptive solution suitable for integration with other receiver functions [52].

In [10], the implementation of an EDC using feed-forward equalizer (FFE) was demonstrated, achieving 100% reach improvement using a 10-Gb/s DML source. Few other studies have also studied electronic equalization using FFE and decision-feedback equalizer (DFE) at the receiver end for 10-Gb/s systems based on DMLs [9, 12]. Figure 2.4 shows the structure of FFE/DFE EDC.

Although electronic equalization techniques have relatively low first installed cost, the loss of the optical phase information after direct detection of intensity modulated signals limits the amount of dispersion that can be effectively compensated [53]. Another difficulty in these techniques is that they require electronic logic circuits, which should operate at a speed as high as the data rate, whose complexity increases exponentially with the number of bits over which an optical pulse has spread due to the chirp effects [50].

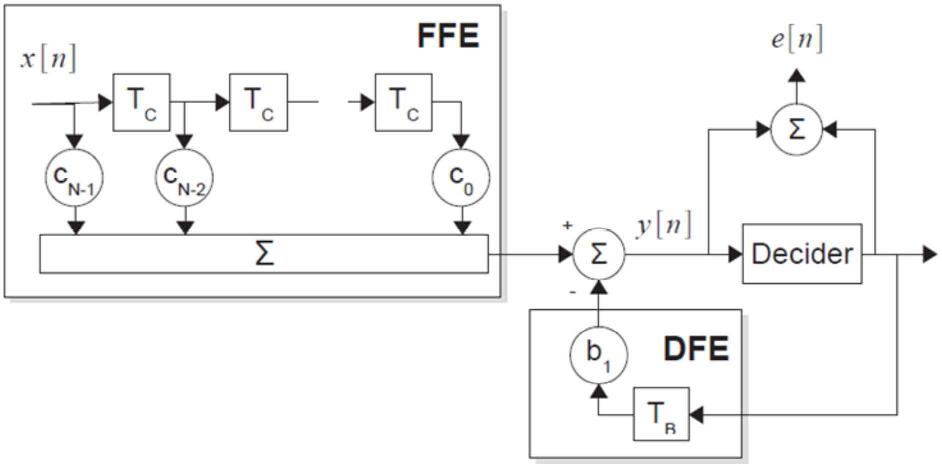

Figure 2.4: Feed-forward decision feed-back equalizer structure (FFE/DFE) [54]. T_B and T_c indicate 1-bit delay stages.

2.2.2.3 Optical Compensation

In contrast to the electrical compensation techniques at the transmitter or receiver described above, the frequency chirping can be alleviated in the fiber span by employing negative dispersion fibers (NDFs) or dispersion compensation modules (DCMs).

a) Negative Dispersion Fiber

As stated earlier, the interaction between the positive chirp of DMLs and the positive dispersion of conventional SSMF degrades the system performance and limits the maximum achievable transmission distance. In [15], a nonzero dispersion-shifted fiber (NZDSF) with a negative dispersion (e.g., Corning MetroCor fiber) was introduced to take advantage of the positive chirp characteristics of the DML and to enhance the transmission distance without the need for dispersion compensation. Over such NDF, the blue-shifted leading edge has a smaller group velocity than the red-shifted components resulting in pulse compression and significant transmission performance improvement [49]. Figure 2.5 shows the dispersion characteristics of MetroCor fiber which has a zero dispersion wavelength at 1630~1640 nm and an average dispersion of about -3 and -8 ps/nm/km in the L- and C-bands, respectively. The loss, the dispersion slope, and the effective area of this fiber are compliant with the ITU-T's G.655 standard [49].

With 2.5 Gb/s DMLs, MetroCor fibers can achieve up to four times the distance achieved over SSMFs at 1550 nm [14, 15]. In [16], the use of MetroCor fiber was demonstrated for the transmission of 10-Gb/s directly modulated signals over 100-km fiber. Chung *et al.* proposed the use of an NDF with a small dispersion of -2.5 ps/nm/km at 1550 nm to further extend the transmission distance. By using this fiber, they reported the transmission of directly modulated 10-Gb/s WDM signals over 320 km without dispersion compensation [8].

Nevertheless, replacing the existing fiber links, which are commonly deployed using SSMF, with new types of optical fiber would involve exorbitant costs, especially that NDF is generally 70-80% more expensive than conventional SSMF, which remains the most economic choice for metro and access networks [55, 56]. In addition, the future systems may require fiber links that can be compensated using standard dispersion compensation devices. Since many of today's DCMs contain an

NDF, they cannot be used in those systems which utilize an NDF as the transmission medium [56]. Therefore, other solutions to combat the frequency chirp are required for the large installed base of standard fibers.

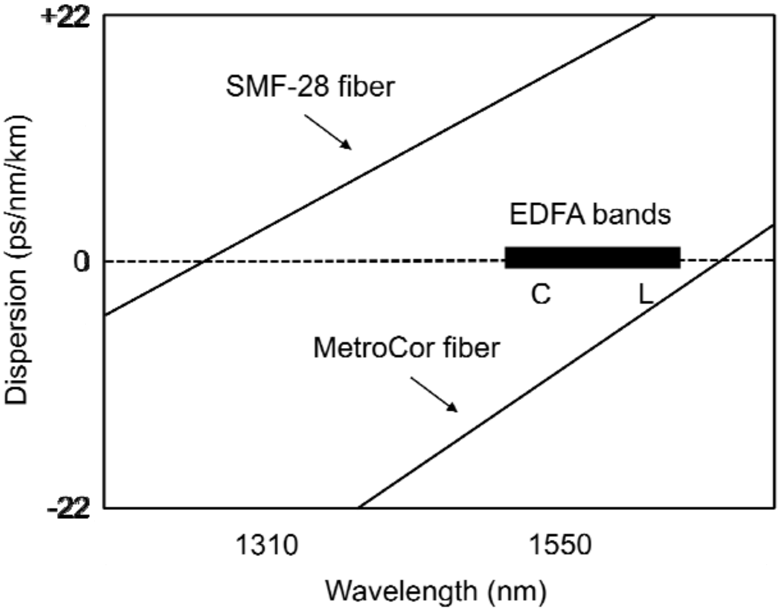

Figure 2.5: Dispersion characteristics of MetroCor and SMF-28 fibers [49].

b) Dispersion-Compensating Fibers

For long-haul systems, accumulative dispersion can be compensated along the deployed fiber transmission line in a periodic fashion [6]. A special kind of fiber with a negative dispersion, known as dispersion-compensating fiber (DCF), was developed for such purpose [57-59]. Therefore, adding a DCF module (comprising 6-8 km of DCF) to optical amplifiers spaced apart by 60~80 km, as illustrated in Figure 2.6, offers a practical solution to upgrade the terrestrial optical transmission systems while making use of the existing SSMFs [13, 60]. These modules have found widespread application to extend the operating distance, with more than 10,000 modules installed worldwide [60].

However, such DCMs are cost-prohibitive for access and metro systems since a DCF may cost as much as the fiber for which it provides compensation [15, 56]. These modules also increase the complexity of the network design since each DCM should be located to ensure a proper compensation [56]. They are also bulky due to the large bending loss. Another problem with DCFs is that they exhibit relatively high loss (attenuation coefficient $\alpha = 0.4 \sim 0.6$ dB/km) and thus the insertion loss of a DCF module typically exceeds 5 dB. In addition, due to the relatively small diameter of DCFs, the effective mode area is only ~20 μm^2. In consequence, the nonlinear effects are considerably enhanced due to the high optical intensity inside the DCF at a given input power [6].

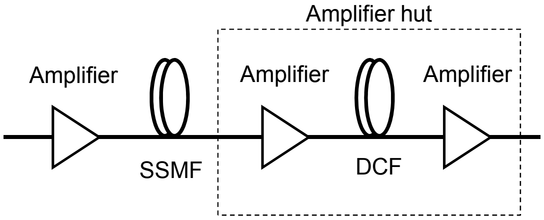

Figure 2.6: Typical transmission system with a DCF module.

2.3 FSK Modulation of DMLs

The methods reviewed in Section 2.2 to mitigate the chirp effects in DML systems including transmitter- and receiver-based electronic compensation [9-12] and optical compensation [8, 13, 15, 16, 60] require either electrical or optical implementations that increase the system complexity and cost. In particular, replacing the existing fiber links, which are widely deployed using SSMF, with NDFs would involve huge costs. On the other hand, the device-based approaches require modifying the laser structure in order to exhibit low frequency chirp [17-19].

In addition to direct intensity modulation, however, semiconductor lasers have direct frequency modulation capability [20, 61]. The FSK modulation of DMLs takes advantage of the frequency chirp and can improve the dispersion-limited transmission distance [62]. It can be realized by driving the DML with a bias current far above the threshold and adding a relatively small modulation current [22]. This scheme requires an FM to IM converter either at the transmitter or the receiver, which can be a narrow optical filter or a delay interferometer (DI) [63].

However, the main problem in this approach is that DMLs exhibit highly non-uniform FM response at low frequencies (typically below 10 MHz), which results in a severe performance degradation [64]. The modulating injection current causes a change in both temperature and carrier density in the active layer, which in turn causes a change in the refractive index, affecting the oscillation frequency [64]. The thermal effect is dominant at low frequencies (below ~10 MHz) while the carrier density-induced FM exhibits a flat response from DC to several GHz. The overall FM response of the laser diode then becomes non-uniform at low frequencies with a frequency dip at ~1 MHz as illustrated in Figure 2.7 [20, 64].

This non-uniform FM response results in a severe pattern dependency [21, 22]. For example, when PRBS with a length of 2^7-1 is used at 10 Gb/s, the signal has its lowest frequency component at 78.7 MHz (= 10 GHz/127), which is well beyond the non-uniform region in the FM response of the DML (i.e., below 10 MHz). Consequently, the signal only utilizes the uniform region of the DML FM response. However, as the pattern length increases, the spectral spacing becomes narrower, and hence the low-frequency contents of the signal will be adversely affected by the non-uniform FM response. Since a short PRBS cannot represent real data, the pattern dependency implies a system penalty in real systems.

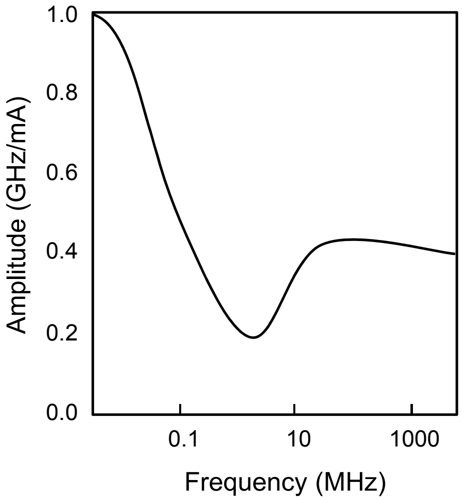

Figure 2.7: Typical FM response of a laser diode at low-frequency range, based on [64]

The following subsections introduce several approaches that have been reported to mitigate the non-uniformity of the DML FM response.

2.3.1 Device Approaches

The most straightforward solution to the non-uniform FM response problem is to use a laser diode with a flat FM-response such as multi-electrode DFB lasers [23-25]. In such devices, the lasing frequency can be controlled by adjusting the current ratio applied to the electrodes (i.e. selective current injection) to obtain sufficiently non-uniform field distribution in order to realize a flat FM response.

These devices, however, require correct bias current to each electrode and correct relative amplitude and phase relationship between the modulation currents to the electrodes in order to achieve a flat FM response which increases the implementation complexity [65]. In addition, simple line coding techniques in combination with conventional DFB lasers, for instance, were found to be nearly as a powerful solution as the use of three-electrode DFB lasers [66].

Section 2.3.2 focuses on system approaches to counteract the performance degradation associated with the non-uniform FM response of the DML without the need to replace the conventional lasers with new ones having modified structure and characteristics.

2.3.2 System Approaches

2.3.2.1 Electrical Equalization at the Transmitter

Unlike in the device approaches described in Section 2.3.1, the non-uniform FM response of the DML can be mitigated by shaping the electrical driving signal at the transmitter. For example, Saito *et al.* have implemented an electrical circuit, by means of an electrical high-pass filter (HPF), to equalize the laser driving signal in order to suppress the large frequency deviation at low frequencies, and hence realize uniform FM modulation characteristics [26].

Electrical equalization circuits to shape the laser driving signal were also demonstrated in other studies [27, 28]. However, such equalization circuits should be adjusted depending on the device FM characteristics, which increase the transmitter complexity. These techniques are also based on analog circuits and thus they do not take advantage of the digital mass production.

2.3.2.2 Optical Filtering

Optical filtering has been widely used to narrow the signal spectrum and increase the spectral efficiency in external modulator-based transmission systems [67, 68]. Optical filtering can also improve the performance of directly modulated systems by narrowing the broadened spectrum and converting chirp-induced FM into useful amplitude modulation (AM) [29, 69].

In [29], asymmetric narrowband optical filtering (3-dB bandwidth ~0.3 nm) was used to double the reach of DMLs in a 10-Gb/s WDM system without dispersion compensation. Figure 2.8 illustrates the concept of this scheme for directly modulated systems.

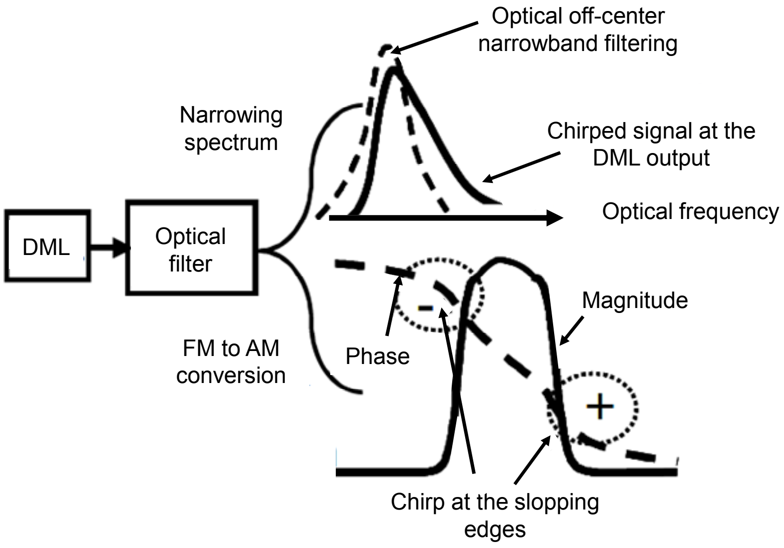

Figure 2.8: Conceptual diagram of asymmetric narrowband optical filtering in directly modulated systems [29].

Unlike in the external modulation case, there are many unwanted frequency components in the broadened spectrum of DMLs. Therefore, optical filtering with a bandwidth narrower than that of the broadened spectrum can remove these frequency components as shown in Figure 2.8 [29]. In addition, optical filtering can increase the ER by suppressing low driving current-induced frequency components. Since the chirp-induced spectrum broadening is not symmetric in directly modulated systems, asymmetric narrow filtering is needed. However, narrow filters are hard to implement, and particularly when this approach is implemented in WDM systems, a filter is required for each channel which increases the system cost and complexity.

Another approach that employs optical filtering to overcoming the limitations of DMLs and enhancing their transmission distance is described in [70]. This approach [known as chirp-managed laser (CML)] utilizes a DML followed by an optical spectrum reshaper (OSR) filter operating at its transmission edge to reshape both the amplitude and the instantaneous frequency profiles of the input pulses as depicted in Figure 2.9.

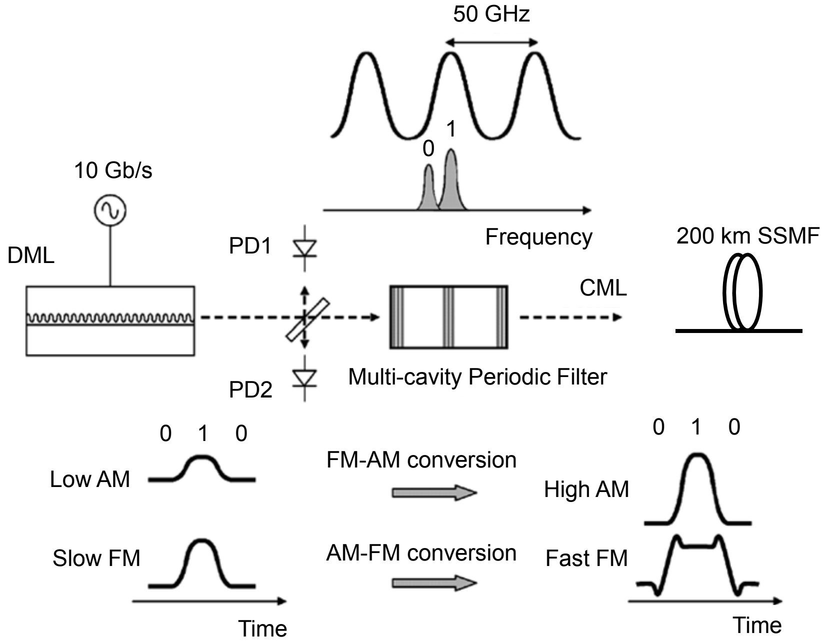

Figure 2.9: Principle of operation of CML [70]. PD: photodiode.

The laser wavelength is aligned on the transmission edge of the OSR, so that the blue-shifted ‘1’ bits can pass while the red-shifted ‘0’ bits are attenuated. This FM to AM conversion increases the ER at the output of the OSR as illustrated in Figure 2.9. The dispersion tolerance of this scheme results mainly from the high ER and also relatively narrow optical spectrum. Using this approach, a transmission distance of up to 250 km over SSMF was reported at 10 Gb/s without dispersion compensation [71]. In this scheme, however, a locking circuit composed of two photodiodes is required to lock the DML wavelength to the transmission edge of the OSR, which makes the concept more complex.

2.3.2.3 DC-Balanced Line Coding

When non-return-to-zero (NRZ) direct modulation is utilized, the thermal modulation of the laser causes drifts in the optical frequency during long strings of zeros or ones. The resulting baseline wander in the received signal leads to erroneous detection for long PRBS lengths [72]. Since DC-balanced formats contain low or no DC components, the laser temperature stays constant even during long strings of NRZ ones and zeros. Therefore, by using DC-balanced coding, the low-frequency contents of the signals can be depleted as shown in Figure 2.10, and hence only the uniform region of the FM response at higher frequency range will be exploited.

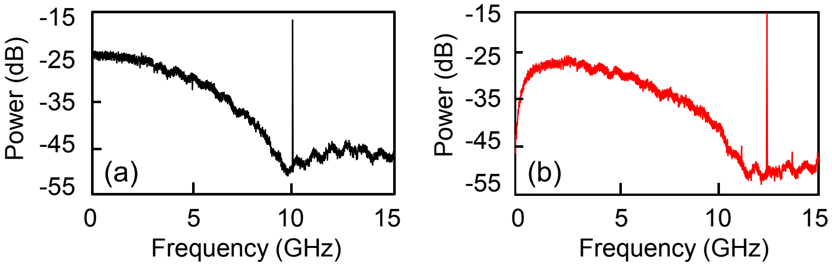

Figure 2.10: Schematic of RF spectra of (a) uncoded signal, and (b) signal coded with a DC-balanced line coding.

Few studies have shown the effectiveness of line coding techniques such as Manchester coding [33] and alternate mark inversion (AMI) [30-32] in overcoming the low-frequency non-uniform FM response of DMLs.

Manchester coding provides a transition in the center of every bit as illustrated in Figure 2.11 (a), and hence this coding induces 100% bandwidth increase as two signals are used to transmit a single bit.

In AMI coding, the binary 0 is represented by zero voltage and the ones are represented alternately by positive and negative pulses as shown in Figure 2.11 (b). Therefore, AMI coding provides 50% bandwidth increase as a ternary symbol is used to transmit a binary digit.

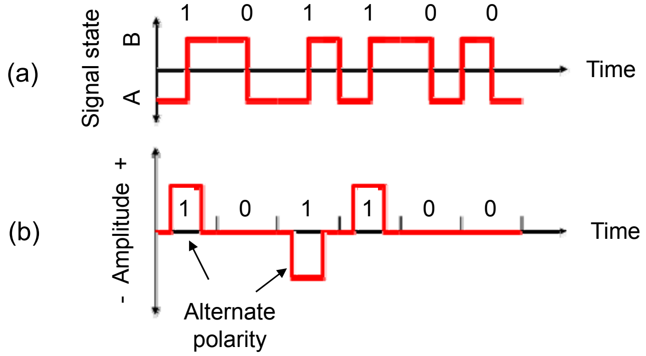

Figure 2.11: Illustration of (a) Manchester coding, and (b) AMI coding.

Recently, Baroni *et al.* have proposed the use of 8B/10B line coding to ameliorate the performance degradation induced by the non-uniform FM response of the DML [21]. The 8B/10B coding translates each source byte into a predefined 10-bit codeword with a maximum run length of 5 and a disparity of either 0 or ±2 in each 10-bit codeword. The run length is defined as the number of identical contiguous '1's or '0's which appear in the signal stream and the disparity is the difference between the number of 1's and 0's in the codeword. Since the disparity is bounded, the 8B/10B code is DC-balanced, i.e., provides a low DC content [73]. However, 8B/10B coding imposes a large overhead of 25%, which requires 25% larger bandwidth for the transmission devices (e.g., drivers, DMLs, receivers) and makes the system 56% (= 1.25^2-1) more vulnerable to fiber dispersion.

2.4 Summary

In this chapter, we have explored the literature related to DMLs. We first reviewed the basic characteristics and limitations of DMLs in Section 2.1. Section 2.2 is focused on directly intensity modulated lasers and their chirp-induced limitations. This section covers a verity of techniques proposed to mitigate the frequency chirp in intensity modulation-based DMLs. Section 2.3, concerns FSK modulation in DMLs which makes good use of the chirp-induced frequency modulation in DMLs. This scheme, however suffers from severe performance degradation associated with the non-uniform FM response of the laser diode. Several methods reported to combat this issue are introduced in this section. DC-balanced line coding can provide cost-effective and efficient way to alleviate the degradation caused by the non-uniform FM response. From the next chapter onwards, we will focus on the use of simple and bandwidth-efficient DC-balanced line codes to improve the performance of DML-based transmission systems.

Chapter 3

DC-Balanced Line Coding for 10-Gb/s Directly Modulated Lasers

3.1 Introduction

As aforementioned in Section 2.2, the intensity modulation in DMLs is always accompanied by phase modulation which in turn causes a large frequency chirp resulting in a considerable pulse broadening and significant chirp-induced power penalty after transmission over dispersive fiber [4, 6]. On the other hand, FSK modulation of DMLs makes good use of the frequency chirp and can improve the dispersion-limited transmission distance of DMLs [62]. But the main problem in this approach, as discussed in Section 2.3, is that DMLs exhibit highly non-uniform FM response at low frequencies resulting in a significant performance degradation [21, 64]. Section 2.3 reviewed several approaches that have been reported to combat this problem. Recently, Baroni *et al.* have proposed the use of 8B/10B DC-balanced line coding to deplete the low-frequency spectral contents of the signal in order to utilize the uniform region of the laser FM response only [21]. However, this line coding has a relatively large overhead of 25%, which requires 25% larger bandwidth for the transmission devices (e.g., drivers, DML, receiver) and makes the system 56% ($=1.25^2-1$) more vulnerable to fiber dispersion.

In this chapter, we experimentally investigate the use of various DC-balanced line coding schemes, including 8B/10B, 5B/6B, 7B/8B, 9B/10B, and 64B/66B to find a suitable code for 10-Gb/s directly modulated systems in terms of performance and bandwidth efficiency. Unlike in [21], we take the bandwidth expansion of each code into account to accurately assess the performance. Additionally, the target BER in [21] was 10^{-6} whereas it is 10^{-9} in our experimental demonstration. This chapter is structured as follows. We introduce the basic characteristics of the examined line codes in Section 3.2. The experimental setup employed to evaluate the performance of the coding formats is described in Section 3.3, while the experimental results are reported and discussed in Section 3.4. A short summary of this chapter is presented in Section 3.5.

3.2 DC-Balanced Line Coding

The 8B/10B, 5B/6B, 7B/8B, and 9B/10B codes are based on mapping blocks of data into predefined codewords that satisfy the run length and disparity constraints as defined in the coding lookup tables of each line coding. As defined in Chapter 2, the run length is the number of identical contiguous ones or zeros in the signal stream and the disparity is the difference between the number of ones and zeros in the codeword. For example, 8B/10B line coding maps each source byte into a predefined 10-bit transmission pattern with a maximum run length of 5 and a disparity of either 0 or ±2 [73]. Similarly, the 9B/10B code translates 9 bits of data into a 10-bit codeword, with a maximum run length of 7. The permitted disparity in each 10-bit codeword is 0, ±2 and ±4. Running disparity control is used to maintain this DC balance by which the transmitter keeps track of the running disparity [74]. The 5B/6B and 7B/8B codes map 5-bit and 7-bit blocks into predefined 6-bit and 8-bit codewords, respectively [73, 75]. More details about the construction of these codes are found in Appendices A through D.

Unlike the codes described above, 64B/66B coding is not based on mapping 64-bit blocks into predefined 66-bit codewords. Instead, each 64-bit block is scrambled using a self-synchronous scrambler of polynomial $x^{58} + x^{39} + 1$, and then a 2-bit preamble is added ('01' if the scrambled block is only data and '10' if it is only control or a mix of data and control) [76]. The 64B/66B code has an overhead of only 3.12% but at the expense of poorer transition density and longer run length compared to the mapping codes described above. Table 3-1 summarizes the basic characteristics of the line codes examined in this chapter. The line rate is defined as the total transmission data rate including the overhead.

Table 3-1: Basic characteristics of the utilized line codes

	8B/10B	5B/6B	7B/8B	9B/10B	64B/66B	PRBS (2^{20}-1)
Overhead (%)	25.00	20.00	14.29	11.11	3.12	0.00
Line rate (Gb/s)	12.44	11.94	11.37	11.06	10.26	9.95
Maximum run length	5	6	7	7	64*	20
Disparity per codeword	0 or ±2	0 or ±2	0, ±2 or ±4	0, ±2 or ±4	64**	N/A

* The maximum run length is 64 when the input block to the 64B/66B encoder is a sequence of zeros. However, when the input is a PRBS of length 2^n-1, the maximum run length is ~n.

** When the input block to the 64B/66B encoder is a sequence of zeros.

3.3 Experimental Setup

The experimental setup to evaluate the performance of the DML-based transmission system using different line codes is depicted in Figure 3.1. We generate line-coded data at a personal computer and then port them to a pulse pattern generator. A 2^{20}-1 PRBS is used as an input to the offline encoder throughout the experiment. The generated signals are fed to a commercial butterfly-packaged DML (NEL NLK5C5EBKA) operating at 1549.2 nm. We measure the light power versus input current (L-I curve) characteristics of the DML at 20°C and plot in Figure 3.2. As observed from this figure, the threshold current of the DML is 10 mA in this case.

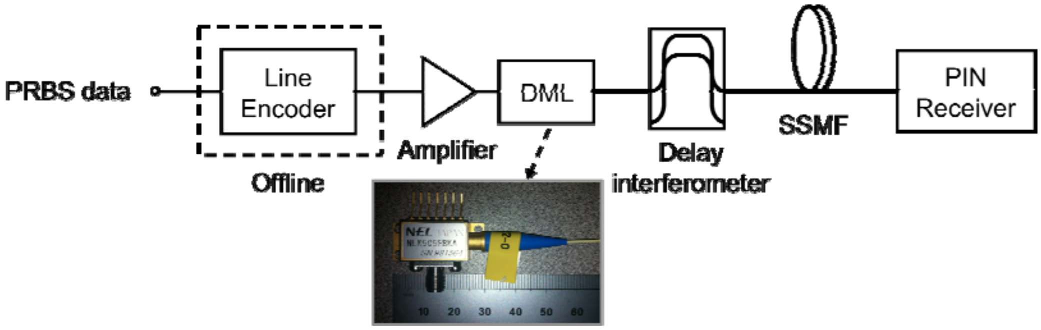

Figure 3.1: Experimental setup to evaluate the performance of DC-balanced line coding in a DML-based transmission system. The photo shows the DML used in this experiment (the scale is in millimeters).

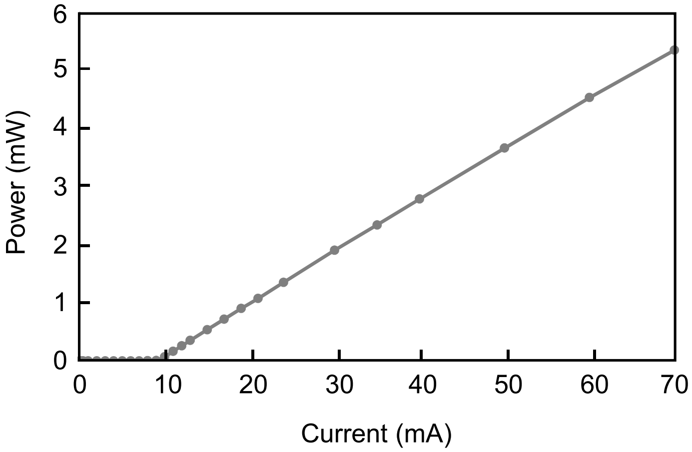

Figure 3.2: The light power versus input current (L-I curve) characteristics of the utilized DML at 20°C.

The DML is biased at 60 mA (~6 times the threshold current to make the adiabatic chirp dominant over the transient chirp), obtaining an output power of 5.3 dBm. We also measure the frequency response of the DML at these operating conditions as shown in Figure 3.3. The DML has a relaxation resonance frequency at around 18 GHz and the 3-dB modulation bandwidth is measured to be 25 GHz.

Figure 3.3: Measured frequency response of the DML used in the experiment.

The FSK-modulated signal at the DML output, the optical spectrum of which is plotted in Figure 3.4 (a), is sent to a DI to be converted into continuous-phase FSK/amplitude-shift keying (CPFSK/ASK) signal. Figure 3.4 (b) shows the optical spectrum of the signal at the DI output.

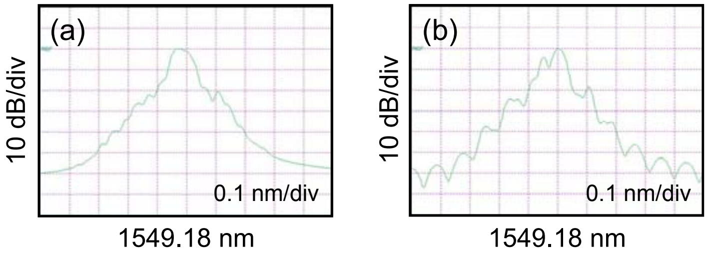

Figure 3.4: Optical spectra measured at the output of (a) DML, and (b) DI.

The wavelength response of the DI employed in the experiment is shown in Figure 3.5. The figure shows that the free spectral range (FSR) (i.e., the wavelength spacing between two successive peaks) is 10.7 GHz. To be noted that the poor ER in Figure 3.5 is due to the limited resolution bandwidth of our optical spectrum analyzer (0.02 nm). The DI phase is adjusted to locate its spectral null at the mark wavelength, which results in a better dispersion tolerance compared to the case where the spaces are suppressed. The CPFSK-ASK signals at the DI output have a 3-dB bandwidth of 7.7 GHz and optical power of 0 dBm. These signals are then launched into an SSMF and detected with a PIN receiver.

It is worth noting that the DI can be alternatively placed at the receiver. However, when it is placed at the transmitter, the receiver implementation can be simpler. In addition, this implementation can be beneficial for WDM systems thanks to the periodicity of the DI frequency response, which allows us to use a single DI for all the WDM channels. This scenario will be explained in more detail in Section 3.4.

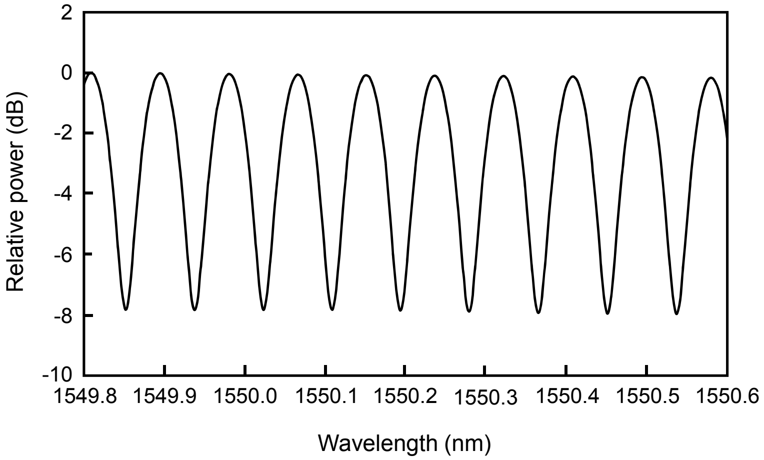

Figure 3.5: Wavelength response of the DI used in the experiment.

We optimize the DML driving voltage. Figure 3.6 shows the measured receiver sensitivity at a BER of 10^{-9} (i.e., the minimum received optical power required to achieve a BER of 10^{-9}) as a function of the peak-to-peak driving voltage. In this measurement, we utilize 2^7-1 PRBS at 9.95 Gb/s. The optimum driving voltage is found to be 1.28 V_{pp} in this case. This optimum driving voltage remains unchanged for different PRBS lengths and line codes running at their corresponding line rates.

Since the FM efficiency of the DML is measured to be 0.184 GHz/mA, the frequency deviation between the mark and space of the FSK signal at the DML output is 4.7 GHz (= 0.184 GHz/mA × 1.28 V / 50 Ω), which is approximately half the data rate.

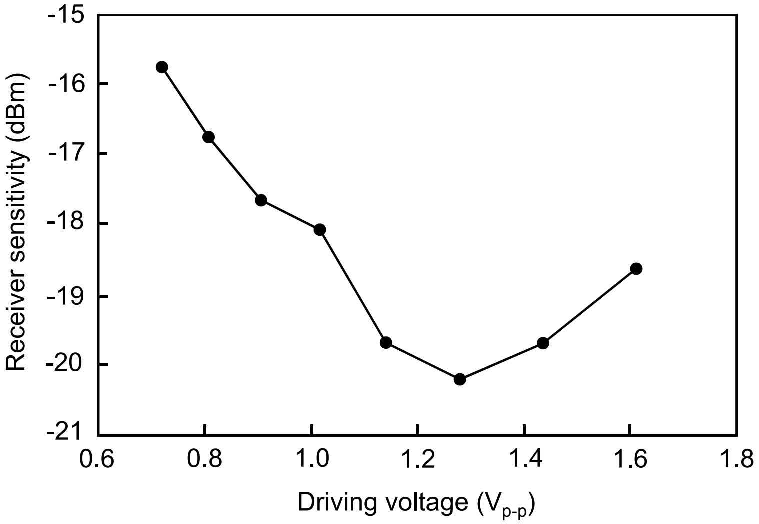

Figure 3.6: Receiver sensitivity as a function of the peak-to-peak driving voltage to the DML measured with uncoded 2^7-1 PRBS at 9.95 Gb/s.

3.4 Experimental Results

Figure 3.7 shows the back-to-back BER curve using each line code operating at its corresponding line rate. Also plotted are the BER curves using uncoded PRBS with lengths of 2^7-1, 2^{15}-1, and 2^{20}-1 for comparison.

The measured receiver sensitivities for the line-coded signals range from -19.3 to -16.9 dBm except for the 64B/66B-coded signal where an error floor is observed at around 10^{-8}. This should be attributed to the little depletion of the low-frequency signal content by the 64B/66B line coding as evident in the RF spectra of the coded signals plotted in Figure 3.8 and 3.9. Unlike the other line codes, 64B/66B [Figure 3.8 (b)] induces only a little change in the power level of the low-frequency spectral content of the signal compared to uncoded 2^{20}-1 PRBS [Figure 3.8 (a)]. Nevertheless, in Figure 3.7, 64B/66B coding exhibits more than an order-of-magnitude improvement in BER over 2^{20}-1 PRBS.

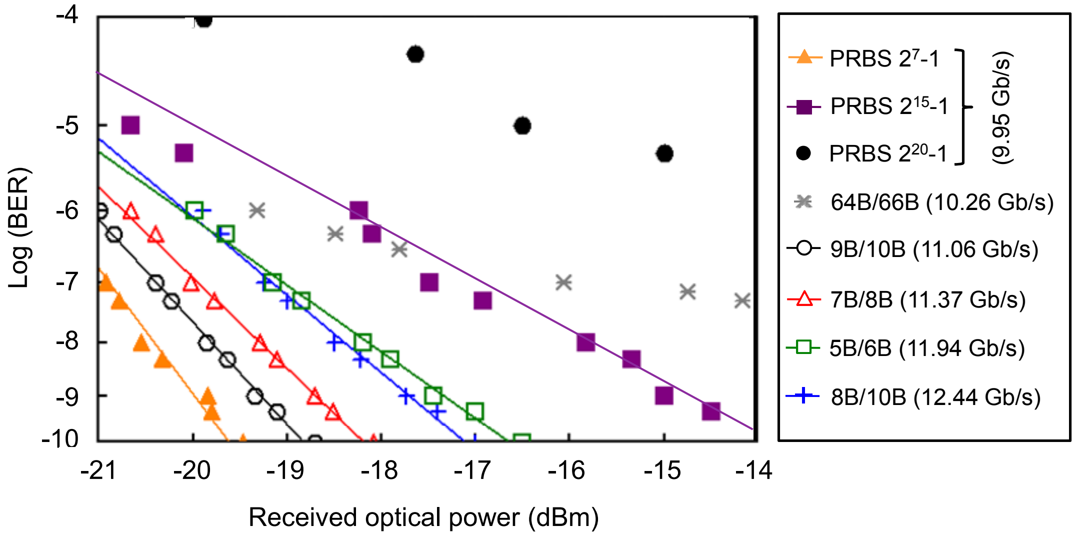

Figure 3.7: Back-to-back BER curves of the line-coded signals at their corresponding line rates. Also plotted are the BER curves using uncoded PRBS with lengths of 2^7-1, 2^{15}-1, and 2^{20}-1 for comparison. If not stated otherwise, the PRBS length used in these measurements is 2^{20}-1.

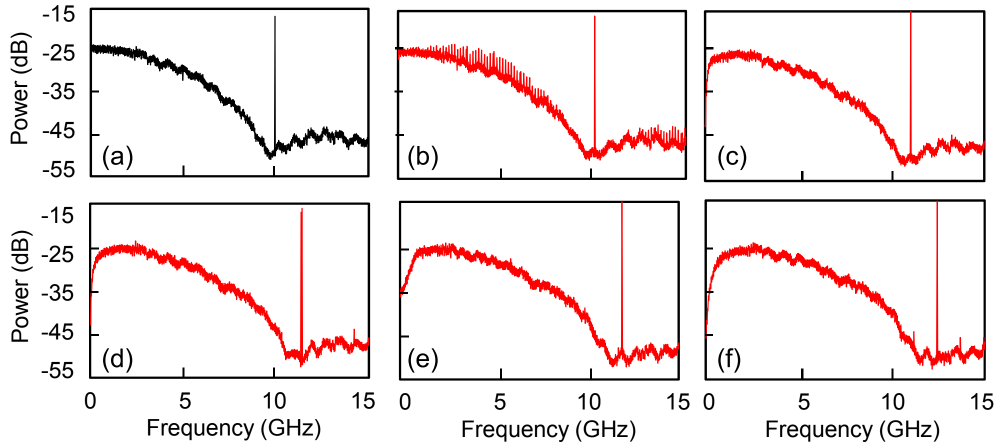

Figure 3.8: Measured RF spectra of (a) uncoded 2^{20}-1 PRBS, (b) 64B/66B, (c) 9B/10B, (d) 7B/8B, (e) 5B/6B, and (f) 8B/10B signals. The PRBS length used in these measurements is 2^{20}-1.

Figure 3.7 shows that 9B/10B exhibits the best receiver sensitivity among the five examined line codes. This is because this line coding greatly depletes the low-frequency spectral content of the signal as evident in Figure 3.8 (c) and Figure 3.9, yet it has a small overhead of 11.11%. The receiver sensitivity using 9B/10B line coding is measured to be -19.3 dBm, which is only ~0.7 dB worse than that using 2^7-1 PRBS. To be noted that 2^7-1 PRBS, however, cannot represent real data and it is used just as a reference.

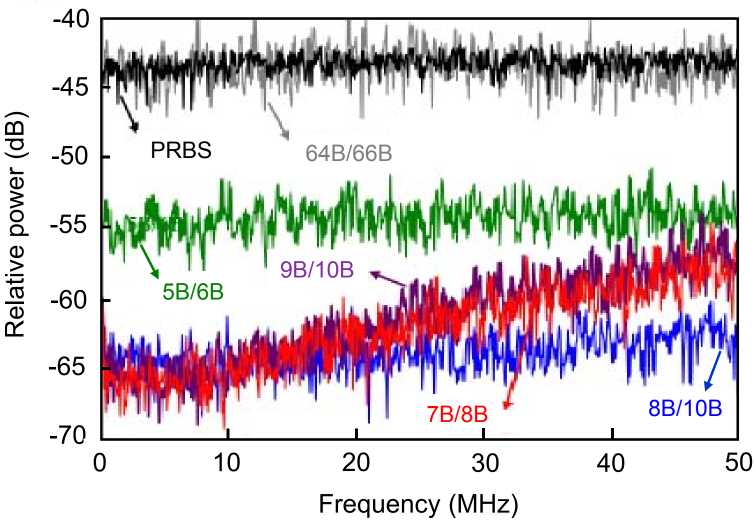

Figure 3.9: Measured RF spectra of the coded and uncoded signals at low-frequency range (<50 MHz).

The BER measurements using different PRBS lengths also show the importance of the absence of low-frequency spectral contents of the signals. For example, the receiver sensitivity using 2^7-1 PRBS is -20.0 dBm whereas it is measured to be -15.0 dBm for 2^{15}-1 PRBS and a poor BER of 5×10^{-6} is observed at a received signal power of -15 dBm with 2^{20}-1 PRBS. This is because the lowest spectral tone using 2^7-1 PRBS is located at 78.37 MHz (= 9.953 Gb/s / 127), which is much higher than the FM dip of the DML (at ~ 10 MHz) and thus this signal utilizes the flat region of the

DML FM response. However, 2^{15}-1 and 2^{20}-1 PRBSs have their lowest spectral tones at 304 kHz and 9.5 kHz, respectively. Therefore, they suffer performance degradation induced by the non-uniform FM response of the DML at low frequencies.

It is interesting to note that when we utilize different line codes, the line rate varies with the overhead. For fair comparison among the line codes with different line rates, we should thereby optimize the bandwidth of the electrical and optical devices for each line coding. Due to the limitation of our experimental setup, however, we utilize the same devices with all the line codes. Therefore, we measure the receiver sensitivity penalty incurred by the limitation of the experimental setup. To this end, we measure the sensitivity penalty using 2^7-1 PRBS as we increase the data rate from 9.95 to 12.44 Gb/s and plot in Figure 3.10. The penalties are plotted with reference to the receiver sensitivity of the 9.95-Gb/s signals.

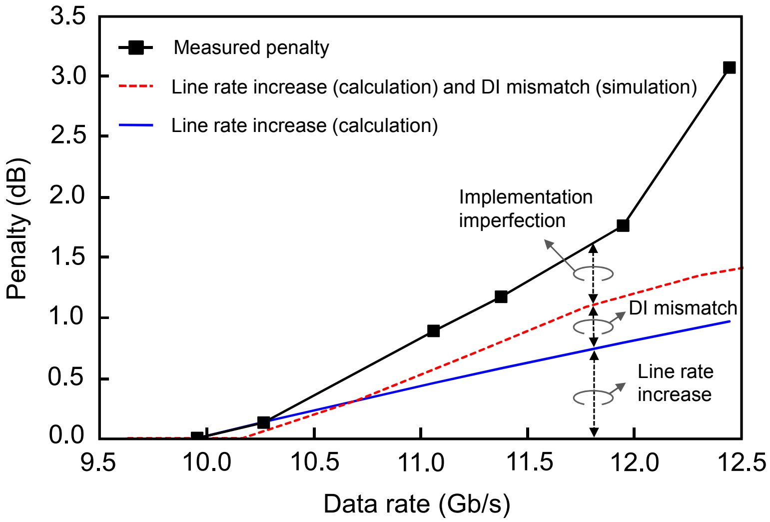

Figure 3.10: Receiver sensitivity penalty as a function of the data rate measured with 2^7-1 PRBS.

The results show that the penalty increases with the data rate. For example, a penalty of 3.1 dB is incurred at a data rate of 12.44 Gb/s. This penalty should be attributed to (1) data-rate increase, (2) delay-to-line rate mismatch of the DI, and (3) implementation imperfection (e.g., caused by using a fixed bandwidth amplifier). To see the contribution of these effects, we analyze the penalty caused by the data-rate increase and the delay-to-line rate mismatch using a theoretical calculation and computer simulation, respectively. As the data rate increases, the received signal power should increase with the data rate to maintain the signal-to-noise ratio (SNR). Therefore, the penalty due to the data-rate increase (solid line in Figure 3.10) is proportional to the data rate. The relative delay between the two arms of the DI utilized in this experiment is 93.5 ps, which best matches to 10.7-Gb/s signals. However, when the line rate deviates from this number, a sensitivity penalty is incurred. The computer simulation (VPI TransmissionMaker) shows that a penalty of 0.4 dB is expected when 12.44-Gb/s signals are used with the 93.5-ps DI. Therefore, Figure 3.10 shows that the penalty of 3.1 dB for 12.44-Gb/s signal can be broken down into 1.0 dB by the data-rate increase, 0.4 by the delay-to-line rate mismatch, and 1.7 dB by implementation imperfection.

It is interesting to note that in Figure 3.7 the sensitivity penalties of the line-coded signals with respect to the sensitivity of 2^7-1 PRBS are smaller than the results of Figure 3.10. For example, the sensitivity penalty of 12.44-Gb/s 8B/10B-coded signal is measured to be 2.1 dB in Figure 3.7 but the sensitivity penalty of 12.44-Gb/s 2^7-1 PRBS is 3.1 dB in Figure 3.10. This implies that even 2^7-1 PRBS is a little affected by the FM dip of the DML and the line coding is very effective in utilizing the flat FM response region only. This can be also explained by the sensitivity improvement of the line-coded signals over 2^7-1 PRBS when the line coding is applied at 9.95 Gb/s (i.e., without taking the overhead into account). For example, 9.95-Gb/s 8B/10B signals result in a sensitivity improvement of 0.2 dB with respect to 9.95-Gb/s 2^7-1 PRBS.

Figure 3.11 illustrates the optical eye diagrams measured at the DI output. The eye diagrams for 2^7-1 PRBS, 5B/6B, 7B/8B, 8B/10B and 9B/10B show clear eye opening, while 2^{20}-1 PRBS and 64B/66B show degraded eye diagrams with scattered dots in the middle of the eyes. The ER is measured to be 9~10 dB for all the cases.

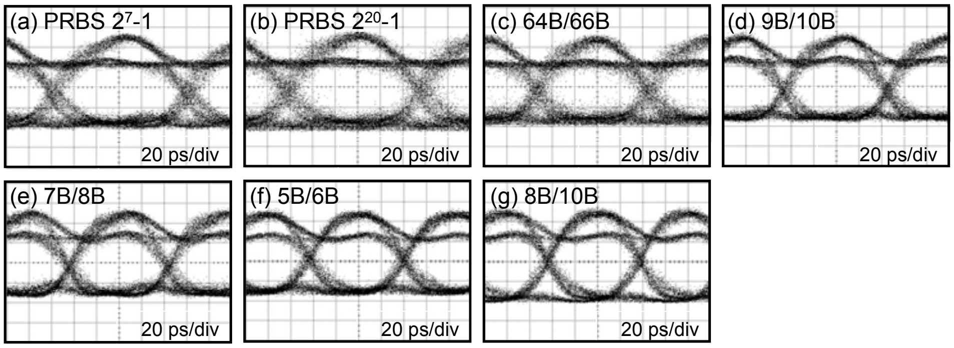

Figure 3.11: Optical eye diagrams of (a) uncoded 2^7-1 PRBS, (b) uncoded 2^{20}-1 PRBS, (c) 64B/66B, (d) 9B/10B, (e) 7B/8B, (f) 5B/6B, and (g) 8B/10B signals measured at the DI output. If not stated otherwise, the PRBS length used in these measurements is 2^{20}-1.

The dispersion tolerance of the line-coded signals is measured using SSMF. Figure 3.12 shows the receiver sensitivity versus the transmission distance. The results for 64B/66B are not included because we are not able to achieve a BER of $<10^{-9}$ even at the back-to-back case.

The results in Figure 3.12 show a couple of decibels improvement in receiver sensitivity after 15-km transmission. This is because of the duobinary-like phase characteristics of the generated CPFSK-ASK signals [63, 77]. Since the frequency deviation between the mark and space at the DML output is equal to half the line rate, the phase slide of the signals at the space becomes π, just like duobinary signals [77].

The difference between duobinary and CPFSK-ASK signals is that duobinary has an abrupt π phase jump at the center of the space whereas CPFSK-ASK has a smooth phase shift over the bit duration of the space [77]. Only with 9B/10B and 7B/8B coding, we successfully transmit 10-Gb/s signals over 65-km SSMF. The dispersion penalties are measured to be 2.5 and 3.5 dB for 9B/10B and 7B/8B, respectively.

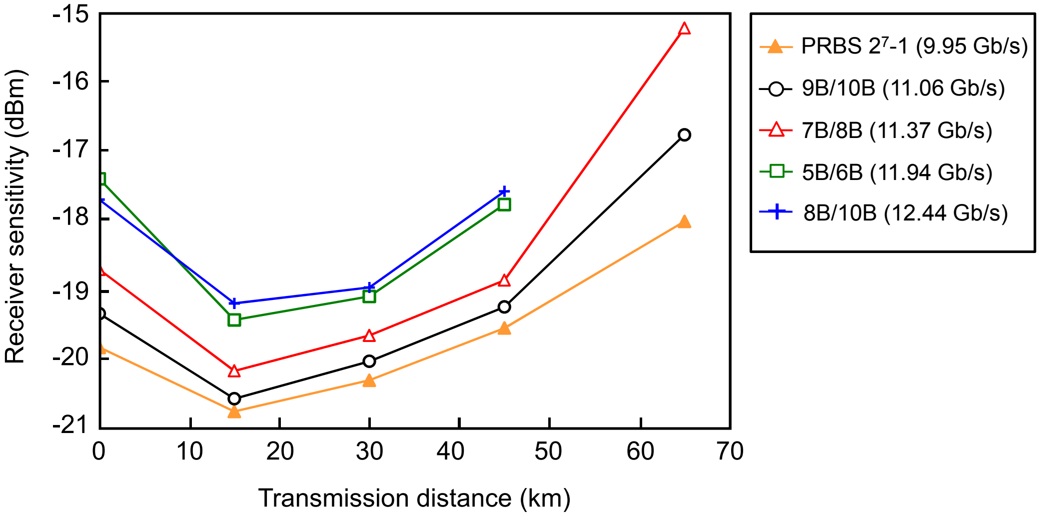

Figure 3.12: Measured dispersion tolerance for the uncoded 2^7-1 PRBS signal and the line-coded signals at their corresponding line rates. If not stated otherwise, the PRBS length used in these measurements is 2^{20}-1.

Figure 3.13 demonstrates the BER curves measured after 65-km transmission. There is no evidence of error floors using 5B/6B and 8B/10B coding. Due to the large bandwidth expansion by the overhead, however, there are large dispersion-induced penalties, and thus, we are not able to achieve a BER of 10^{-9} at the maximum received signal power of -14 dBm.

It should be noted that the laser wavelength should be precisely aligned to the DI. This could be achieved by applying a low-frequency electrical tone signal to the DML and then utilizing Fabry-Perot etalon-based monitoring module [78]. By monitoring the wavelength drift between the DML and DI, we can control the laser wavelength to be locked to the DI. This can be readily applied to WDM systems without additional DI or monitoring modules. Figure 3.14 shows the schematic diagram of such WDM systems.

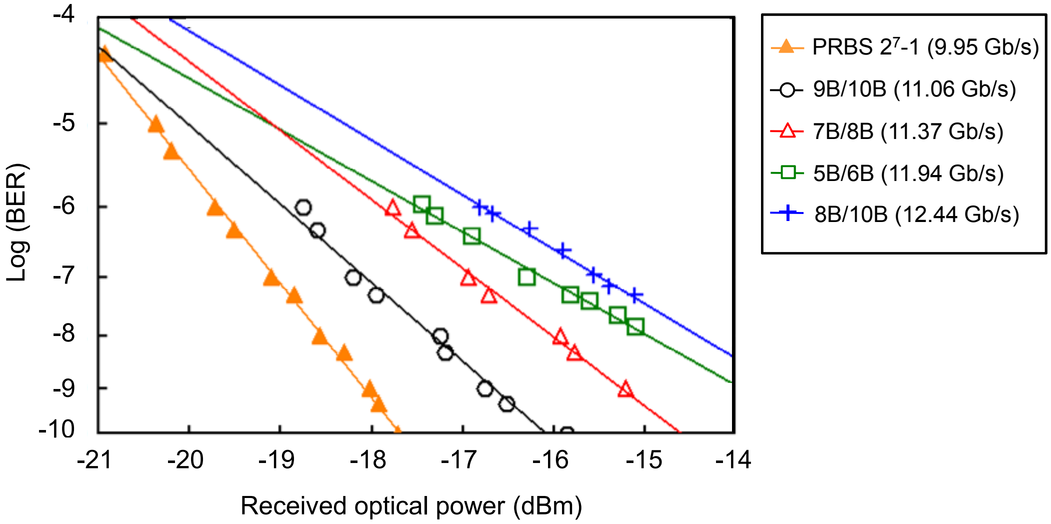

Figure 3.13: BER curves after 65-km transmission over SSMF for the uncoded 2^7-1 PRBS signal and the line-coded signals at their corresponding line rates. If not stated otherwise, the PRBS length used in these measurements is 2^{20}-1.

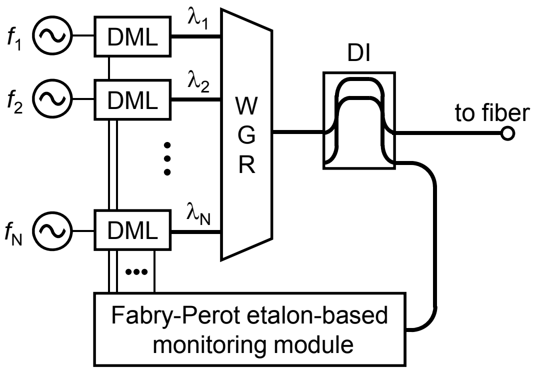

Figure 3.14: Schematic diagram of wavelength-division-multiplexed CPFSK-ASK directly modulated systems. WGR: wavelength grating router.

In this case, the channel spacing should be adjusted according to the FSR of the DI such that the DI spectral nulls are aligned to the marks of the channels. To discriminate between the channels, each DML is applied with a tone signal having a unique frequency. Since the line coding depletes the low-frequency spectral contents of the signal, the tone signal would not interfere with the data signal, provided that the tone frequency is lower than tens of MHz.

3.5 Summary

We have experimentally investigated the application of various line codes (8B/10B, 5B/6B, 7B/8B, 9B/10B, and 64B/66B) to enhance the performance of 10-Gb/s CPFSK-ASK signals generated with a DML and a DI. We take into consideration the bandwidth expansion induced by the overhead of each line code for fair comparison. A long PRBS length of 2^{20}-1 is also used for all the line codes to accurately examine the pattern dependency.

We have performed a set of receiver sensitivity measurements over SSMF to evaluate the performance of the line codes. Among the five codes we tested, 9B/10B exhibits the best performance whereas a marginal improvement is achieved with 64B/66B. This is because 9B/10B coding can greatly deplete the low-frequency spectral contents of the signals, yet it expands the bandwidth by 11.11% only. Using this line coding, we achieve 65-km transmission of directly modulated 10-Gb/s signals without any dispersion compensation. The dispersion-induced penalty is measured to be 2.5 dB. Therefore, we believe that the use of 9B/10B for DMLs can be beneficial for implementing cost-sensitive access transmission systems.

Chapter 4

Directly-Modulated Laser Driven by Low-Bandwidth Duobinary Signals

4.1 Introduction

Despite their merits, one of the biggest stumbling blocks to the widespread use of DMLs is the modulation bandwidth limitation (typically <20 GHz) by the nonlinear gain effect and the carrier transport lifetime [5, 37, 79]. In a typical semiconductor laser, the resonance frequency f_R is a figure-of-merit which determines the maximum direct modulation bandwidth [80]. For most lasers, the 3-dB modulation bandwidth (f_{3dB}), defined as the frequency at which the modulation output is reduced by a factor of 2 (i.e., 3 dB), can be approximated by [6]

$$f_{3dB} \approx \frac{f_R\sqrt{3}}{2\pi} \approx \left(\frac{3GP_b}{4\pi^2\tau_p}\right)^{1/2} \tag{4.1}$$

where G is the net rate of stimulated emission, P_b is the output power at the bias level, and τ_p is the photon life time related to the excited energy level.

Several studies have been reported to increase the resonance frequency of DMLs including optical injection locking [80-82]. In a conventional laser, as the bias current increases, both the damping and resonance frequency increase, thereby limiting the maximum modulation bandwidth. In injection-locked lasers, the damping may actually decrease as the resonance frequency increases, allowing very efficient modulation response at extremely high frequencies.

In this chapter, we propose a system approach rather than changing the device structure to alleviate the modulation bandwidth limitation of the DML. We demonstrate a 10-Gb/s DML-based transmitter driven by 3.5-GHz-bandwidth electrical signals. This greatly relieves the modulation bandwidth requirements of the DML and it is expected that 20-Gb/s signals can be accommodated with a 7-GHz-bandwidth DML using this approach. To be noted that the proposed scheme can be applied in conjunction with the device approaches descried above (e.g., using optical injection locking) to support even higher modulation speeds.

In the proposed system, the DML is driven by duobinary signals generated by filtering NRZ signals with a low-pass filter (LPF) [83]. The ternary FSK signals generated at the DML output are then converted into binary CPFSK/ASK signals using a DI [84]. To avoid the performance degradation caused by the non-uniform FM response of the DML especially at low frequencies, we employ DC-balanced 9B/10B line coding [63]. Two schemes are demonstrated in this chapter, one using the destructive port of the DI (hereafter referred to as destructive-port scheme) and the other using the constructive port (hereafter referred to as constructive-port scheme).

This chapter is organized as follows. Section 4.2 is devoted to discuss proposed transmitter using the destructive-port scheme. The principle of operation is first introduced in Section 4.2.1, followed by the experimental setup and results in Section 4.2.2 and 4.2.3, respectively. Section 4.3 focuses on the constructive-port scheme. The remaining sections introduce the principle of operation, experimental demonstration and results using this scheme. Finally the chapter is summarized in Section 4.4.

4.2 Destructive-Port Scheme

4.2.1 Principle of Operation

The proposed transmitter is depicted in Figure 4.1. It consists of a DML, a DI, and an optical band-pass filter (OBPF).

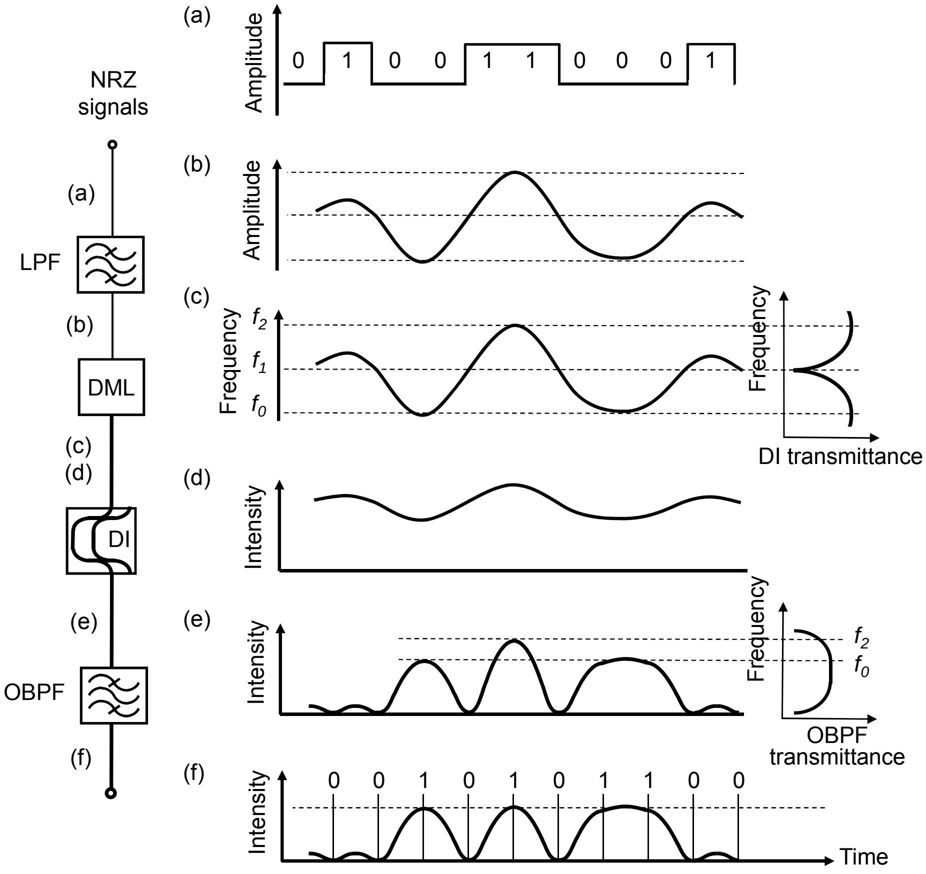

Figure 4.1: Principle of operation using the destructive-port scheme (a) NRZ data, (b) duobinary-encoded DML driving signal, (c) ternary FSK signal at the DML output (frequency profile), (d) intensity profile of the signal at the DML output, (e) CPFSK/ASK signal at the DI output, and (f) mark-level-equalized CPFSK/ASK signal at the OBPF output.

The data are first encoded using 9B/10B encoder and then precoded. The purpose of precoding is to avoid error propagation at the receiver, just like in duobinary systems [85]. The precoded data are then encoded into duobinary signals after passing through an LPF as illustrated in Figure 4.1 (b). The duobinary signals are applied directly to the DML to generate ternary FSK signals with corresponding frequencies f_0, f_1, and f_2 [Figure 4.1 (c)]. The FSK signals are then converted into CPFSK/ASK signals by passing through the *destructive* port of the DI, where the peak frequencies of the DI are located at f_0 and f_2 while its null frequency at f_1, as shown in Figure 4.1 (c). The f_1 components at the DML output are then suppressed by the DI, constituting the spaces of the signals (i.e., '0' bits), whereas both f_0 and f_2 components are given high transmittance, and hence constitute the marks (i.e., '1' bits) [Figure 4.1 (e)]. However, the current modulation of the DML is always accompanied by intensity modulation as illustrated in Figure 4.1 (d). As a result, the marks have two different intensity levels, a low level which corresponds to the f_0 component and a high level corresponding to the f_2 component as shown in Figure 4.1 (e). This split in the mark level can be readily suppressed by using an OBPF with its skirt located at f_2 which gives a low transmittance to the high-level marks, and consequently equalizes the split in the mark level as shown in Figure 4.1 (f).

4.2.2 Experimental Setup

The experimental demonstration of the destructive-port scheme is verified using the setup shown in Figure 4.2. NRZ signals with a PRBS length of 2^{20}-1 are first encoded offline by a 9B/10B line encoder and then precoded. Due to the overhead of the 9B/10B coding, the line rate is increased by 11.11%. The precoded signals are encoded into duobinary signals using a 3.5-GHz LPF and then fed to a commercial DML operating at 1549 nm. The LPF bandwidth falls within the typical range of duobinary transmitters (i.e., 1/4 to 1/3 of the line rate) [86, 87]. The DML is biased at 80 mA (~8 times the threshold current to make the adiabatic chirp dominant), obtaining an output power of 6.5 dBm. The optimum driving voltage to the DML is found to be 2.0 V_{pp}, at which the peak-to-peak frequency deviation of the ternary FSK signals is estimated to be ~8 GHz, which is close to the line rate.

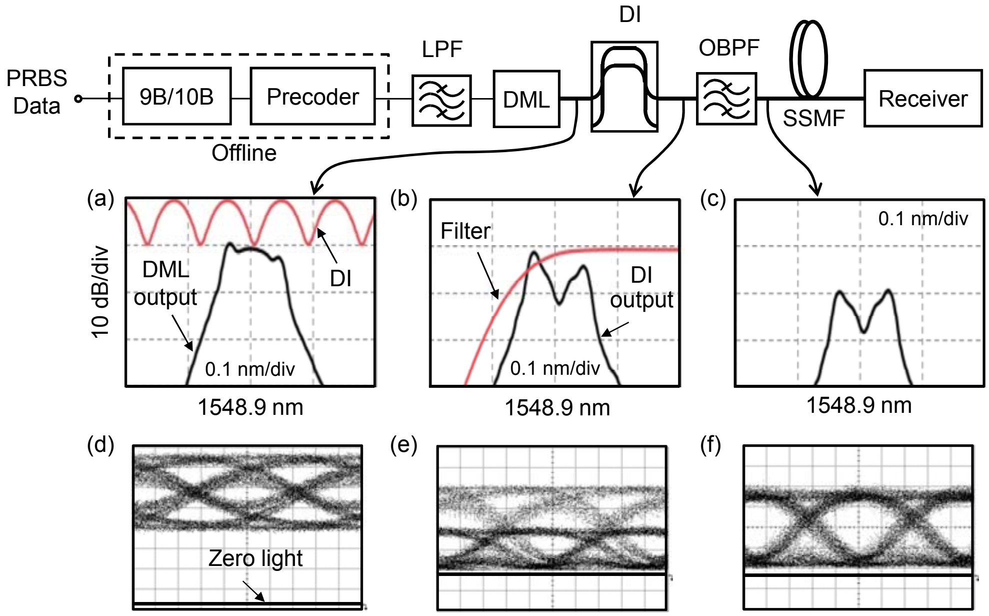

Figure 4.2: Experimental setup for demonstration of the destructive-port scheme. The insets are the measured optical spectra at (a) DML output (the DI wavelength response is plotted in red), (b) DI output (the OBPF wavelength response is plotted in red), and (c) OBPF output, and the measured eye diagrams at (d) DML output, (e) DI output, and (f) OBPF output.

The optical spectrum and eye diagram at the DML output are depicted in Figure 4.2 (a) and (d), respectively. The DML output is sent to a DI with an FSR of 10.7 GHz. Figure 4.2 (b) and (e) show the optical spectrum and eye diagram at the DI output, respectively. A split in the mark levels caused by the intensity modulation of the DML is clearly observed in Figure 4.2 (e). However, the use of OBPF equalizes the mark level as shown in Figure 4.2 (f). The optical spectrum in Figure 4.2 (c) also shows the identical optical powers at f_0 and f_2. The ER of the signals is measured to be

~8 dB. CPFSK/ASK signals with -3-dBm optical power are launched into an SSMF and detected with a PIN receiver.

4.2.3 Experimental Results

We first measure the back-to-back performance of the proposed system using the destructive-port scheme. Figure 4.3 shows the BER curve of the 9B/10B-coded signals running at 11.06 Gb/s. Also plotted, for comparison, are the BER curves measured with uncoded PRBSs of length 2^7-1 and 2^9-1 at 9.95 Gb/s.

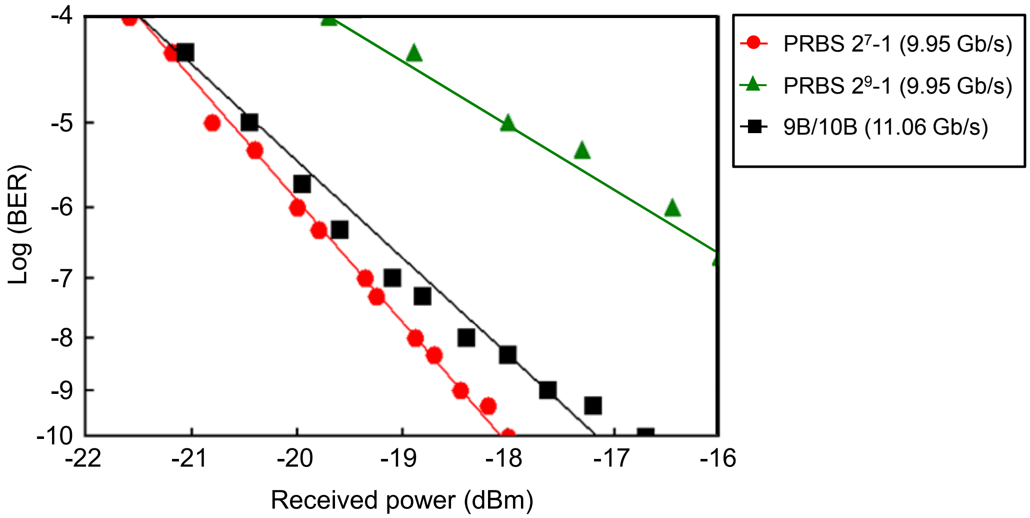

Figure 4.3: Measured back-to-back BER of the destructive-port scheme. The BER curves using uncoded PRBS of length 2^7-1 and 2^9-1 at 9.95 Gb/s are plotted for comparison.

The receiver sensitivities (at BER=10^{-9}) using 2^7-1 and 2^9-1 PRBSs are measured to be -18.5 and -11 dBm, respectively, whereas an error floor is observed at a BER of ~10^{-4} with uncoded 2^{20}-1 PRBS (not shown in Figure 4.3). As explained in Chapter 2, a short PRBS length cannot represent real data, and thus, the pattern dependency implies a system penalty in real systems. The pattern dependency observed in Figure 4.3 is ascribed to the non-uniform FM response of the DML at low frequencies. The

9B/10B coding depletes the low frequency contents of the signal, and thereby mitigates these pattern-length dependencies. Using 9B/10B line coding, we achieve a good receiver sensitivity of -17.6 dBm at a PRBS length of 2^{20}-1. The 0.9-dB penalty with respect to the uncoded 2^{7}-1 PRBS should be in part attributed to the line-rate increase [63]. The efficacy of mark-level equalization using OBPF is also evaluated using BER measurements. Without the OBPF, a poor BER of 7×10^{-3} is observed at a received power of -12 dBm.

We next measure the dispersion tolerance of the proposed scheme. Figure 4.4 shows the receiver sensitivity as a function of the accumulated dispersion. The corresponding eye diagrams are demonstrated in Figure 4.5. The dispersion window, defined as the allowable amount of dispersion inducing less than 2-dB power penalty, is measured to be ±300 ps/nm. This indicates that the generated 10-Gb/s signals at 1550 nm can travel ~20 km over SSMF without dispersion compensation.

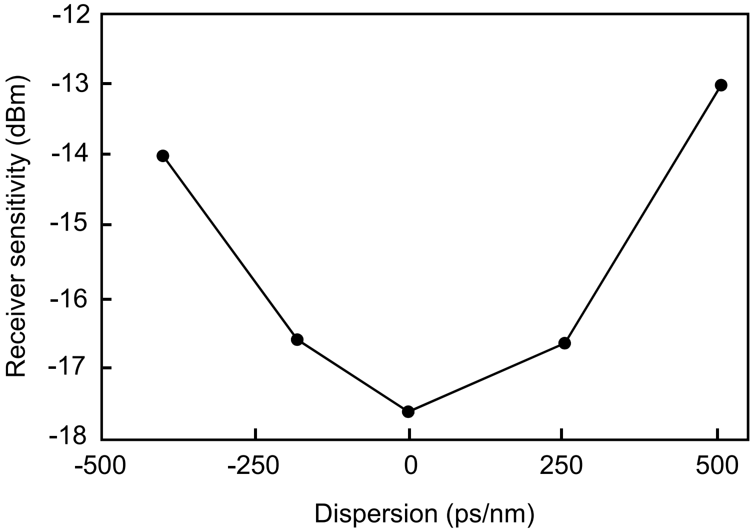

Figure 4.4: Measured dispersion tolerance using the destructive-port scheme.

Finally, we measure the sensitivity penalty incurred by the frequency offset between the DML and the optical filters and plot in Figure 4.6. In these measurements, we stabilize the optical filters and vary the bias current of the DML to fine tune the operating wavelength. The figure shows that the frequency offset should be kept within around ±150 MHz to keep the penalty below 2 dB. Since both the DML and DI are located at the transmitter side, the DML wavelength could be precisely aligned to the optical filters by utilizing a frequency monitoring module [78].

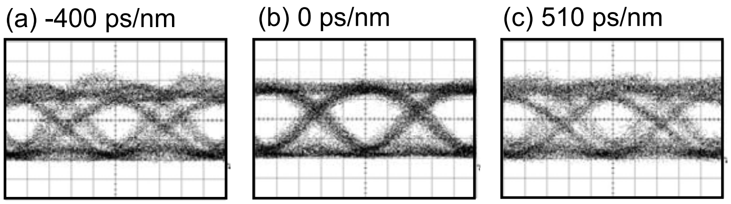

Figure 4.5: Measured eye diagrams using the destructive-port scheme when the accumulated dispersion is (a) -400, (b) 0, and (c) 510 ps/nm.

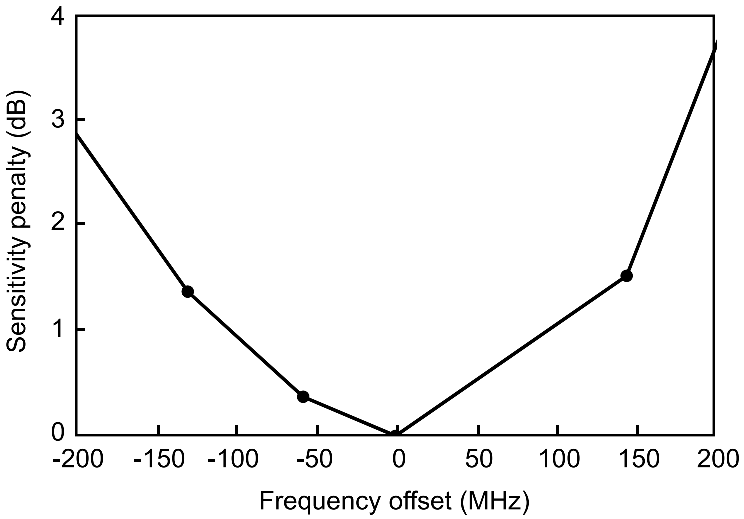

Figure 4.6: Measured sensitivity penalty incurred by the frequency offset between the DML and the optical filters using the destructive-port scheme.

4.3 Constructive-Port Scheme

4.3.1 Principle of Operation

The DI has two output ports and both ports can convert the FSK signals at the DML output into CPFSK/ASK signals. Figure 4.7 shows the principle of operation when the *constructive* port of the DI is employed.

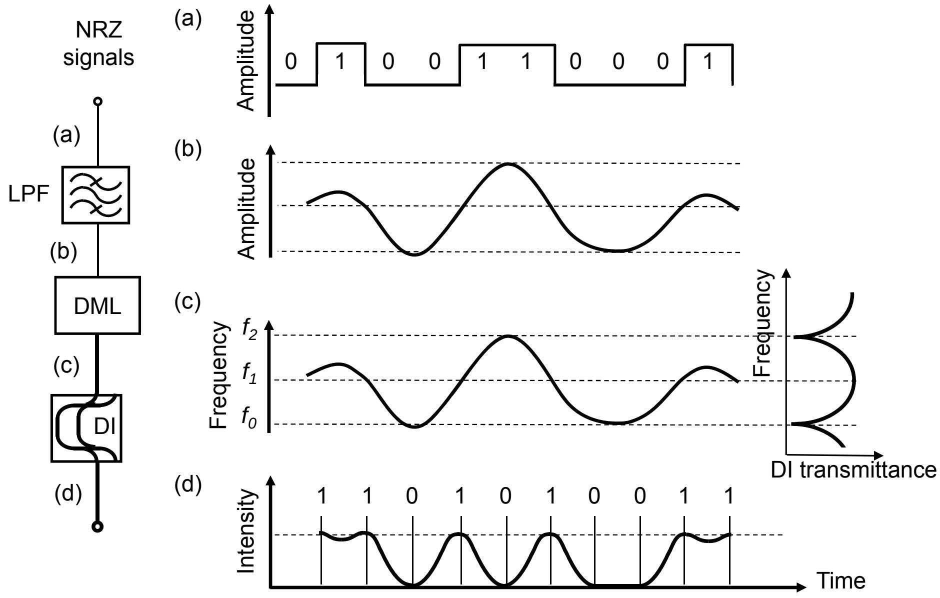

Figure 4.7: Principle of operation using the constructive-port scheme (a) NRZ data, (b) duobinary-encoded DML driving signal, (c) ternary FSK signals at the DML output (frequency profile), and (d) CPFSK/ASK signals at the DI output.

Just like the case with the destructive-port scheme, the precoded NRZ signals first pass through the LPF to be encoded into duobinary signals as illustrated in Figure 4.7 (b), which are fed directly to the DML. The ternary FSK-modulated signals at the DML output are then converted into CPFSK/ASK signals by passing through the constructive port of the DI. The peak frequencies of the DI are aligned to the f_1 components of the signal while the null frequencies of the DI to the f_0 and f_2 components, as shown in Figure 4.7 (c). The marks are therefore composed of the f_1

components whereas both the f_0 and f_2 components constitute the spaces [Figure 4.7 (d)]. Unlike the destructive-port scheme in Section 4.2, the OBPF, which is required to equalize the mark levels, is not needed since the marks of the constructive-port scheme are composed of a single frequency component.

4.3.2 Experimental Setup

The constructive-port scheme is also experimentally demonstrated using the same setup as in Figure 4.2. In this case, however, we remove the OBPF and utilize the constructive port of the DI. The optimum driving voltage to the DML is found to be 2.3 V_{pp} in this case, at which the peak-to-peak frequency deviation of the FSK signals at the DML output is ~9 GHz. Figure 4.8 (a) shows the optical spectrum of the signal at the DML output together with the DI wavelength response.

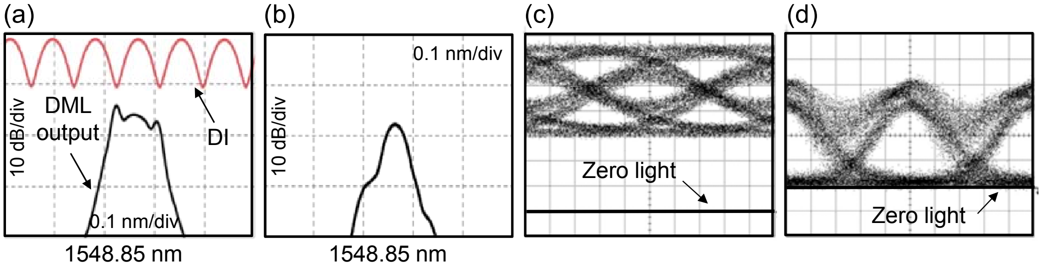

Figure 4.8: Measured optical spectra using the constructive-port scheme at (a) DML output (DI wavelength response is plotted in red), and (b) DI output. Optical eye diagrams at (c) DML output and (d) DI output.

As explained in Section 4.3.1, the null frequencies of the DI are positioned to extinguish the edge frequency components of f_0 and f_2. The optical spectrum and eye diagram of the CPFSK/ASK signals at the DI output are shown in Figure 4.8 (b) and (d), respectively. The ER of the signals is measured to be ~11 dB. The signals are then launched into the SSMF with an optical power of 1.7 dBm and detected with a PIN receiver. It is worth noting that the absence of the OBPF helps to emit higher output power than the destructive-port scheme.

Throughout the demonstration using the constructive-port scheme, the line rate is fixed to 9.95 Gb/s regardless of whether the line coding is used or not. This is because the FSR of the DI is not optimized for this scheme. In the destructive-port scheme, the DI suppresses the f_1 component only. Thus, even though $|f_2\text{-}f_0|$ deviates from the FSR of the DI, it induces power loss only. In the constructive-port scheme, on the other hand, the DI needs to suppress two frequency components, f_0 and f_2. The mismatch between $|f_2\text{-}f_0|$ and the FSR thereby leads to a poor ER and degraded performance.

4.3.3 Experimental Results

The back-to-back BER performance is depicted in Figure 4.9. Also plotted are the BER curves using uncoded PRBSs of length 2^7-1, 2^9-1, and 2^{11}-1, for comparison.

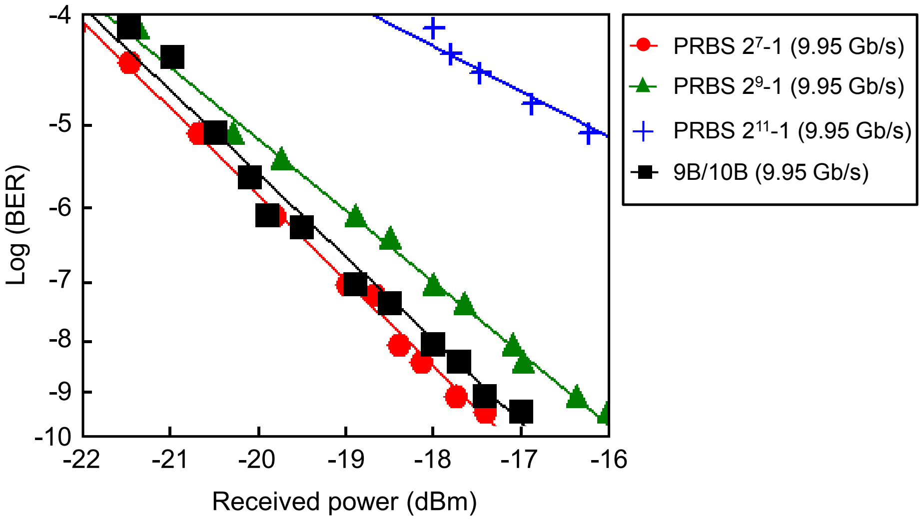

Figure 4.9: Measured back-to-back BER of the constructive-port scheme. The BER curves using uncoded PRBSs of length 2^7-1, 2^9-1, and 2^{11}-1 are plotted for comparison. The signals operate at 9.95 Gb/s.

The receiver sensitivities are measured to be -17.7 and -16.4 dBm using uncoded 2^7-1 and 2^9-1 PRBSs, respectively, whereas an error floor is observed at a BER of

~10^{-7} with the uncoded 2^{11}-1 PRBS. Using 9B/10B line coding, however, we achieve a good receiver sensitivity of -17.4 dBm at a PRBS length of 2^{20}-1.

The dispersion tolerance of the constructive-port scheme is shown in Figure 4.10. The dispersion window is measured to be -200~800 ps/nm, exhibiting asymmetry around the zero dispersion in favor of positive dispersion. We ascribe this to the asymmetric optical spectrum of the signals. Due to the narrower spectral width, the constructive-port scheme has wider dispersion window than the destructive-port scheme.

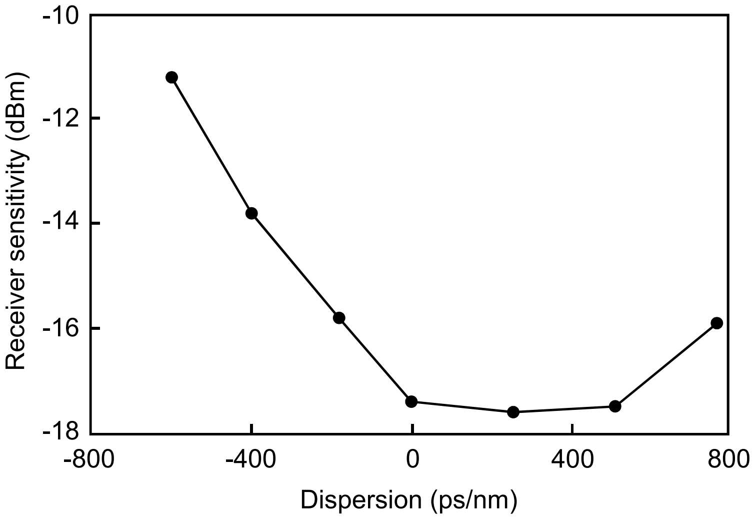

Figure 4.10: Measured dispersion tolerance using the constructive-port scheme.

Finally, we measure the sensitivity penalty caused by the frequency offset between the DML and the DI and depict in Figure 4.11. In this measurement, we stabilize the DI and vary the bias current of the DML to fine tune the operating wavelength. Figure 4.11 shows that the frequency offset should be kept within around ±150 MHz to keep the sensitivity penalty below 2 dB.

It is worth noting that in a wavelength-division multiplexed system, the cost incurred by the DI and OBPF can be shared by multiple users via replacing the OBPF for each channel with a single wavelength-offset WGR as shown in Figure 4.12. The periodicity of the DI also enables us to utilize a single DI at the output of the WGR. The increased cost per customer (caused by the OBPF and DI) thereby becomes insignificant as the number of users increases.

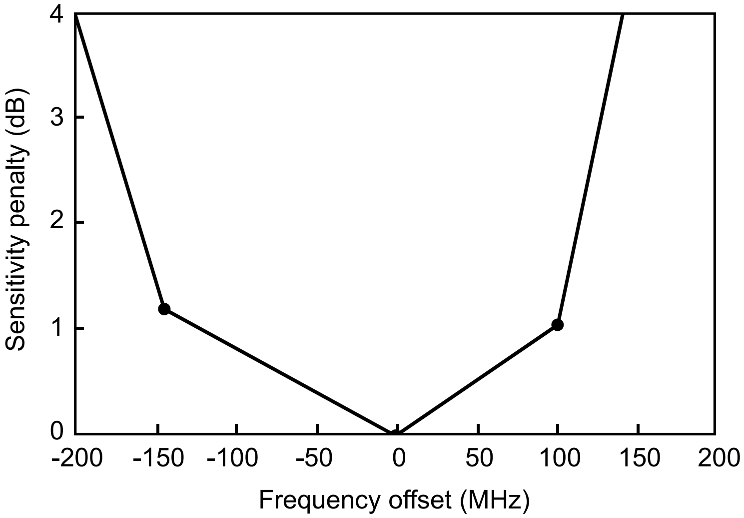

Figure 4.11: Measured sensitivity penalty incurred by the frequency offset between the DML and the DI using the constructive-port scheme.

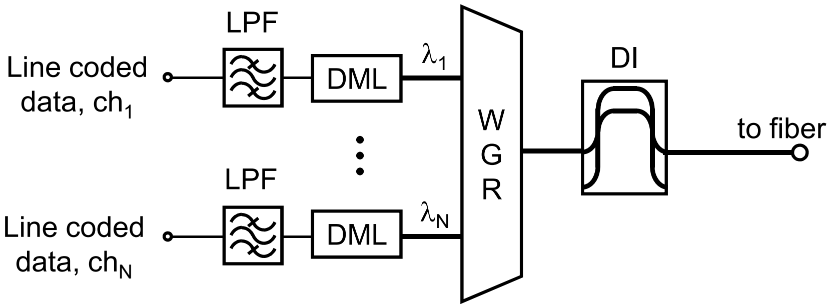

Figure 4.12: Schematic diagram of WDM downstream transmission system using the proposed transmitter.

4.4 Summary

In this chapter, we have proposed and demonstrated the generation of 10-Gb/s NRZ signals using a DML driven by highly band-limited electrical signals (3.5-GHz-bandwidth duobinary signals) followed by a DI. The ternary FSK signals at the DML output are converted into binary CPFSK/ASK signals through the DI. We utilize 9B/10B line coding to overcome the non-uniform FM response of the DML. Using the proposed transmitter, we have experimentally demonstrated two schemes: one using the constructive port of the DI and the other using the destructive port. Both schemes exhibit good receiver sensitivity and dispersion tolerance large enough to be used for optical access networks. The destructive-port scheme, however, outperforms the constructive-port one. Using the former scheme, the 2-dB dispersion window is measured to be ±300 ps/nm indicating that the generated 10-Gb/s signals can travel up to ~20 km over SSMF at 1550 nm without any dispersion compensation.

Chapter 5

DC-Balanced Line Coding for the Dual Modulation of Directly Modulated Lasers and Electro-absorption Modulators

5.1 Introduction

Long-reach access networks (>20 km) have recently received a great deal of attention as a promising solution that can substantially reduce the operation expenditure (OPEX) of broadband service providers [1], [2]. Increasing the transmission distance in these networks to >100 km is desirable to merge into metro networks. In this case, long-reach PONs can reduce the number of central offices (COs) and place numerous optical line terminal (OLT) equipment at a centralized location. Thus, these networks not only save the lease and operation fees for the COs but also they greatly simplify the operation and maintenance of the networks. As the data rate and transmission distance increase, however, high-performance, high-power optical transmitters are required for these cost-sensitive applications. Although DMLs offer a low-cost solution for access networks, the achieved reach does not support long reach access networks. The EML, composed of a laser diode and an EAM integrated on a single chip, offer several advantages for long reach access networks including small footprint and cost-effectiveness. However, compared to $LiNbO_3$ MZM-based counterparts, EMLs still exhibit large frequency chirp with a chirp parameter typically ranging from -3 to 3, decreasing as the bias voltage increases [88]. This, in turn, limits the transmission distance over SSMF at 1550-nm window to ~80 km at 10 Gb/s [77].

Different approaches have been reported to increase the dispersion-limited transmission distance of EMLs. One common approach is to operate the device at highly negative voltage such that the output signal exhibits a negative chirp [89]. However, the average output power of the EML is significantly reduced in this case, and thus an optical amplifier may be needed at the EML output to satisfy the power budget, which increases the cost and complexity of the system [77, 90]. The use of low ER can further increase the reach [78]. This, however, results in a relatively poor performance for short-distance transmission [77].

In [77], a new approach was proposed to extend the reach of conventional EMLs without the need to sacrifice the optical power or ER. This approach proposes the dual modulation of the laser diode and EAM. The dual modulation-based transmitter generates CPFSK/ASK signals by directly frequency-modulating the laser diode on top of the data modulation of the EAM to establish a special phase correlation between the adjacent bits. The FM produced by the DML induces π phase shifts at every space. These phase shifts are known to provide optical duobinary with increased dispersion tolerance compared to conventional ON-OFF keying (OOK) format. The π phase shift is achieved at every space when the FM of the DML is equal to half the data rate. Using this approach, a dispersion-uncompensated transmission at 10 Gb/s was reported over 175- and 125-km SSMF when the DML was modulated with inverted and non-inverted data, respectively. In this approach, however, a large pattern dependency was observed at long transmission distance due to the non-uniform FM response of the DML at low frequency range [63, 91]. When the FM efficiencies of the DML are not constant over the entire frequency range of a long PRBS, both the amount of phase slip at the space and the frequency chirp at the leading and trailing edges of the signal would vary with the data pattern [77].

To cope with this problem, a new DML integrated with EAM was designed using a semi-insulated semiconductor buried heterostructure (SI-BH) and a shorter cavity length in order to enhance the non-uniform FM response of the DML and produce a flat FM response [92]. Similarly, in [93] a new device using sub-mount QW AlGaInAs structure was utilized to exhibit a flat FM response, and the modulation indices of the DML and EAM were balanced for optimum performance. However, such approaches require modifying the laser structure in order to produce a highly flat FM response.

In this chapter, a system approach is introduced rather than changing the device structure and characteristics. The use of DC-balanced line coding is proposed to enhance the performance of the dually modulated DML-EAM transmitter. The line coding depletes the low-frequency spectral contents of the signal falling in the non-uniform region of the DML FM response such that only the uniform region at higher frequency range is utilized [63, 91]. After introducing the principle of operation of the dual-modulation-based DML-EAM transmitter in Section 5.2, the experimental setup to evaluate the performance of the proposed system is described in Section 5.3. The experimental results are then illustrated and discussed in Section 5.4. Finally, Chapter 5 is summarized in Section 5.5.

5.2 Principle of Operation of DML-EAM Transmitter

In the DML-EAM dual modulation scheme, CPFSK/ASK signals are generated by the FSK modulation of the DML on top of the data modulation of the EAM to establish a special phase correlation between the bits as mentioned earlier. Figure 5.1 illustrates the time-resolved intensity and phase waveforms when the DML and EAM are modulated with inverted data and non-inverted data (i.e., push-pull configuration), respectively.

When the DML operates at far beyond the threshold current, its FM characteristics are mainly determined by the adiabatic chirp. The frequency deviation of the DML is then proportional to the modulation current, which is expressed as [77]

$$f_1 - f_0 = \eta \cdot \Delta I \tag{5.1}$$

where f_1 and f_0 are the frequencies at the mark and space, respectively, η is the FM efficiency of the DML, and ΔI is the modulation current. Figure 5.1 (a) and (b) show the output intensity waveforms of the DML and EAM, respectively. The high ER of the EAM eliminates the mark portion of the DML signal, leaving the space portion at the output of the EAM. In the frequency domain, this can be understood in a way that the EAM carves out the f_1 components of the signal, just like a narrow optical filter centered at f_0 and filtering out the f_1 components. Figure 5.1 (c) shows the relative optical phase of the EAM output carried over f_0.

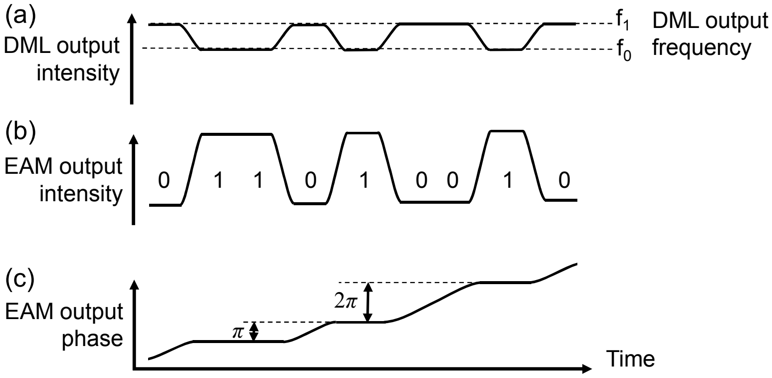

Figure 5.1: Principle of operation of the DML-EAM dual modulation system: (a) intensity and frequency waveforms at the DML output, (b) intensity waveform at the EAM output, and (c) phase waveform at the EAM output [77].

The chirp of the EAM is assumed to be negligible in Figure 5.1 since the DML typically has larger chirp than the EAM. The relative optical phase varies as the DML frequency deviates from f_0. In order to achieve π phase shift at every space, the phase difference over a single space should be equal to π. With a raised cosine-shaped waveform, it can be achieved when the frequency deviation is half the data rate. For 10-Gb/s signals, this corresponds to 5 GHz. When the aforementioned condition is met, the optical phase at the center of the mark slips by π every time it encounters a space. This phase shift at every space can greatly increase the dispersion tolerance of the optical signals as mentioned earlier [77]. Section 5.3 presents the experimental setup implemented to evaluate the performance of the proposed DML-EAM dual modulation scheme using DC-balanced line coding to mitigate the non-uniform FM response of the DML.

5.3 Experimental Setup

The experimental setup of the proposed DML-EAM dual modulation system is depicted in Figure 5.2. Since an EML with a direct-modulation capability for the laser diode was not available, a commercially available DML followed by an external EAM is utilized as an alternative to EML.

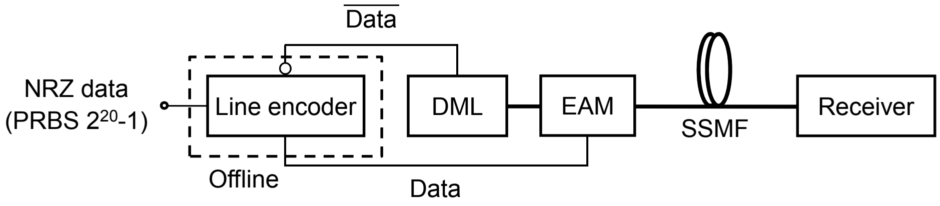

Figure 5.2: Experimental setup of the proposed DML-EAM dual-modulation scheme (push-pull configuration).

NRZ data running at 9.95 Gb/s with a PRBS length of 2^{20}-1 are first encoded offline at a personal computer and then uploaded to the pulse pattern generator. In this experiment, we examine two line coding formats; 8B/10B and 9B/10B. The coded data and inverted data are then fed to the EAM and DML (push-pull scheme), respectively. Due to the coding overhead, the line rate increases accordingly to 12.44 or 11.06 Gb/s after 8B/10B or 9B/10B coding, respectively. The DML (operating at 1548.7 nm) is biased at 60 mA (~6 times the threshold current to make the adiabatic chirp dominant), obtaining an output power of 5.6 dBm.

Unlike MZMs, EMLs have a variety of chirp and transmission characteristics, varying not only from vendor to vendor but also from device to device [88]. For this reason, we measure the transmission characteristics of the utilized EML in Figure 5.3 in order to estimate the optimum driving conditions.

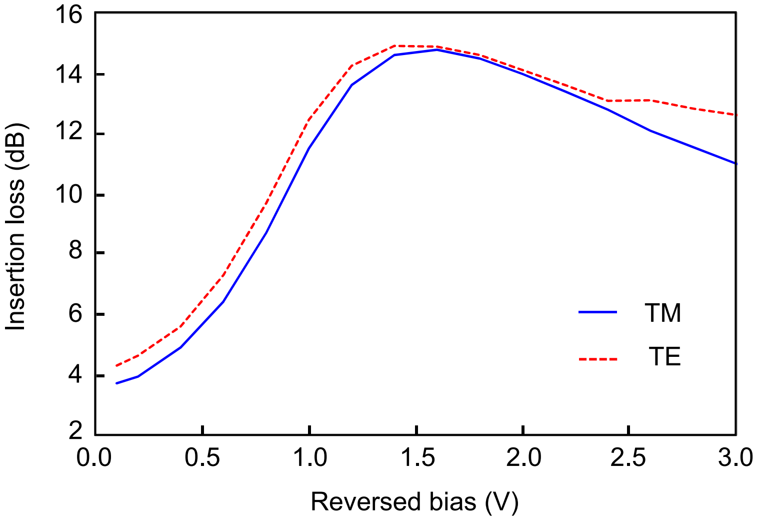

Figure 5.3: Bias characteristics of the utilized EAM. TM: transverse magnetic mode, and TE: transverse electric mode.

Throughout the experiment, the bias voltage to the EAM is set to -0.7 V. At this bias condition, the optimum driving voltage is found to be 1 V_{pp}. Since the FM efficiency of the DML is 0.184 GHz/mA, the frequency deviation between the marks and spaces of the FSK signals at the DML output is ~4 GHz, which is approximately half the data rate.

Next, we measure the chirp characteristics of the utilized EML using the measurement method reported in [94], the experimental setup of which is depicted in Figure 5.4. We use an EAM driven by a sinusoidal signal from a signal generator with 0-dBm power level and a frequency ranging from 5 to 15 GHz. The DC bias of the EAM is varied from 0.3 to 1.2 V. A 110- and 130-km SSMF is deployed as a dispersive medium, after which the signals are photo-detected and then the frequency response of the EAM at each bias voltage is measured using a spectrum analyzer. The chip parameter α_{chirp} is then calculated using [94]

$$f_u^2 L = \frac{c}{2D\lambda^2}\left(1 + 2u - \frac{2}{\pi}\arctan(\alpha_{\text{chirp}})\right) \qquad [5.2]$$

where f_u is the resonance frequency corresponds to the u^{th} null of the frequency response, L is the optical fiber length of dispersion D, and λ is the operating wavelength (i.e., 1548.7 nm).

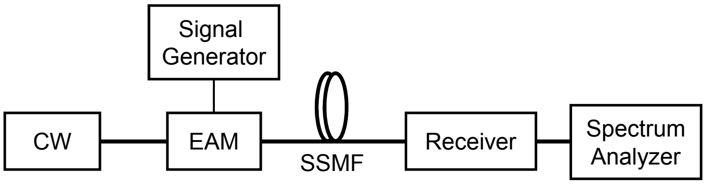

Figure 5.4: Experimental setup used to measure the chirp parameter of the EAM.

Figure 5.5 shows the measured chirp parameter as a function of the reversed bias of the EAM. The figure shows that the chirp parameter depends strongly on the bias voltage. For example, at -0.7 V the chirp parameter is equal to -0.29. We also measure the chirp parameter of the DML at the driving conditions used during the experiment and it is found to be 4.7.

The dynamic ER of the CPFSK/ASK signals at the output of the dually modulated transmitter is >7 dB. The generated signals with -3-dBm optical power are launched into an SSMF and detected using an optically preamplified receiver (optical 3-dB bandwidth: 0.17 nm).

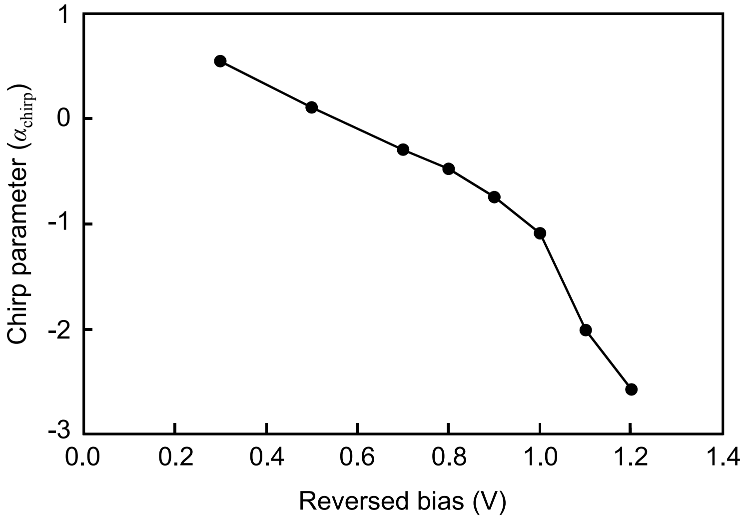

Figure 5.5: Measured chirp parameter (α_{chirp}) versus the reversed bias of the EAM.

5.4 Experimental Results

5.4.1 Push-Pull Configuration

We first evaluate the performance of the proposed system using the push-pull configuration (i.e., the DML and EAM are modulated with inverted and non-inverted encoded data, respectively) as depicted in Figure 5.2. Figure 5.6 shows the measured receiver sensitivities versus the transmission distance over SSMF obtained using this configuration. For comparison, the dispersion tolerance of the uncoded PRBS data with lengths of 2^7-1 and 2^{20}-1 are measured along with that of the signal modulated with the EAM alone (i.e., DML modulation is OFF).

The results show that with EAM modulation alone, we can barely achieve 80-km transmission over SSMF without dispersion compensation, and a large power penalty of 6.2 dB is observed with reference to the back-to-back case. We are unable to obtain a BER less than 10^{-9} when the distance exceeds 100 km. To be noted that this is achieved with the help of the negative chirp of the EAM.

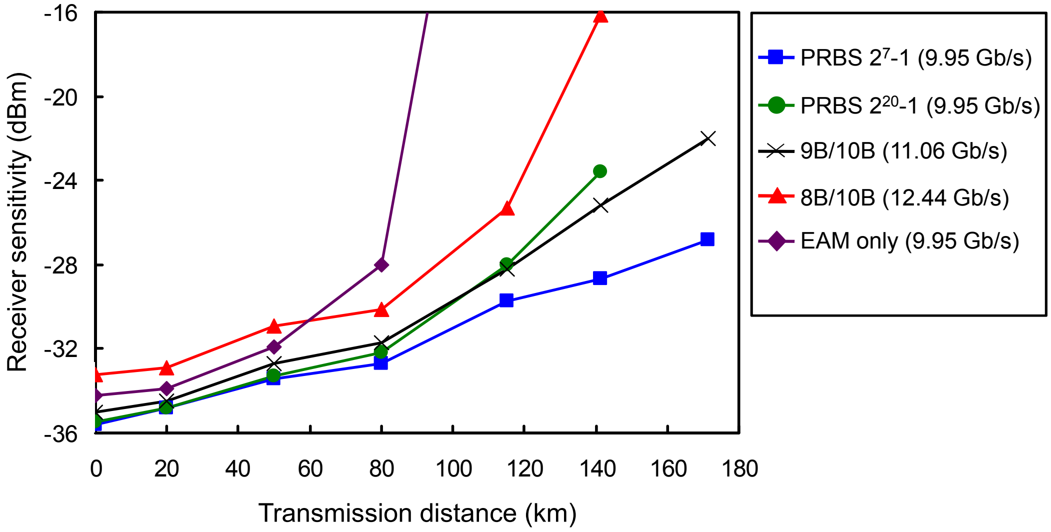

Figure 5.6: Measured dispersion tolerance using the push-pull configuration. For comparison, the dispersion tolerance of the uncoded PRBS data with lengths of 2^7-1 and 2^{20}-1 are measured along with that of the signal modulated with the EAM alone (i.e., DML modulation is OFF). If not stated otherwise, the PRBS length used in these measurements is 2^{20}-1.

As demonstrated in [77, 92, 93], the reach is significantly extended using the dual modulation scheme, and the receiver sensitivity using 2^7-1 PRBS is measured to be -26.8 dBm after 171 km (8.8-dB penalty with respect to the back-to-back case).

However, we are unable to achieve this reach using a long PRBS. For example, a sensitivity penalty of ~12 dB is observed after 141-km transmission using 2^{20}-1 PRBS. This pattern dependency implies a system penalty in real systems, and in this case, it should be attributed to the non-uniform FM response of the DML. Therefore, we employ DC-balanced line coding to cope with this problem.

Figure 5.6 shows that the use of 9B/10B coding can extend the reach to 171 km. Compared to uncoded 2^7-1 PRBS, additional 4.8-dB penalty is observed with the 9B/10B coding after 171 km. To be noted that 2^7-1 PRBS cannot represent real data and is only used as a reference. To investigate this 4.8-dB penalty, the receiver sensitivity is measured as a function of the transmission distance without taking the overhead into consideration as shown in Figure 5.7. The line rate is maintained to 9.95 Gb/s throughout these measurements. For comparison, the measured receiver sensitivities using uncoded 2^7-1 PRBS are reproduced from Figure 5.6.

Figure 5.7 shows that as long as the line rate is the same, both 8B/10B and 9B/10B-coded signals exhibit nearly the same dispersion tolerance as the uncoded 2^7-1 PRBS. This leads to the conclusion that both 8B/10B and 9B/10B codes are effective in eliminating the pattern dependency in the dual-modulation scheme and the additional penalty with respect to the uncoded 2^7-1 PRBS observed in Figure 5.6 comes from the line-rate increase. Since the dispersion tolerance is sensitive to the line rate, the use of low-overhead line coding schemes, such as 9B/10B (coding overhead = 11.11%), is beneficial to improve the performance of dual modulation-based EML systems. This is also evident from the performance of the 8B/10B-coded signal in Figure 5.6 which is by far worse than that of the 9B/10B-signal with a receiver sensitivity of -16.1 dBm after 141 km. Although 8B/10B line coding can efficiently deplete the low-frequency contents of the signal, the bandwidth expansion corresponding to the relatively large overhead (i.e., 25%) results in a large power penalty after transmission.

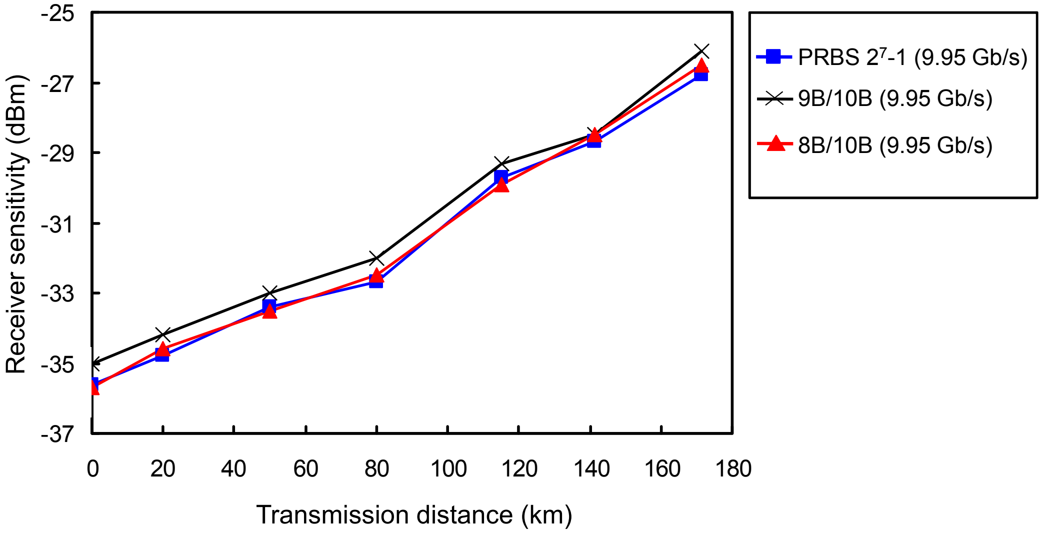

Figure 5.7: Measured dispersion tolerance using the push-pull configuration without taking the coding overhead into account. The signals operate at 9.95 Gb/s and the PRBS length used is 2^{20}-1. For comparison, the measured receiver sensitivities using 2^7-1 PRBS are reproduced from Figure 5.6.

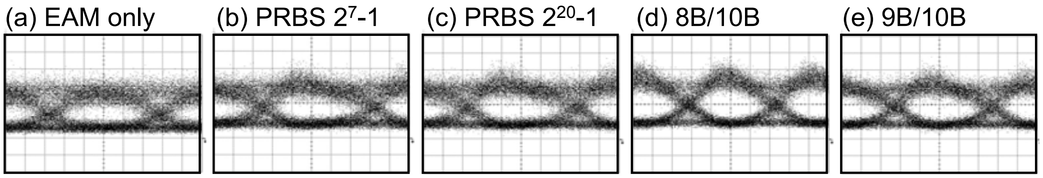

Figure 5.8: Optical eye diagrams at the back-to-back case achieved with (a) EAM-modulation alone (DML modulation is OFF), and dual modulation scheme (push-pull configuration) using (b) uncoded 2^7-1 PRBS, (c) uncoded 2^{20}-1 PRBS, (d) 8B/10B-, and (e) 9B/10B-coded signals. If not stated otherwise, the pattern length used is 2^{20}-1.

The measured optical eye diagrams at the back-to-back condition with and without line coding are shown in Figure 5.8. Figure 5.9 shows the eye diagrams at the maximum reach achieved in each case. The ER is measured to be 6.5~7.5 dB for all the cases.

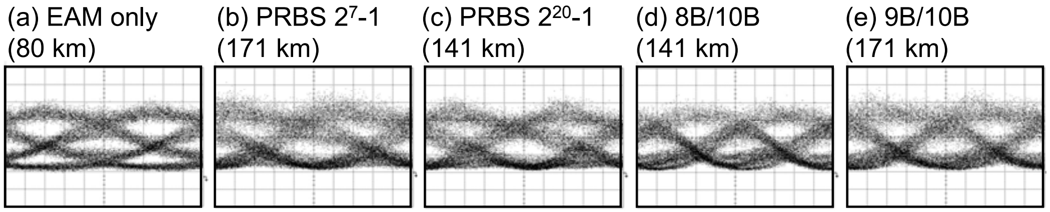

Figure 5.9: Optical eye diagrams at the maximum reach achieved with (a) EAM-modulation alone (DML modulation is OFF), and dual modulation scheme (push-pull configuration) using (b) uncoded 2^7-1 PRBS, (c) uncoded 2^{20}-1 PRBS, (d) 8B/10B-, and (e) 9B/10B-coded signals. If not stated otherwise, the pattern length used is 2^{20}-1.

5.4.2 Push-Push Configuration

Next we evaluate the performance of the proposed system using the push-push scheme where the DML is modulated with non-inverted data. The major advantage of this configuration is that the DML and EAM are both modulated with the same non-inverted data. Since the DML requires a small current for modulation, only a tiny portion of the EAM input signal can be tapped off and applied to the DML, which will simplify the packaging of the dual-modulation-based transmitter [77].

Figure 5.10 shows the dispersion tolerance measured using the push-push configuration. The back-to-back receiver sensitivity of the 9B/10B-coded signal is measured to be -30.5 dBm (4.5-dB penalty compared to the push-pull configuration). The receiver sensitivity is degraded by ~7 dB at 50 km owing to the pulse broadening by the positive chirp. After 141 km, the receiver sensitivity is measured to be -16 dBm with a power penalty of 14.5 dB with respect to the back-to-back case. However, using 2^{20}-1 PRBS (without any line coding), the maximum reach we can achieve is 115 km with a large power penalty of 16.7 dB.

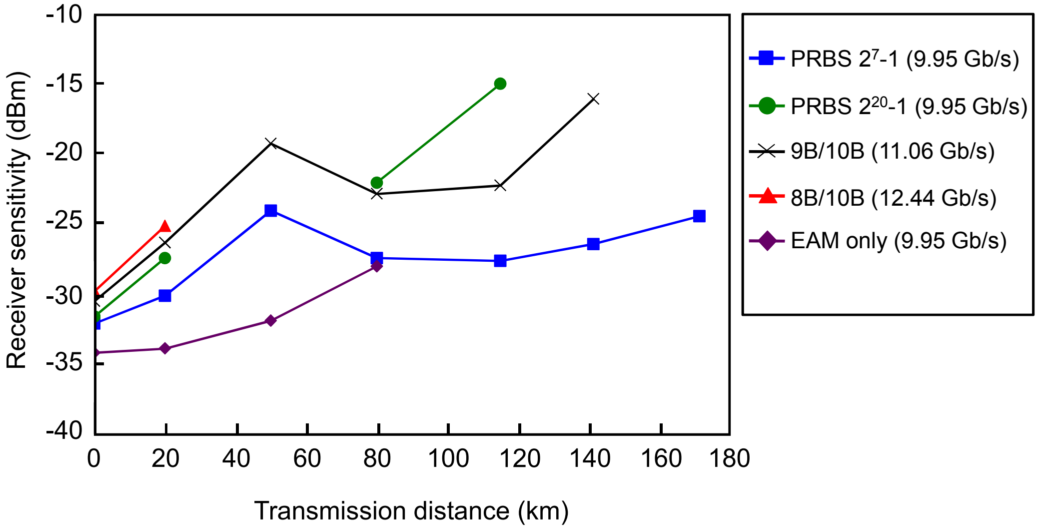

Figure 5.10: Measured dispersion tolerance using the push-push configuration. For comparison, the dispersion tolerance of the uncoded PRBS data with lengths of 2^7-1 and 2^{20}-1 are measured along with that of the signal modulated with the EAM alone (i.e., DML modulation is OFF). If not stated otherwise, the PRBS length used in these measurements is 2^{20}-1.

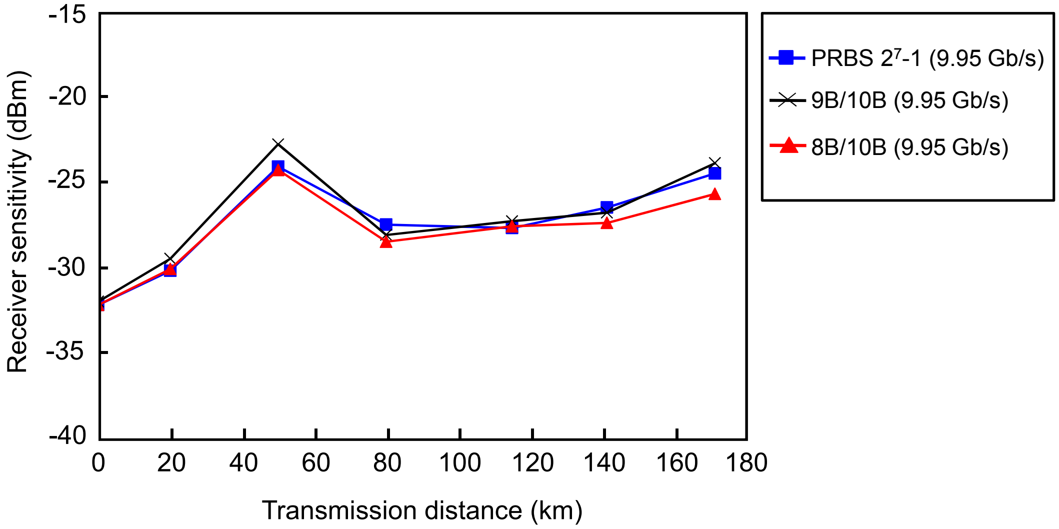

Figure 5.11: Measured dispersion tolerance using the push-push configuration without taking the coding overhead into account. The signals operate at 9.95 Gb/s and the PRBS length used is 2^{20}-1. For comparison, the measured receiver sensitivities using 2^7-1 PRBS are reproduced from Figure 5.10.

We also measure the BER performance of the 9B/10B- and 8B/10B-coded signals at 9.95 Gb/s using the push-push configuration as demonstrated in Figure 5.11. The receiver sensitivities after 171 km are -23.8 and -25.6 dBm for the 9B/10B- and 8B/10B-coded signals, respectively, which correspond to 0.6-dB penalty using 9B/10B coding and 1.2-dB improvement using 8B/10B format with respect to 2^7-1 PRBS.

The measured eye diagrams for the push-push configuration are shown in Figure 5.12 and Figure 5.13. The ER is measured to be 5.5~6.5 dB for all the cases.

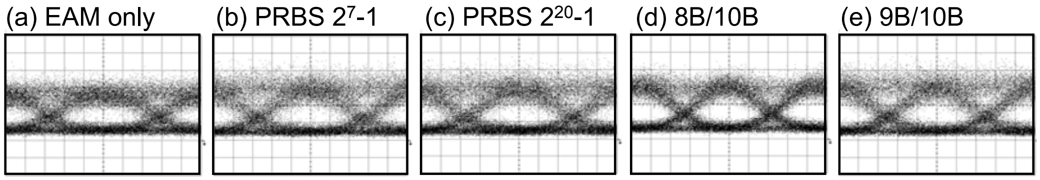
(a) EAM only
(b) PRBS 2^7-1
(c) PRBS 2^{20}-1
(d) 8B/10B
(e) 9B/10B

Figure 5.12: Optical eye diagrams at the back-to-back case achieved with (a) EAM-modulation alone (DML modulation is OFF), and dual modulation (push-push configuration) using (b) uncoded 2^7-1 PRBS, (c) uncoded 2^{20}-1 PRBS, (d) 8B/10B-, and (e) 9B/10B-coded signals. If not stated otherwise, the pattern length used is 2^{20}-1.

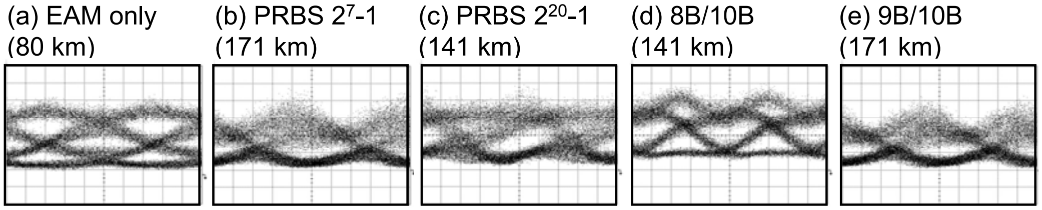
(a) EAM only (80 km)
(b) PRBS 2^7-1 (171 km)
(c) PRBS 2^{20}-1 (141 km)
(d) 8B/10B (141 km)
(e) 9B/10B (171 km)

Figure 5.13: Optical eye diagrams at the maximum reach achieved with (a) EAM-modulation alone (DML modulation is OFF), and dual modulation (push-push configuration) using (b) uncoded 2^7-1 PRBS, (c) uncoded 2^{20}-1 PRBS, (d) 8B/10B-, and (e) 9B/10B-coded signals. If not stated otherwise, the pattern length used is 2^{20}-1.

5.5 Summary

The use of DC-balanced line coding has been proposed and demonstrated to avoid the non-uniform FM response of the DML in the dual modulation-based DML-EAM transmitter. The proposed scheme is experimentally demonstrated using two configurations: (1) push-pull configuration where the DML and EAM are modulated with inverted and non-inverted encoded data, respectively, and (2) push-push configuration where the DML and EAM are both modulated with non-inverted encoded data.

We have evaluated the performance of the proposed system by measuring the receiver sensitivity over SSMF. The measurements show that DC-balanced line coding is effective in eliminating the pattern dependency in the dual modulation-based transmitter caused by the non-uniform FM-response of the DML. However, the low overhead is essential to gain benefit from the line coding. The results also show that the push-pull configuration outperforms the push-push scheme. Using 9B/10B line coding, we achieve 171- and 141-km transmission over SSMF using push-pull and push-push configurations, respectively, without any dispersion compensation.

Chapter 6

DC-Balanced Line Coding for Downlink Modulation using DMLs in Wavelength-Shared, Bidirectional WDM PONs

6.1 Introduction

High bandwidth applications such as storage networking, video streaming/sharing, and online gaming continue to drive greater bandwidth demands for next-generation broadband access networks. To address the growing capacity, security, and distance requirements while leveraging the benefits of a passive infrastructure, WDM PONs are considered to be the most scalable and future-proof solution. A key advantage of WDM PONs is the assignment of dedicated wavelength channels to each optical network unit (ONU) while having double-star architecture. This not only guarantees large capacity and high security for each ONU, but also facilitates graceful upgradability and network flexibility [95-97]. Figure 6.1 shows a schematic diagram of a WDM-PON system.

The DML-based transmitters demonstrated in Chapter 3 through 5 of this thesis, offer cost-effective solutions for *downstream* transmission in WDM PONs. These transmitters, however, are not *colorless* and thus their implementation at the ONUs for *upstream* transmission is not only cost-prohibitive but also poses inventory management issues. To lower the cost and make WDM PONs a viable solution for broadband access networks, it is highly desirable to utilize colorless optical transmitters for upstream transmission. Identical optical transmitters, which operate at any wavelength, can be used for any ONU to substantially lower the operation cost and consequently alleviate the inventory problem. For this purpose, a couple of optical transmitters based on reflection-type opto-electronic devices, such as RSOA and incoherent light-injected Fabry-Perot laser diode, have been reported [96, 98-100].

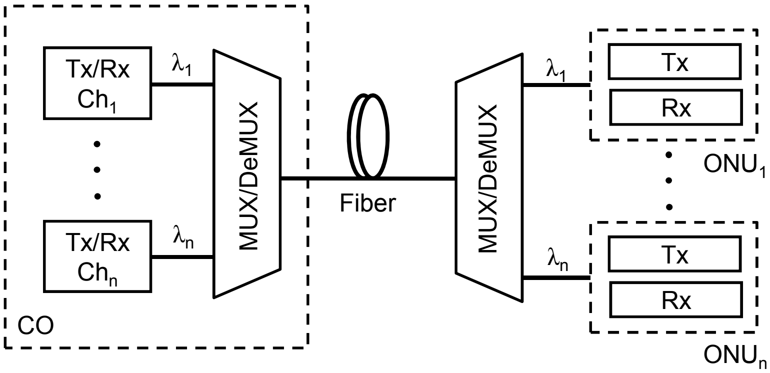

Figure 6.1: Schematic diagram of a WDM-PON system. MUX: multiplexer, and DeMUX: demultiplexer.

In these approaches, the reflection-type devices operate in a colorless manner by imposing upstream data on the incoming seed light from the CO. Therefore, the wavelength-specific light sources can be all located at the CO, providing service providers with centralized management of the failure-prone light sources. In most of these schemes, however, the seed light is CW light and it is expected that an additional light source operating at a different wavelength should be provided for each ONU to support downstream transmission. From the viewpoint of implementing WDM PONs in a very cost-effective way, it is highly desirable to utilize a single light source for both downlink and uplink [101-105]. In such wavelength reuse schemes, a portion of the downstream signal is detected at the ONU and the other portion can be reused for upstream transmission. As aforementioned, DML-based transmitters offer a cost-effective solution for this purpose.

Nevertheless, the performance of these wavelength-shared schemes is limited by the interference between the downstream and upstream data at the CO. Several approaches have been proposed to mitigate the unwanted interference. One previous approach is to operate the RSOA in the saturation regime [101, 106]. Provided that the ER of the downstream signals is low (e.g., 3 dB) and the injection power into the RSOA is high, the saturated RSOA keeps its output power fairly constant regardless of the injected downstream data pattern and erases the downstream data at the ONU. However, this benefit comes at the expense of poor downstream performance attributed to the low ER. Moreover, the modulation bandwidth of the RSOA is limited by the carrier lifetime to <2 GHz [107, 108], which in turn limits the upstream data rate typically to ~1.25 Gb/s.

Another approach is to use orthogonal (i.e., independent) modulation formats for the downlink and uplink. This can minimize the interference between the downstream and upstream data since one modulation format can be detected without being affected by the other. A good example of such approach is to utilize phase-shift keying (PSK) or FSK modulation formats for the downstream transmission whereas OOK is utilized for the uplink [107, 109]. The constant-envelope downstream light injected into the RSOA does not interfere with the OOK-modulated RSOA output, enabling independent operation of both downstream and upstream transmission. However, the constant envelope of the downstream signals is guaranteed only in the absence of fiber dispersion. Thus, the advantages of orthogonality between the downstream and upstream modulation formats subside as the transmission distance over dispersive fiber increases. More importantly, this approach requires an optical PSK or FSK demodulator at each ONU, making the subscribers' premises costly and complicated. It obviously weakens the original purpose of developing a centralized light source for simple and cost-effective ONUs.

A proper choice of line coding can also greatly reduce the interference between the downstream and upstream data, especially in asymmetric bidirectional WDM PONs [110]. For instance, Manchester coding, a DC-free line coding with at least one transition per symbol duration, can deplete the signal contents at low frequencies allowing the low-data-rate upstream signals to reside at these frequencies without interfering with the downstream signals [111]. However, Manchester coding doubles the signal bandwidth, as mentioned in Chapter 2, which in turn, limits the downstream data rate and makes the signals more vulnerable to fiber dispersion. This is also the case for inverse return-to-zero (IRZ) line coding [112].

In this chapter, we demonstrate a cost-effective single-fiber 10-Gb/s downlink, 2.5-Gb/s uplink WDM-PON system using DMLs and RSOAs for downlink and uplink, respectively. For high cost-effectiveness, we utilize a single centralized light source based on DML at the CO for bidirectional transmission. We examine the use of various DC-balanced line codes, including 9B/10B, 7B/8B, 5B/6B, and 8B/10B, to ameliorate the performance of both the downlink and uplink. Particularly, we employ DC-balanced line coding for the downstream modulation for two purposes: (1) to improve the performance of the FSK-modulated DML signals, and (2) to reduce the interference between the downstream and upstream signals.

This chapter is organized as follows. The principle of operation is first introduced in Section 6.2, followed by the experimental setup and results in Section 6.3 and 6.4, respectively. Finally the chapter is summarized in Section 6.5.

6.2 Principle of Operation

The proposed WDM-PON system is depicted in Figure 6.2. DMLs are utilized for downlink transmission and they also provide seed light to the RSOAs at the ONUs.

The downlink data at the CO are first encoded and then fed to the DML for FSK modulation. The FSK-downstream signals are multiplexed through a WGR and fed to the DI to be converted into OOK format. The signals are then launched into the feeder fiber to be demultiplexed by another WGR at the remote node. The optical power received at the ONU is split into the downlink receiver and the RSOA. For uplink, the light injected into the RSOA is remodulated by the upstream data. The OOK upstream signals from the ONUs are multiplexed at the remote node and then sent back over the same feeder fiber to the CO for detection.

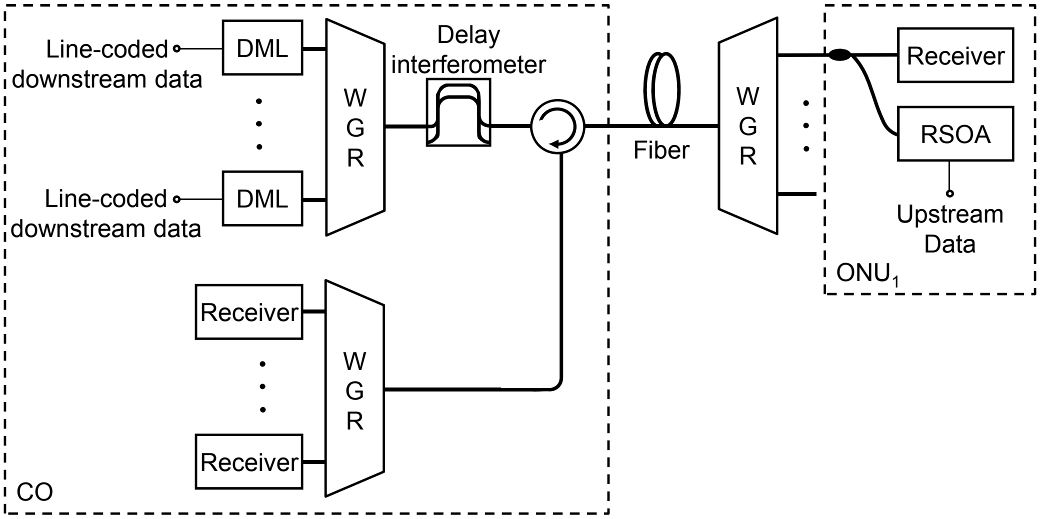

Figure 6.2: The proposed wavelength-shared bidirectional WDM-PON system.

In this system, we exploit DC-balanced line coding for two purposes. First, the line coding can alleviate the performance degradation of the FSK-modulated downstream signal induced by the non-uniform FM response of the DML as discussed in Chapter 3 [63]. Second, the DC-balanced line coding can reduce the power fluctuation of the injected seed light averaged over the upstream symbol duration. This is because the DC-balanced line coding suppresses the disparity (i.e., the difference between the number of ones and zeros) in the downstream data, and thus when the encoded downstream data are averaged over the upstream symbol duration (assuming that the upstream symbol duration is larger than the downstream symbol duration) they tend to converge at $(P_1+P_0)/2$, where P_1 and P_0 are the powers of '1' and '0' bits, respectively. The power fluctuation of the injected seed light averaged over the upstream symbol duration is thereby reduced, which in turn, suppresses the interference between the downlink and uplink data [105]. We use computer simulation (VPI TransmissionMaker) to plot the waveforms of the downstream signal with and without DC-balanced line coding (8B/10B code is used as an example) as shown in Figure 6.3. The figure clearly shows that the line coding suppresses the long runs of zeros observed in the uncoded waveform [Figure 6.3 (a)], which would be problematic for remodulation.

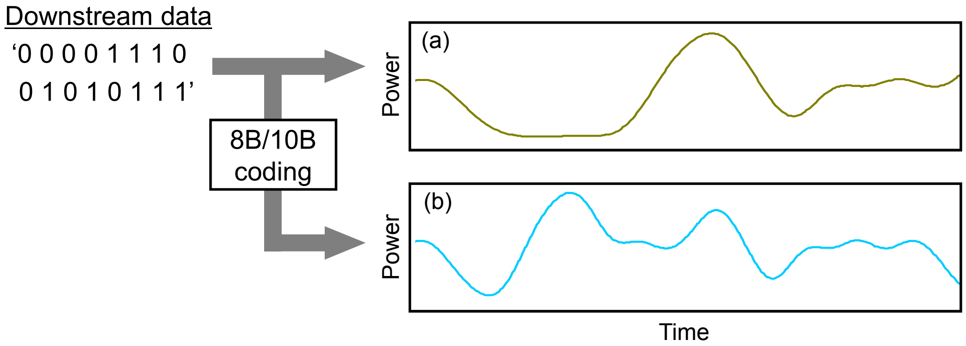

Figure 6.3: Waveform of the downstream data averaged over the upstream symbol duration (a) uncoded downstream data, and (b) 8B/10B-coded downstream data. The input downstream data pattern is '0000 1110 0101 0111.' The data-rate ratio between downlink and uplink is 4.

To show the efficacy of power fluctuation reduction by the line coding, we calculate the disparities of the downstream data over 4-symbol durations and plot them in Figure 6.4. This is because in our system, the data-rate ratio between uplink and downlink is ~4, which implies that for each upstream symbol, 4 bits of the downstream data are involved in average. Therefore, the interference between the upstream and downstream data is determined by the power fluctuation of the downstream data averaged over 4-symbol durations (i.e., one upstream symbol duration). As shown in Figure 6.4, the disparity can be -4, -2, 0, 2, or 4. For example, when four consecutive bits are all '0's, the disparity is -4. But, if we have one '0' and three '1's among four adjacent bits, the disparity becomes 2.

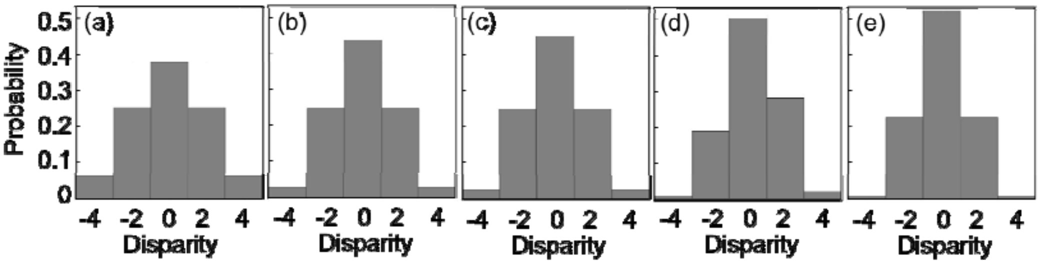

Figure 6.4: Probability distribution of disparity per upstream symbol duration when the downstream data are (a) uncoded PRBS, (b) 9B/10B-, (c) 7B/8B-, (d) 5B/6B-, and (e) 8B/10B-coded signals. The PRBS length is 2^{20}-1 for all the cases.

The results clearly show that the line coding suppresses the power fluctuation compared to the uncoded PRBS. For instance, the probability of the worst-case disparity (i.e., disparity=±4) is 6% without the use of line coding as illustrated in Figure 6.4 (a). This probability is, however, reduced to 3% and 2.5% using 9B/10B and 7B/8B codes, respectively. It is further reduced by using codes with better DC characteristics such as 5B/6B and 8B/10B, resulting in probabilities of 0.8%~1.9% and 0.9%, respectively, but at the expense of larger overhead (Table 3-1 in Chapter 3 summarizes the basic characteristics of the used codes).

We also experimentally measure the average power fluctuations of the downstream signals. The 1-mW downstream signals are first photo-detected and then averaged by using a 1.9-GHz electrical LPF which is the bandwidth of the uplink receiver. Figure 6.5 shows the measured standard deviation of the power fluctuations. The standard deviation is measured to be 435 μW for the uncoded downstream signals, but it is reduced to 370~405 μW when line coding is applied.

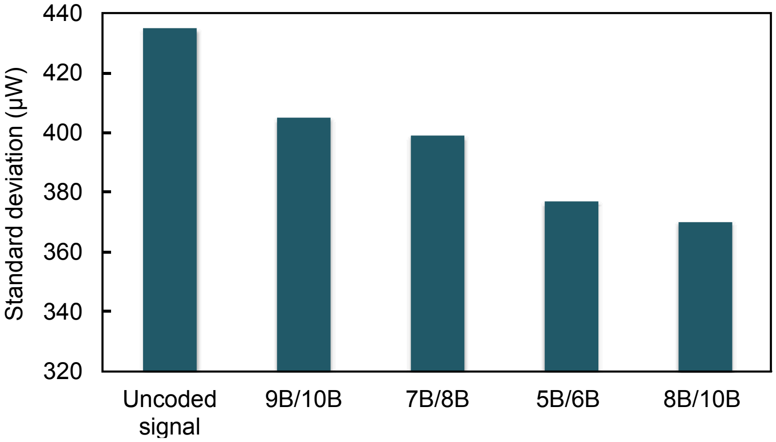

Figure 6.5: Standard deviation of the downstream power fluctuation averaged over the upstream symbol duration.

It should be noted in Figure 6.2 that we place the DI at the CO rather than in the ONUs. Since the DML output is FSK-modulated with relatively small power fluctuation (caused by the current modulation of the DML), the use of FSK modulation for downlink is beneficial to substantially reduce the power fluctuation of the seed light, as explained above. However, this scheme requires the DI to be placed at each ONU, which in turn, makes the ONU costly and complicated. Besides, the periodicity of the DI frequency response allows us to place a single DI at the CO for all the WDM channels. This makes the system simple and cost-effective. In the future, the DI can be possibly integrated with the multiplexer for further cost reduction [113].

6.3 Experimental Setup

The experimental setup of the proposed scheme is shown in Figure 6.6.

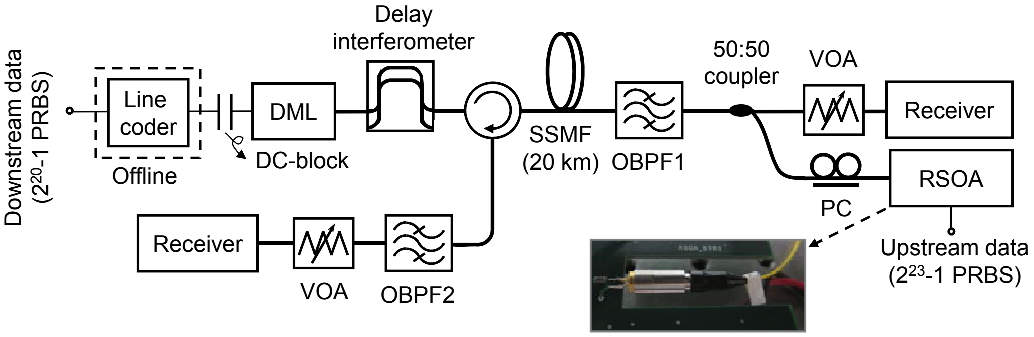

Figure 6.6: Experimental setup. VOA: variable optical attenuator, and PC: polarization controller. The photo shows the RSOA used in the experiment.

For downlink, NRZ downstream data running at 9.95-Gb/s (PRBS length = 2^{20}-1) are first encoded offline using a line encoder and then passed through a DC-block (low cut-off frequency: 45 MHz) to further deplete the low frequency contents before being fed to a DML operating at 1549.5 nm and biased at 60 mA (~6 times the threshold current to make the adiabatic chirp dominant). Due to the coding overhead, the line rate increases to 11.06, 11.37, 11.94, or 12.44 Gb/s after 9B/10B, 7B/8B, 5B/6B, or 8B/10B coding, respectively, as illustrated earlier in Table 3-1 in Chapter 3. The optimum driving voltage to the DML is found to be 2.5 V_{pp}. Since the FM efficiency of the DML is 0.184 GHz/mA, the frequency deviation between the marks and spaces of the FSK-modulated signals at the DML output is 9.2 GHz, which is approximately equal to the data rate. The FSK-modulated signal at the DML output is sent to a DI (FSR = 10.7 GHz) to be converted into CPFSK/ASK signal. The ER of the downstream signal is measured to be 9~10 dB. The downstream signal is then launched into 20-km SSMF through an optical circulator. After transmission, the downstream signal passes through OBPF1 with a 3-dB bandwidth of 0.6 nm. This optical filter emulates a WGR at the remote node. The signal is then split two ways using a 50:50 optical coupler; one to the downlink receiver and the other to the upstream modulation using RSOA. We use a PIN receiver to detect the downstream signals.

For upstream transmission, we employ an uncooled, InP buried heterostructure RSOA packaged in a transistor outline (TO) can. The RSOA is biased at 30 mA and directly modulated with 2.67-Gb/s NRZ signals (PRBS length = 2^{23}-1). Here we assume Reed-Solomon (255, 239) forward-error correction (FEC)-coded data with 7% overhead which means that the actual data rate is 2.5 Gb/s. The injected power into the RSOA is -11 dBm. We measure the gain curve of the utilized RSOA as a function of the input power and plot in Figure 6.7. The input saturation power, defined as the input optical power at which the signal gain is compressed by 3 dB from its small signal gain, is measured to be -21 dBm, thus the RSOA operates in the saturation region in this case.

A polarization controller is inserted at the input of the polarization-sensitive RSOA to adjust the state of polarization in order to maximize the seeding efficiency. Polarization-insensitive RSOAs can be used for real deployment to eliminate the need for polarization controllers. The upstream signal passes through OBPF1 and is then sent back over the same feeder fiber as the downstream transmission. After transmission, the upstream signal passes through OBPF2 (3-dB bandwidth = 0.6 nm) which emulates a WGR at the CO to demultiplex the WDM channels. The upstream signal is then detected using a PIN detector.

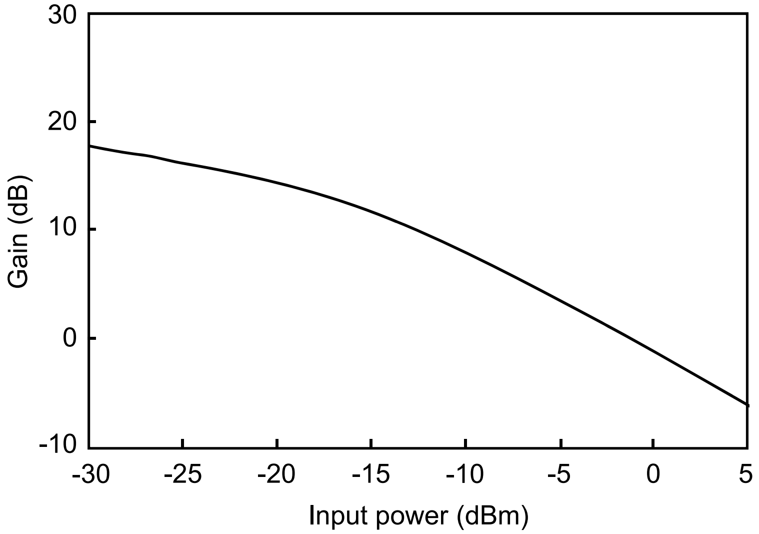

Figure 6.7: Gain versus input power of the RSOA used in the experiment. The bias current is 30 mA.

6.4 Experimental Results

We measure the BER curves of the downstream signals for both back-to-back and 20-km transmission and plot in Figure 6.8 (a) and (b), respectively. The uplink modulation is ON in these measurements. We also plot the BER curve of the 9B/10B-encoded downstream signal when the RSOA is OFF for comparison.

An error floor is observed at a BER of 9×10^{-4} after 20-km transmission when the downstream signal is uncoded [solid circles in Figure 6.8 (b)]. This is clearly because of the non-uniform FM response of the DML. The downstream performance is, however, remarkably improved after the use of line coding which depletes the low frequency contents of the signal by >15 dB, allowing the signal to utilize the flat region of the DML FM response [63]. The receiver sensitivities (at BER= 1×10^{-9}) are measured to -16.8 and -17.0 dBm using 8B/10B and 5B/6B codes, respectively. The receiver sensitivities are further improved to -17.5 and -18.0 dBm using 9B/10B and 7B/8B coding formats, respectively.

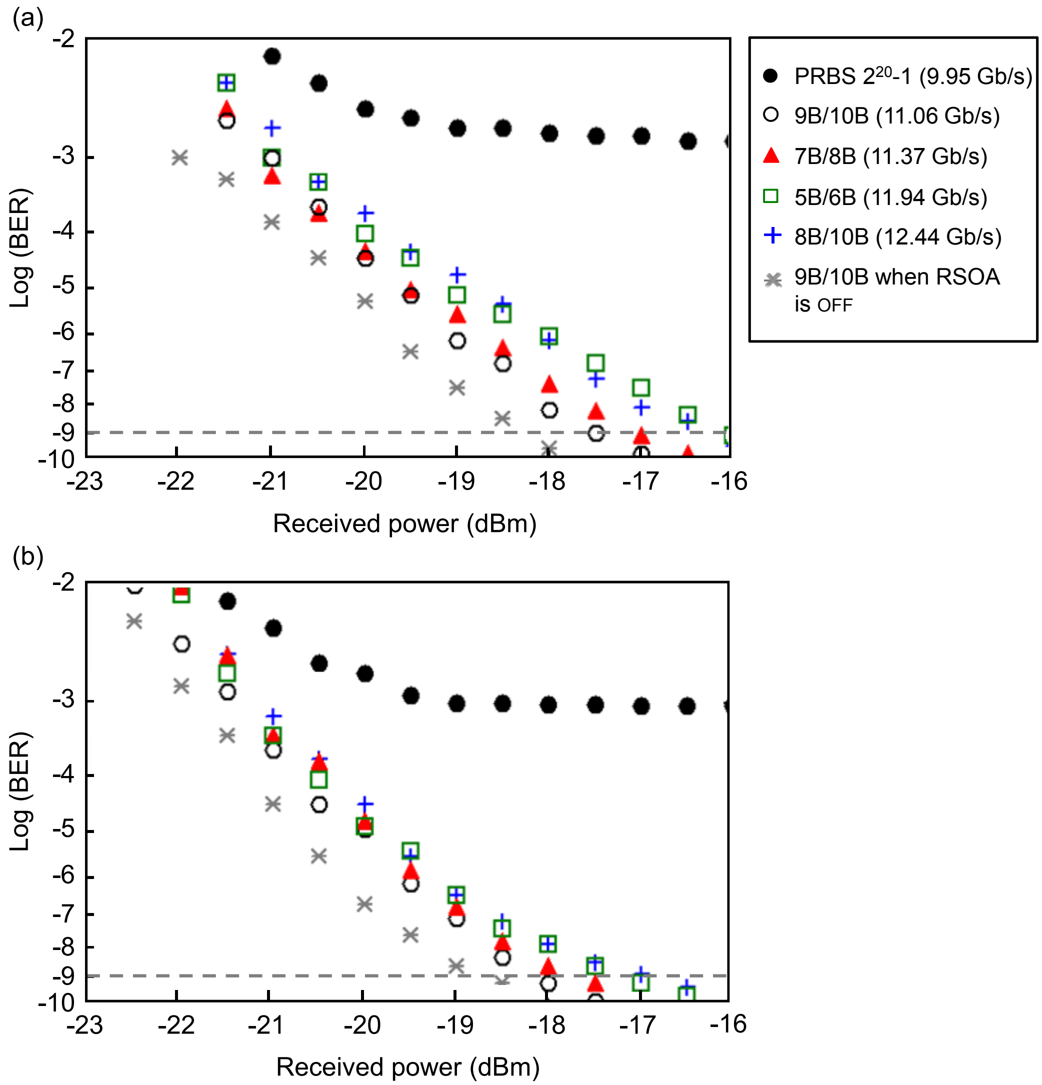

Figure 6.8: BER curves of the downstream signals when the upstream modulation is ON: (a) back-to-back, and (b) after 20-km transmission. Also plotted, for comparison, the BER curve of the downstream signal (9B/10B-encoded) when the RSOA is OFF. The dotted line indicates the BER threshold of 1×10^{-9}.

Therefore, among the four examined line codes, 9B/10B [empty circles in Figure 6.8 (b)] outperforms the others thanks to its low overhead (i.e., 11.11%), whereas

8B/10B coding [empty squares in Figure 6.8 (b)] exhibits the worst downstream performance due to its relatively large overhead (i.e., 25%). We also measure the BER curve of the downstream signal when the RSOA is turned off and a penalty of 0.5~2.0 dB is observed with respect to the downstream performance when the upstream modulation is ON. This should be attributed to the crosstalk between the downstream signal and the Rayleigh-backscattered upstream signal in the single-fiber loopback network.

The back-to-back BER curves of the downstream signals are depicted in Figure 6.8 (a). In this case, we replace the fiber link with an optical attenuator with the same loss (i.e., ~5.5 dB) so that the power injected into the RSOA remains unchanged. The measured receiver sensitivities are -17.5, -17.0, -16.2, and -16.0 dBm using 9B/10B, 7B/8B, 8B/10B, and 5B/6B codes, respectively. On the other hand, an error floor is observed at a BER of 1.5×10^{-3} with the uncoded downstream signal [solid circles in Figure 6.8 (a)]. With respect to Figure 6.8 (a), we observe a sensitivity improvement of 0.5~1.0 dB after 20-km transmission [Figure 6.8 (b)], which should be attributed to the duobinary-like phase characteristics of the downstream signals which makes some amount of the fiber dispersion acts favorably on the system performance as explained earlier in Section 3.4 [63].

Figure 6.9 shows the measured eye diagrams of the downstream signals at the back-to-back and after 20-km transmission. The eye diagrams for 9B/10B-coded signal [Figure 6.9 (a) and (f)] show clean eye openings. Clear eyes are also observed using 7B/8B, 5B/6B, and 8B/10B codes, while uncoded 2^{20}-1 PRBS shows degraded eye diagrams [Figure 6.9 (e) and (j)] with scattered dots in the middle of the eyes.

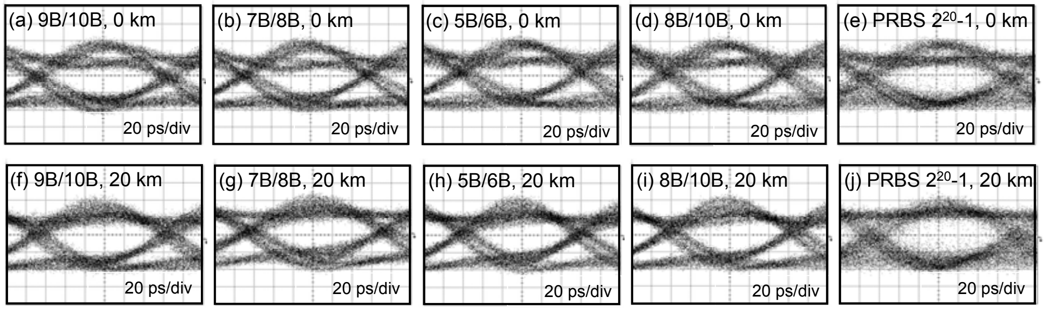

Figure 6.9: Measured eye diagrams of the downstream signals when the upstream modulation is ON at the back-to-back and after 20-km transmission using different line codes for the downstream modulation. Also shown is the eye diagram using uncoded PRBS downstream signal for comparison. The PRBS length is 2^{20}-1 for all the cases.

The BER measurements of the upstream signals are depicted for the back-to-back case and after 20-km transmission in Figure 6.10 (a) and (b), respectively. In the back-to-back case as shown in Figure 6.10 (a), we observe an error floor at a BER of 1×10^{-9} even when the downstream modulation is OFF. This should be attributed to reflection-induced optical crosstalk since such error floor was not observed in a non-loopback configuration.

When the downstream modulation is ON, the downstream data interfere with the upstream data, and thus, we observe a poor BER floor of 6×10^{-4} without line coding [solid circles in Figure 6.10 (a)]. However, the application of line coding improves the error floor to be better than the FEC threshold (uncorrected BER=1.8×10^{-4}). The error floor is improved to ~1×10^{-5} using 9B/10B and 7B/8B codes. It is further improved to 5×10^{-6} and 3×10^{-6} using 5B/6B and 8B/10B codes, respectively. The receiver sensitivities of the upstream signals range between -22.1 dBm (using 9B/10B coding) and -22.8 dBm (using 8B/10B coding). Therefore, the upstream signal exhibits the best performance when the downstream signal is coded using 8B/10B coding. This is because, as illustrated in Figure 6.4 and 6.5, 8B/10B-coded downstream signal exhibits the least power fluctuations leading to better upstream performance.

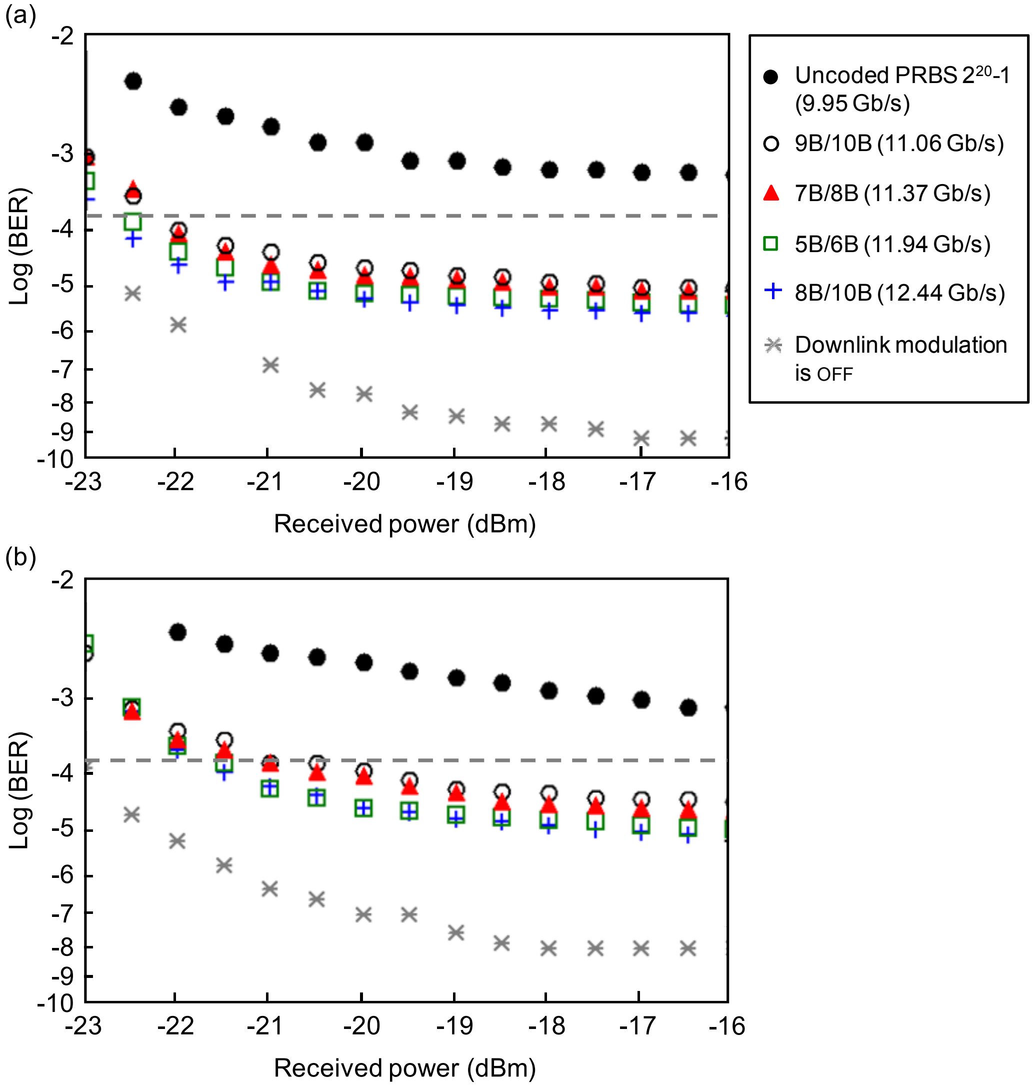

Figure 6.10: BER curves of the upstream signals when the downstream modulation is ON: (a) back-to-back, and (b) after 20-km transmission. Also plotted, for comparison, the BER curve of the upstream signal when the downstream modulation is OFF. The dotted line indicates the BER threshold of FEC at 1.8×10^{-4}.

The BER curves of the upstream signals after 20-km transmission are depicted in Figure 6.10 (b). As expected from Figure 6.4 and 6.5, the line codes with lower power fluctuations exhibit better upstream performance. For example, the receiver sensitivity is measured to be -20.5 dBm using 9B/10B coding. The receiver sensitivity is improved to -21.5 dBm using 8B/10B coding thanks to the low power fluctuations of the downstream signal in this case. Compared to the back-to-back results in Figure 6.10 (a), the upstream signals exhibit 1.0~1.5-dB penalty after 20-km transmission, which should be attributed to Rayleigh backscattering. In a single-fiber loopback network, Rayleigh backscattering-induced crosstalk can limit the upstream performance in two ways: Rayleigh backscattered seed light interferes with the upstream data signal (type I) and Rayleigh backscattered upstream data signal is modulated again by RSOA and interferes with the upstream data signal (type II) [114].

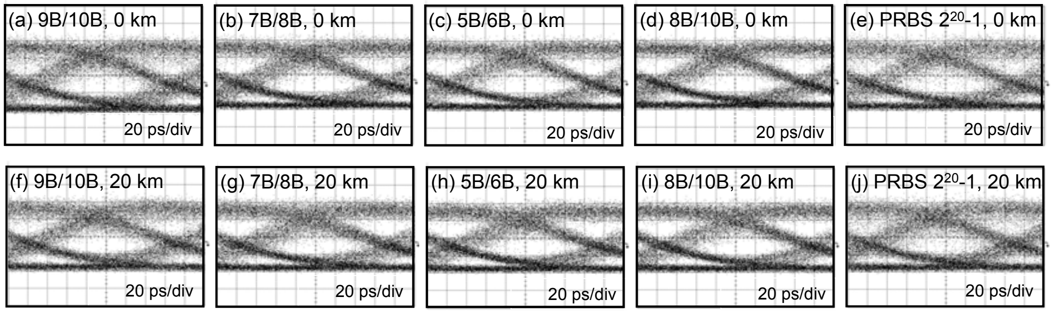

Figure 6.11: Measured eye diagrams of the upstream signals when the downstream modulation is ON at the back-to-back and after 20-km transmission using different line codes for the downstream modulation. Also shown are the eye diagrams using uncoded PRBS downstream signals for comparison. The PRBS length is 2^{20}-1 for all the cases.

Figure 6.11 shows the measured eye diagrams of the upstream signals. When the downstream data are uncoded [Figure 6.11 (e) and (j)], the upstream signal exhibits degraded eye diagrams with scattered dots in the middle of the eyes. When DC-balanced line coding is applied to the downstream signal, the eye diagrams exhibit clearer eye openings.

Finally, we make the power budget analysis of the proposed system depicted in Figure 6.2 using different line codes and summarize in Table 6-1.

Table 6-1: Power budget analysis

		Downlink		Uplink	
	Transmitter power (dBm)	6.0		3.5	
Loss (dB)	WDM (×2)	8.0		8.0	
	Delay interferometer	5.0		N/A	
	Optical circulator	1.0		1.0	
	20-km fiber link	5.0		5.0	
	Optical coupler	3.0		3.0	
	Total	22.0		17.0	
		Sensitivity (dBm)	Margin (dB)	Sensitivity (dBm)	Margin (dB)
Code	9B/10B	-18.0	2.0	-20.5	7.0
	7B/8B	-17.5	1.5	-20.7	7.2
	5B/6B	-17.0	1.0	-21.4	7.9
	8B/10B	-16.5	0.5	-21.6	8.1

The output power of the DML is ~6 dBm, and the total loss in the downlink is estimated to be 22 dB. When 9B/10B coding is used, the downlink can accommodate up to 2.0-dB additional loss before the BER drops below 1×10^{-9}, thanks to its low coding overhead (i.e., 11.11%). The downlink power margin is reduced to 1.5 and 1.0 dB with 7B/8B and 5B/6B codes, respectively, whereas it is as low as 0.5 dB using 8B/10B line coding.

Table 6-1 also shows that the uplink exhibits large power margins of 7~8 dB, given that the RSOA output power is 3.5 dBm. Since the overall power budget is limited by the downstream performance, one way to improve this is to use a coupler at the ONU with an asymmetric coupling ratio favorable to the downlink (e.g., 30:70). Both the downlink and uplink power budgets can be also improved by using avalanche photo-detectors.

6.5 Summary

In summary, we have examined the use of a few DC-balanced line codes for downstream modulation in a wavelength-shared WDM PON using a DML for downlink and an RSOA for uplink.

We show that the advantage of line coding is twofold. First, it significantly improves the performance of the FSK-downstream signals by depleting their low-frequency contents in order to overcome the performance degradation associated with the non-uniform FM response of the DML at low frequencies. Second, it greatly suppresses the interference between the downstream and upstream data, which in turn, remarkably improves the upstream performance.

Among the examined codes, the 9B/10B line coding exhibits the best downlink performance providing sufficient power margins. However, the use of line codes with better DC characteristics (e.g., 8B/10B) can improve the uplink performance, but at the expense of limited downlink power margins due to the downlink performance degradation caused by the overhead-induced bandwidth expansion.

Chapter 7

Conclusions and Future Works

7.1 Conclusions

In this thesis, we have utilized FSK modulation of DMLs to make good use of the chirp-induced frequency modulation at 10 Gb/s. We employed a DI to convert the FSK signals into ASK format. DC-balanced line coding was used to overcome the performance degradation associated with the non-uniform FM response of the DML. The line coding depletes the low-frequency spectral contents of the signal, which fall in the non-flat region of the FM response (i.e., <10 MHz), such that the signal only utilizes the uniform region at higher frequency range. However, the application of line coding induces coding overhead leading to higher bandwidth requirements for the transmission devices. For example, 8B/10B code (mapping code based on lookup tables) increases the signal bandwidth by 25% due to the coding overhead (i.e., the raw data rate of 10 Gb/s increases to 12.5 Gb/s after coding). On the other hand, 64B/66B coding (based on scrambling techniques) has a small overhead of 3.1% but with poor efficiency in eleminating the DC contents compared to the mapping codes. Therefore, the utilized DC-balanced line codes need to efficiently maintain low DC characteristics while inducing low overheads. In the case of mapping codes, developing such codes may significantly increase the size of the lookup tables. In this thesis, we only considered mapping codes having lookup tables with not more than 512 source vector entries, in order to maintain relatively low complexity in the utilized encoders.

In Chapter 3, various DC-balanced line codes, including 8B/10B, 5B/6B, 7B/8B, 9B/10B, and 64B/66B, were investigated in a 10-Gb/s DML-based transmission system. The bandwidth expansion induced by the coding overhead of each line code was taken into consideration for a fair comparison. Among the examined codes, 9B/10B exhibited the best performance whereas a marginal improvement was achieved with 64B/66B coding. This is because 9B/10B coding can greatly deplete the low-frequency spectral contents of the signals, yet it expands the bandwidth by 11.11% only. Using this line coding, we were able to achieve 65-km transmission of directly modulated 10-Gb/s signals over SSMF (dispersion-induced penalty was 2.5 dB) without any dispersion compensation. Therefore, applying suitable DC-balanced line coding for directly modulated systems can be beneficial for implementing cost-effective 10-Gb/s access transmission systems.

In the remaining chapters of this thesis, we have utilized line coding to improve the performance of different DML-based optical transmitters. In Chapter 4, we demonstrated the generation of 10-Gb/s NRZ signals using a DML driven by 3.5-GHz-bandwidth electrical duobinary signals followed by a DI. The DI converts the ternary FSK signals at the DML output into binary CPFSK/ASK signals. We utilized 9B/10B line coding to overcome the non-uniform FM response of the DML. Using the proposed transmitter, we demonstrated two configurations using both the destructive and constructive ports of the DI. An OBPF was needed in the destructive-port scheme to equalize the observed split in the mark level. Both configurations exhibited good receiver sensitivities and dispersion tolerance large enough to be used for optical access networks. For example, using the destructive-port scheme, the generated 10-Gb/s signals could travel up to ~20 km over SSMF at 1550 nm (2-dB dispersion penalty) without any dispersion compensation.

In Chapter 5, we employed DC-balanced line coding to avoid the non-uniform FM response of the DML in the dual modulation-based EML composed of a DML and an EAM. We demonstrated this transmitter using two configurations: push-pull configuration where the DML and EAM were modulated with inverted and non-inverted encoded data, respectively, and push-push configuration where the DML and EAM were both modulated with non-inverted encoded data. The DC-balanced line coding was effective in eliminating the performance degradation caused by the non-uniform FM-response of the DML in these systems. However, the low overhead was essential to gain benefit from the line coding. Using 9B/10B line coding, we were able to achieve 171- and 141-km transmission over SSMF using the push-pull and push-push configurations, respectively, without dispersion compensation.

Finally, in Chapter 6, we applied DC-balanced line coding including 8B/10B, 5B/6B, 7B/8B, and 9B/10B for the downstream modulation in a wavelength-shared WDM PON using a DML for downlink and an RSOA for uplink. The use of DC-balanced line coding has two purposes. First, it alleviates the performance degradation of the downstream signal associated with the non-uniform FM response of the DML. Second, it greatly suppresses the interference between the downstream and upstream data, which in turn, remarkably improves the upstream performance. Among the line codes we tested, the 9B/10B line coding exhibited the best downlink performance providing sufficient power margins for downlink and uplink. However, the use of line codes with better DC characteristics (i.e., shorter run length and more even distribution of ‘1’s and ‘0’s), such as 8B/10B coding, improved the uplink performance but at the expense of limited downlink power margins due to the downlink performance degradation caused by the overhead-induced bandwidth expansion.

The findings of this thesis can help implementing optical access networks in a cost-effective way by utilizing DMLs with DC-balanced line coding. The use of line coding is beneficial for cost-sensitive access applications since it is a digital solution and can be used with the commercially available DMLs without the need to replace the deployed fiber links or the existing devices at the transmitter or receiver sides.

7.2 Future Works

In this section, some research topics are proposed for further investigation:

- ***Effective DC-balanced line codes with higher bandwidth efficiency***

It will be worthy of significance to investigate more bandwidth-efficient DC-balanced line codes that can effectively deplete the low-frequency contents of the signal while inducing a small coding overhead. Since developing low-overhead mapping codes (e.g., 16B/17B coding) may increase the size of the lookup tables and consequently the complexity of the encoder, incorporating suitable scrambling techniques (e.g., scramble-and-select line coding [115]) can be of importance to design a simple and yet efficient encoder for directly modulated systems.

- ***WDM systems using the proposed transmitters***

It is desirable to apply the proposed transmitters in Chapter 3 and 4 for WDM systems. In this case, the cost incurred by the DI (and OBPF in Chapter 4) can be shared by multiple users. The periodicity of the DI enables us to utilize a single DI at the output of the WGR for all the users. Also the OBPF required for each channel in Chapter 4 can be replaced with a single wavelength-offset WGR. The increased cost per customer incurred by the DI and optical filters will thereby become insignificant as the number of users increases.

- ***DML wavelength stabilization***

In the proposed systems in Chapter 3, 4, and 6, the laser wavelength should be precisely aligned to the DI. This can be achieved by applying a low-frequency electrical tone signal to the DML and then utilizing the Fabry-Perot etalon-based monitoring module [78]. By monitoring the wavelength drift between the DML and DI, the laser wavelength can be locked to the DI. This can be readily applied to WDM systems without any additional DI or monitoring modules thanks to the periodicity of the DI. To discriminate between the different channels in this case, each DML should be applied with a tone signal having a unique frequency. Since the proposed line coding depletes the low-frequency spectral contents of the signal, the tone signal will not interfere with the data signal, provided that the tone frequency is lower than tens of MHz.

- ***Supporting higher modulation speeds using DMLs***

The proposed scheme in Chapter 4 greatly relieves the modulation bandwidth requirements of the DML and it is expected that 40-Gb/s signals can be accommodated with a 14-GHz-bandwidth DML using this approach. In addition, it will be advantageous to implement the proposed scheme in conjunction with the device approaches described in Chapter 4 (e.g., using optical injection locking [80-82]) to support even higher modulation speeds.

- ***Incorporating powerful FEC codes and avalanche photo-detectors***

In Chapter 6, we assumed Reed-Solomon (255, 239) FEC coding with 7% overhead for the upstream data. To further improve the power margins, it is suggested to utilize FEC for the downlink whereas more powerful FEC codes can be used for the uplink to increase the FEC threshold from 1.8×10^{-4} to even higher levels. Additionally, both the downlink and uplink power budgets can be improved by using avalanche photo-detectors.

- ***DC-balanced line coding for other transmission systems***

One of the other important aspects of the proposed schemes using FSK modulation along with DC-balanced line coding is that they can be applied to other transmission systems such as vertical-cavity surface-emitting lasers (VCSELs)-based systems to alleviate the chirp effects and extend the dispersion-limited transmission distance.

Appendix A

5B/6B Coding

The 5B/6B encoder used in this thesis follows the coding plan and rules of Table A-1 [73]. The first column in Table A-1, under "Name" heading represents the 32 decimal equivalents for the 5-bit source vectors (i.e., input blocks of data) *ABCDE*, assuming *A* is the least significant bit (LSB) and *E* is the most significant bit (MSB). For regular data D.x, where $0 \leq x \leq 31$, the line *K* is set to 0. Few source vectors can be part of special characters[*] which are recognizable as other than data. For such cases *K* is set to x or 1. To encode special characters, *K* line must be 1.

In the "Classification" columns, the logic function L04 means that there are no 1's and four 0's in *ABCD*, L13 means that there are one 1 and three 0's in *ABCD*, and so on. An accent to the right of a symbol is used to represent complementation (e.g., E' means the complement of *E*). A dot $(\cdot)$ represents the logical AND function.

All the 6-bit codewords which are generated directly by the 5B/6B logic functions from the *ABCDE* inputs are listed under the column headed by "*abcdei*." The coding table is designed so that a minimal number of bits must be changed on passing through the encoder. All the bits in column *abcdei* which undergone changes by the 5B/6B logic functions are in bold type, assuming that the extra digit "*i*" is added with a normal value of 0. When the source vector meet the logical conditions listed on the left side under "bit encoding," then the bold type bits are changed to the values shown

---

[*] Special characters are defined here as extra data blocks beyond the 32 needed to encode 6 bits of data. They are generally used to establish byte synchronization, to mark the start and end of packets, and sometimes to signal control functions such as ABORT, RESET, SHUTOFF, IDLE, and link diagnostics. They all comply with the general coding constraints of disparity and maximum run length [69].

in the “*abcdei*” column. For example, if L04 holds, *b* and *c* digits are forced to 1’s, as shown for D.0 and D.16.

Table A-1: 5B/6B encoding lookup table [69]

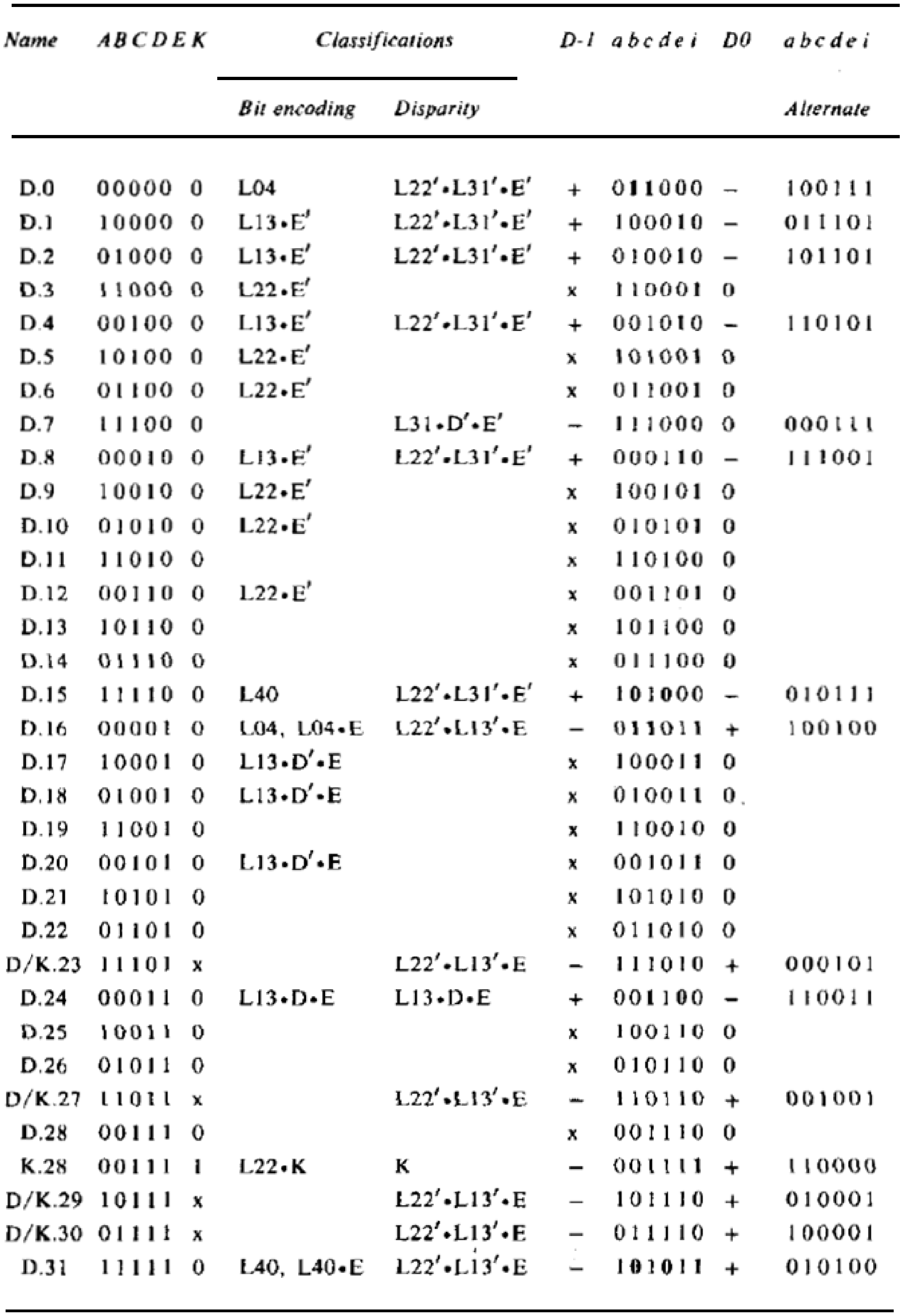

Name	*ABCDE*	*K*	*Classifications*		*D-1*	*abcdei*	*D0*	*abcdei*
			Bit encoding	*Disparity*				*Alternate*
D.0	00000	0	L04	L22′•L31′•E′	+	011000	−	100111
D.1	10000	0	L13•E′	L22′•L31′•E′	+	100010	−	011101
D.2	01000	0	L13•E′	L22′•L31′•E′	+	010010	−	101101
D.3	11000	0	L22•E′		x	110001	0	
D.4	00100	0	L13•E′	L22′•L31′•E′	+	001010	−	110101
D.5	10100	0	L22•E′		x	101001	0	
D.6	01100	0	L22•E′		x	011001	0	
D.7	11100	0		L31•D′•E′	−	111000	0	000111
D.8	00010	0	L13•E′	L22′•L31′•E′	+	000110	−	111001
D.9	10010	0	L22•E′		x	100101	0	
D.10	01010	0	L22•E′		x	010101	0	
D.11	11010	0			x	110100	0	
D.12	00110	0	L22•E′		x	001101	0	
D.13	10110	0			x	101100	0	
D.14	01110	0			x	011100	0	
D.15	11110	0	L40	L22′•L31′•E′	+	101000	−	010111
D.16	00001	0	L04, L04•E	L22′•L13′•E	−	011011	+	100100
D.17	10001	0	L13•D′•E		x	100011	0	
D.18	01001	0	L13•D′•E		x	010011	0	
D.19	11001	0			x	110010	0	
D.20	00101	0	L13•D′•E		x	001011	0	
D.21	10101	0			x	101010	0	
D.22	01101	0			x	011010	0	
D/K.23	11101	x		L22′•L13′•E	−	111010	+	000101
D.24	00011	0	L13•D•E	L13•D•E	+	001100	−	110011
D.25	10011	0			x	100110	0	
D.26	01011	0			x	010110	0	
D/K.27	11011	x		L22′•L13′•E	−	110110	+	001001
D.28	00111	0			x	001110	0	
K.28	00111	1	L22•K	K	−	001111	+	110000
D/K.29	10111	x		L22′•L13′•E	−	101110	+	010001
D/K.30	01111	x		L22′•L13′•E	−	011110	+	100001
D.31	11111	0	L40, L40•E	L22′•L13′•E	−	101011	+	010100

The second entry in the "bit encoding" column for D.16 ($L04 \cdot E$) and D.31 ($L40 \cdot E$) applies to the *i*-digit. For lines with no classification entry, the *ABCDE* bits translate unchanged into *abcde* and the added *i*-bit is '0'.

Nonzero-disparity codewords are assigned in complementary pairs to a single source vector. The "Alternate *abcdei*" column on the right of Table A-1 indicates the complement for those *ABCDE* inputs with alternate codewords. The 6-bit codewords are complemented in conformity with the disparity[*] rules which require that the polarity of nonzero-disparity codeword should alternate. In any 6-bit codeword, the running disparity is either +1 or -1 and never 0. The encoder determines the disparity and polarity in the 6-bit codeword, and then the running disparity parameter is passed along for encoding of the next 6-bit. The majority of the codewords are of zero disparity and are, with some exceptions, independent of the running disparity (i.e., they do not have a complement).

The column "*D-1*" shows the required running disparity for entry of the adjacent codeword to the right. An 'x' in the "*D-1*" column means that "*D-1*" can be positive or negative. For example, if the running disparity matches (*D-1*) = +, the output of the encoder will be 011000; otherwise the codeword is complemented to 100111. The "*D0*" column indicates the disparities of the codewords under "*abcdei*", which are either 0, +2, or -2. As in bit encoding, the encoder hardware determines directly from the *ABCDE* and *K* inputs the disparity of a codeword. The respective logic functions for classification of codewords in terms of disparity requirements are shown in a separate column in Table A-1. For example, for D.7 line, a pair of zero-disparity

---

[*] The disparity of a block of data is defined as the difference between the number of 1's and 0's in that block. Positive and negative disparity numbers refer to an excess of 1's and 0's, respectively. For the 6-bit codeword in 5B/6B coding, the permitted disparity is either 0, +2, or -2.

codewords (111000 and 000111) is assigned to a single data pattern with an entry disparity constraint similar to those applicable to nonzero-disparity codewords.

Appendix B

8B/10B Coding

The 8B/10B encoding is accomplished by consolidating 5B/6B and 3B/4B encoders. Therefore, each incoming byte is partitioned into two subblocks. The 5-bit subblock *ABCDE* is encoded into 6-bit subcodeword *abcdei*, following the directions of the logic functions and the disparity control of the 5B/6B encoder stated in Table A-1. Similarly, the 3-bit subblock *FGH* is encoded into 4-bit subcodeword *fghj* according to Table B-1.

Table B-1: 3B/4B encoding lookup table [73]

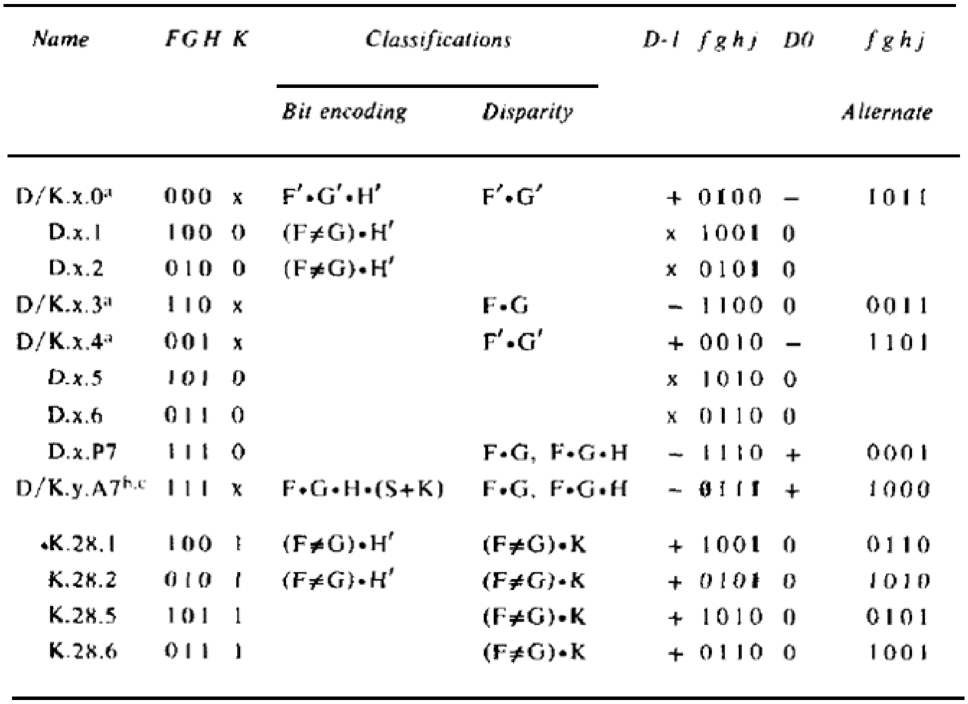

Name	*FGH*	*K*	*Classifications*		*D-1*	*fghj*	*D0*	*fghj*
			Bit encoding	*Disparity*				*Alternate*
D/K.x.0^{a}	000	x	$F'\cdot G'\cdot H'$	$F'\cdot G'$	+	0100	−	1011
D.x.1	100	0	$(F\neq G)\cdot H'$		x	1001	0	
D.x.2	010	0	$(F\neq G)\cdot H'$		x	0101	0	
D/K.x.3^{a}	110	x		$F\cdot G$	−	1100	0	0011
D/K.x.4^{a}	001	x		$F'\cdot G'$	+	0010	−	1101
D.x.5	101	0			x	1010	0	
D.x.6	011	0			x	0110	0	
D.x.P7	111	0		$F\cdot G$, $F\cdot G\cdot H$	−	1110	+	0001
D/K.y.A7^{b,c}	111	x	$F\cdot G\cdot H\cdot(S+K)$	$F\cdot G$, $F\cdot G\cdot H$	−	0111	+	1000
•K.28.1	100	1	$(F\neq G)\cdot H'$	$(F\neq G)\cdot K$	+	1001	0	0110
K.28.2	010	1	$(F\neq G)\cdot H'$	$(F\neq G)\cdot K$	+	0101	0	1010
K.28.5	101	1		$(F\neq G)\cdot K$	+	1010	0	0101
K.28.6	011	1		$(F\neq G)\cdot K$	+	0110	0	1001

The 3B/4B encoding in Table B-1 follows the conventions and notations of Table A-1 in Appendix A. In Table B-1, some data blocks have two entries in the "Disparity" column: The left classification refers to the entry disparity *D-1*, and the right one to *D0*. The D/K.y.A7 (alternate 7) source vector was introduced to eliminate the run length[*] of 5 sequence in digits *eifgh*. The A7 code replaces the P7 encoding whenever $[(e = i = 1) \cdot (D - 1 = -)]$ OR $[(e = i = 0) \cdot (D - 1 = +)]$ OR $(K = 1)$. To be noted that whenever $K = 1$, $FGH = 111$ is always translated into $fghj = 0111$ or its complement. The D/K.y.A7 encoding can generate a run length of 5 across the trailing character boundary in the *ghjab* bits. However, this sequence is preceded by a run length of only 1 in digit 5.

The zero-disparity 4-bit subcodeword of K.28.1, K.28.2, K.28.5, and K.28.6 are handled similarly to D/K.x.3 with respect to complementation in order to generate some special characters[**] with byte synchronizing for example.

As mentioned earlier, the term disparity designates the difference between the number of 1 and 0 bits in a defined block of digits. All 6-bit *abcdei* and 4-bit *fghj* subcodewords individually, and the complete 10-bit codewords, have a disparity of either 0 or ±2 (i.e., each valid 10-bit codeword either has five 1's and five 0's or six 1's and four 0's or four 1's and six 0's). The coding rules require that the polarity of nonzero disparity codewords should alternate. For this purpose, no distinction is made between 6-bit and 4-bit subcodewords (i.e., a surplus of two 1's in a 6-bit subcodeword can be compensated by two excess 0's in either a 6-bit or a 4-bit subcodeword and vice versa).

The determination of disparity and polarity in the 6-bit subcodeword is followed by the corresponding operations of the 4-bit subcodeword, then the running disparity

---

[*] The run length is defined as the number of identical contiguous 1's or 0's in the codeword. The maximum run length in 8B/10B encoding is 5.

[**] Special characters are defined here as extra code points beyond the 256 needed to encode a byte of data. As mentioned earlier, they are generally used to establish byte synchronization, to mark the start and end of packets, and sometimes to signal control functions.

parameter is passed along for encoding of the next byte. The majority of the coded subblocks are of zero disparity and are, with some exceptions, independent of the running disparity (i.e., they do not have a complement).

Appendix C

7B/8B Coding

The 7B/8B encoding used in this thesis is based on Table C-1. As in the case of 5B/6B and 8B/10B encoding schemes, the assignment of the codewords in the 7B/8B encoder to the uncoded source vectors is done in a way that minimizes the complexity of the encoder. This is accomplished by minimizing the number of bits changed in the source vectors.

The “Name” column in Table C-1 represents the 128 decimal equivalents for the 7-bit source vectors STUVWXY. The codewords are generated directly by the 7B/8B logic functions in the column headed by “Coding Class.” The primary codewords generated from the STUVWXY inputs are listed under the column headed by “stuvwxyz.” All the bits in column stuvwxyz which undergone changes by the 7B/8B logic functions are in bold type, assuming that the extra digit “z” is added with a normal value of 0. The “Alternate stuvwxyz” column indicates the complement for stuvwxyz codewords. The 8-bit codewords are complemented in conformity with the disparity rules, which require that the polarity of nonzero-disparity codeword should alternate.

The column headed by “DB” (i.e., block disparity) on the right represents the disparity for the primary codeword. In 7B/8B coding, the permitted disparity is either 0, ±2, or ±4. For example, if there are three 1’s and five 0’s in the codeword, the disparity is -2.

The column headed by “DR” (i.e., required entry disparity) indicates the polarity of the running disparity.

The column with the “Coding Class” heading defines the logic functions defined in [75] to generate the 8-bit codewords. In these logic functions, the first capital letter B, D, or F indicates the disparity of the codeword: B indicates a balanced codeword, P indicates a complementary pair of balanced codewords which are selected based on the polarity of the running disparity, D (dual) indicates a complementary pair of codewords with a disparity of two, and F indicates a complementary pair of codewords with a disparity of four.

The second capital letter indicates the disparity of the codeword using the notation as follows: U and M indicate disparities of +1 and -1, respectively. C and T indicate disparities of +3 and -3, respectively. V and Q indicate disparities of +5 and -5, respectively. H and S indicate +7 and -7 disparities.

A third capital letter, if present, indicates the value of the control input bit, K. The third and following capital letters other than K mark the bits in the source vector, if any, which must be complemented to obtain the respective codeword. The last coded bit ‘z’ is appended with a zero value and complemented to a value of one, if indicated by a classification name ending in Z.

To illustrate, for D0, the source vector is “0000000” with a K bit of 0. The coding class is “DSSVX,” which means that there is a complementary pair of codewords with a disparity of two (D), the disparity of the source vector is -7 (S), and “SVX” indicates that bits S, V, and X need to be complemented (i.e., inverted). The vector belongs to the DR class S which requires positive (+) entry disparity, the DB class of the source vector is S, and the DB block disparity of the codeword is -2.

Table C-1: 7B/8B encoding lookup table [75]

Name	STUVWXY K	Coding Class	Primary stuvwxyz	Alternate stuvwxyz	DR Class	DR	DB Class	DB
D0	0000000 0	DSSVX	10010100	01101011	S	+	S	−2
D1	1000000 0	DQ3mWX	10001100	01110011	Q	+	Q	−2
D2	0100000 0	DQ3mWX	01001100	10110011	Q	+	Q	−2
D3	1100000 0	DTK’4bW	11001000	00110111	T	+	TK’4b	−2
D4	0010000 0	DQ3mWX	00101100	11010011	Q	+	Q	−2
D5	1010000 0	DTK’4bW	10101000	01010111	T	+	TK’4b	−2
D6	0110000 0	DTK’4bW	01101000	10010111	T	+	TK’4b	−2
D7	1110000 0	BMK’4t’Z	11100001			±	MK’4t’	0
D8	0001000 0	DQ3t5tSY	10010010	01101101	Q	+	Q	−2
D9	1001000 0	DTK’4bW	10011000	01100111	T	+	TK’4b	−2
D10	0101000 0	DTK’4bW	01011000	10100111	T	+	TK’4b	−2
D11	1101000 0	BMK’4t’Z	11010001			±	MK’4t’	0
D12	0011000 0	DTK’4bW	00111000	11000111	T	+	TK’4b	−2
D13	1011000 0	BMK’4t’Z	10110001			±	MK’4t’	0
D14	0111000 0	BMK’4t’Z	01110001			±	MK’4t’	0
D15	1111000 0	PU4c	11110000	00001111	U4c	−	U4c	0
D16	0000100 0	DQ3t5tSY	10001010	01110101	Q	+	Q	−2
D17	1000100 0	FT4m	10001000	01110111	T	+	T4m	−4
D18	0100100 0	FT4m	01001000	10110111	T	+	T4m	−4
D19	1100100 0	BMK’4t’Z	11001001			±	MK’4t’	0
D20	0010100 0	FT4m	00101000	11010111	T	+	T4m	−4
D21	1010100 0	BMK’4t’Z	10101001			±	MK’4t’	0
D22	0110100 0	BMK’4t’Z	01101001			±	MK’4t’	0
D23	1110100 0	BU4c’	11101000			±	U4c’	0
D24	0001100 0	FT4m	00011000	11100111	T	+	T4m	−4
D25	1001100 0	BMK’4t’Z	10011001			±	MK’4t’	0
D26	0101100 0	BMK’4t’Z	01011001			±	MK’4t’	0
D27	1101100 0	BU4c’	11011000			±	U4c’	0
D28	0011100 0	BMK’4t’Z	00111001			±	MK’4t’	0
D29	1011100 0	BU4c’	10111000			±	U4c’	0
D30	0111100 0	BU4c’	01111000			±	U4c’	0
D31	1111100 0	DC4cVZ	11101001	00010110	C	−	C	+2
D32	0000010 0	DQ5qTV	01010100	10101011	Q	+	Q	−2
D33	1000010 0	FT4m	10000100	01111011	T	+	T4m	−4
D34	0100010 0	FT4m	01000100	10111011	T	+	T4m	−4
D35	1100010 0	BMK’4t’Z	11000101			±	MK’4t’	0
D36	0010010 0	FT4m	00100100	11011011	T	+	T4m	−4
D37	1010010 0	BMK’4t’Z	10100101			±	MK’4t’	0
D38	0110010 0	BMK’4t’Z	01100101			±	MK’4t’	0
D39	1110010 0	BU4c’	11100100			±	U4c’	0
D40	0001010 0	FT4m	00010100	11101011	T	+	T4m	−4
D41	1001010 0	BMK’4t’Z	10010101			±	MK’4t’	0
D42	0101010 0	BMK’4t’Z	01010101			±	MK’4t’	0

Name	STUVWXY K	Coding Class	Primary stuvwxyz	Alternate stuvwxyz	DR Class	DR	DB Class	DB
D43	1101010 0	BU4c'	11010100			±	U4c'	0
D44	0011010 0	BMK'4t'Z	0011010**1**			±	MK'4t'	0
D45	1011010 0	BU4c'	10110100			±	U4c'	0
D46	0111010 0	BU4c'	01110100			±	U4c'	0
D47	1111010 0	DC4cVZ	111**0**010**1**	00011010	C	–	C	+2
D48	0000110 0	DT4t5tSTW	**11**00**0**100	00111011	T	+	T4t5t	−2
D49	1000110 0	BMK'4t'Z	1000110**1**			±	MK'4t'	0
D50	0100110 0	BMK'4t'Z	0100110**1**			±	MK'4t'	0
D51	1100110 0	BU4c'	11001100			±	U4c'	0
D52	0010110 0	BMK'4t'Z	0010110**1**			±	MK'4t'	0
D53	1010110 0	BU4c'	10101100			±	U4c'	0
D54	0110110 0	BU4c'	01101100			±	U4c'	0
D55	1110110 0	DC4c'	11101100	00010011	C	–	C	+2
D56	0001110 0	BMK'4t'Z	0001110**1**			±	MK'4t'	0
D57	1001110 0	BU4c'	10011100			±	U4c'	0
D58	0101110 0	BU4c'	01011100			±	U4c'	0
D59	1101110 0	DC4c'	11011100	00100011	C	–	C	+2
D60	0011110 0	BU4c'	00111100			±	U4c'	0
D61	1011110 0	DC4c'	10111100	01000011	C	–	C	+2
D62	0111110 0	DC4c'	01111100	10000011	C	–	C	+2
D63	1111110 0	DVK'6vSTW	**00**11**0**100	11001011	VK'	+	VK'	−2
D64	0000001 0	DQ5qTV	010**1**0010	10101101	Q	+	Q	−2
D65	1000001 0	FT4m	10000010	01111101	T	+	T4m	−4
D66	0100001 0	FT4m	01000010	10111101	T	+	T4m	−4
D67	1100001 0	BMK'4t'Z	1100001**1**			±	MK'4t'	0
D68	0010001 0	FT4m	00100010	11011101	T	+	T4m	−4
D69	1010001 0	BMK'4t'Z	1010001**1**			±	MK'4t'	0
D70	0110001 0	BMK'4t'Z	0110001**1**			±	MK'4t'	0
D71	1110001 0	BU4c'	11100010			±	U4c'	0
D72	0001001 0	FT4m	00010010	11101101	T	+	T4m	−4
D73	1001001 0	BMK'4t'Z	1001001**1**			±	MK'4t'	0
D74	0101001 0	BMK'4t'Z	0101001**1**			±	MK'4t'	0
D75	1101001 0	BU4c'	11010010			±	U4c'	0
D76	0011001 0	BMK'4t'Z	0011001**1**			±	MK'4t'	0
D77	1011001 0	BU4c'	10110010			±	U4c'	0
D78	0111001 0	BU4c'	01110010			±	U4c'	0
D79	1111001 0	DC4cVZ	111**0**001**1**	00011100	C	–	C	+2
D80	0000101 0	DT4t5tSTW	**11**00**0**010	00111101	T	+	T4t5t	−2
D81	1000101 0	BMK'4t'Z	1000101**1**			±	MK'4t'	0
D82	0100101 0	BMK'4t'Z	0100101**1**			±	MK'4t'	0
D83	1100101 0	BU4c'	11001010			±	U4c'	0
D84	0010101 0	BMK'4t'Z	0010101**1**			±	MK'4t'	0
D85	1010101 0	BU4c'	10101010			±	U4c'	0

Name	STUVWXY K	Coding Class	Primary stuvwxyz	Alternate stuvwxyz	DR Class	DR	DB Class	DB
D86	0110101 0	BU4c'	01101010			±	U4c'	0
D87	1110101 0	DC4c'	11101010	00010101	C	–	C	+2
D88	0001101 0	BMK'4t'Z	0001101**1**			±	MK'4t'	0
D89	1001101 0	BU4c'	10011010			±	U4c'	0
D90	0101101 0	BU4c'	01011010			±	U4c'	0
D91	1101101 0	DC4c'	11011010	00100101	C	–	C	+2
D92	0011101 0	BU4c'	00111010			±	U4c'	0
D93	1011101 0	DC4c'	10111010	01000101	C	–	C	+2
D94	0111101 0	DC4c'	01111010	10000101	C	–	C	+2
D95	1111101 0	DVK'5v6cSVW	**0**11**00**010	10011101	VK'	+	VK'	–2
D96	0000011 0	DT5qU	00**1**00110	11011001	T	+	T5q	–2
D97	1000011 0	BMK'4t'Z	1000011**1**			±	MK'4t'	0
D98	0100011 0	BMK'4t'Z	0100011**1**			±	MK'4t'	0
D99	1100011 0	BU4c'	11000110			±	U4c'	0
D100	0010011 0	BMK'4t'Z	0010011**1**			±	MK'4t'	0
D101	1010011 0	BU4c'	10100110			±	U4c '	0
D102	0110011 0	BU4c'	01100110			±	U4c'	0
D103	1110011 0	DC4c'	11100110	00011001	C	–	C	+2
D104	0001011 0	BMK'4t'Z	0001011**1**			±	MK'4t'	0
D105	1001011 0	BU4c'	10010110			±	U4c'	0
D106	0101011 0	BU4c'	01010110			±	U4c'	0
D107	1101011 0	DC4c'	11010110	00101001	C	–	C	+2
D108	0011011 0	BU4c'	00110110			±	U4c'	0
D109	1011011 0	DC4c'	10110110	01001001	C	–	C	+2
D110	0111011 0	DC4c'	01110110	10001001	C	–	C	+2
D111	1111011 0	DVK'3c5cSTX	**00**110**0**10	11001101	VK'	+	VK'	–2
D112	0000111 0	DM4tTX	01001**0**10	10110101	M4t	+	M4t	–2
D113	1000111 0	BU4c'	10001110			±	U4c'	0
D114	0100111 0	BU4c'	01001110			±	U4c'	0
D115	1100111 0	DC4c'	11001110	00110001	C	–	C	+2
D116	0010111 0	BU4c'	00101110			±	U4c'	0
D117	1010111 0	DC4c'	10101110	01010001	C	–	C	+2
D118	0110111 0	DC4c'	01101110	10010001	C	–	C	+2
D119	1110111 0	DVK'3c5cSTX	**00**101**0**10	11010101	VK'	+	VK'	–2
D120	0001111 0	BU4c'	00011110			±	U4c'	0
D121	1001111 0	DC4c'	10011110	01100001	C	–	C	+2
D122	0101111 0	DC4c'	01011110	10100001	C	–	C	+2
D123	1101111 0	DVK'2u3uTVW	**10**0**00**110	01111001	VK'	+	VK'	–2
D124	0011111 0	DC4c'	00111110	11000001	C	–	C	+2
D125	1011111 0	DVK'2bVWY	101**00**1**0**0	01011011	VK'	+	VK'	–2
D126	0111111 0	DVK'2bVWY	011**00**1**0**0	10011011	VK'	+	VK'	–2
D127	1111111 0	DHTVWX	1**0**1**000**10	01011101	H	+	H	–2

Appendix D

9B/10B Coding

The 9B/10B line coding employed in this thesis is based on Table D-1 [74]. The table is generated by considering all the combinations of 10-bit patterns, and grouping the patterns by the number of 1's in each pattern, and thus, a simple binomial distribution of bit patterns is found [74]:

Number of 1's	Number of patterns	Disparity	Comment
0 or 10	1	-5	Do not use
1 or 9	10	-4	Do not use
2 or 8	45	-3	Do not use
3 or 7	120	-2	Use in pairs
4 or 6	210	-1	Use in pairs
5	252	0	Use

Of the possible 1024 bit patterns, those with excessive disparity (greater than 2 bits disparity in absolute value) are discarded. This results in 252 balanced codewords, and a number of slightly imbalanced codewords.

To address the imbalance present in the codewords of +/-1 and +/-2 bits, the principle of running disparity control is applied. The transmitter keeps track of the running disparity (i.e., the sum of the disparities of all prior codewords). If the encoder has a positive running disparity, then it will only encode the source vector into a codeword that has zero or negative disparity. Otherwise, if the encoder has a negative running disparity, then it will only choose a codeword that has zero or positive disparity. In this way, the running disparity will be bounded, and tend towards zero always. There are 252 codewords that are balanced, 210 codewords pairs with disparity of 1, and 120 codewords pairs with disparity of 2. Therefore, the total number of codewords is 582, which is more than needed to encode 9 bits of arbitrary user data.

The 70 extra codewords that are not needed should be chosen such that the maximum run length is minimized. This is possible by considering the beginning and ending run lengths of each codeword. For example, the codeword 0010111111 has an ending run length of 6 and a beginning run length of 2. If the 582 codewords are analyzed in this way, the distribution of ending and beginning run lengths is found to be as follows [74]:

Length Of Run	Number of CPs with ending Run of given length	Number of CPs with beginning Run of given length
1	308	308
2	154	154
3	72	72
4	31	31
5	12	12
6	4	4
7	1	1
8, 9, or 10	0	0

Knowing that there are 70 extra codewords, all the codewords that have beginning and trailing runs of 5 or more can be dropped. This amounts to 32 codewords eliminated, because there are two codewords that fall into both lists: 0000011111 and 1111100000. Therefore, 550 codewords remain with a maximum run length of 8 (i.e., a codeword that ends with a run of 4 and be followed by a codeword that begins with a run length of 4). It is not possible to drop all the beginning and ending runs of 4, and thus, only the ending runs of 4 are eliminated. This suggests that 31 codewords are used. However, one of these 31 codewords (i.e., 0000001111) is already counted when the run of 6 codewords were dropped. So, 30 codewords are consumed, arriving at a set of 520 codewords (i.e., 582 – 32 – 30 = 520).

The maximum run length allowed in these 520 codewords is 7. Each codeword has a disparity of -2, -1, 0, 1, or 2.

Table D-1: 9B/10B encoding lookup table [75]

	Data Pattern												Complement of the Data Pattern												
		Place Value of Each Bit												Place Value of Each Bit											
Codepoint Number	Decimal Format	1	2	4	8	16	32	64	128	256	512	Negative Disparity	Positive Disparity	1	2	4	8	16	32	64	128	256	512	Decimal Format	Description	Value
1	19	1	1	0	0	1	0	0	0	0	0	-2	2	0	0	1	1	0	1	1	1	1	1	1004	Special Control	0
2	21	1	0	1	0	1	0	0	0	0	0	-2	2	0	1	0	1	0	1	1	1	1	1	1002	Reserved	
3	22	0	1	1	0	1	0	0	0	0	0	-2	2	1	0	0	1	0	1	1	1	1	1	1001	Reserved	
4	25	1	0	0	1	1	0	0	0	0	0	-2	2	0	1	1	0	0	1	1	1	1	1	998	Reserved	
5	26	0	1	0	1	1	0	0	0	0	0	-2	2	1	0	1	0	0	1	1	1	1	1	997	Reserved	
6	28	0	0	1	1	1	0	0	0	0	0	-2	2	1	1	0	0	0	1	1	1	1	1	995	Control	1
7	35	1	1	0	0	0	1	0	0	0	0	-2	2	0	0	1	1	1	0	1	1	1	1	988	Reserved	
8	37	1	0	1	0	0	1	0	0	0	0	-2	2	0	1	0	1	1	0	1	1	1	1	986	Control	2
9	38	0	1	1	0	0	1	0	0	0	0	-2	2	1	0	0	1	1	0	1	1	1	1	985	Control	3
10	41	1	0	0	1	0	1	0	0	0	0	-2	2	0	1	1	0	1	0	1	1	1	1	982	Control	4
11	42	0	1	0	1	0	1	0	0	0	0	-2	2	1	0	1	0	1	0	1	1	1	1	981	Control	5
12	44	0	0	1	1	0	1	0	0	0	0	-2	2	1	1	0	0	1	0	1	1	1	1	979	Control	6
13	49	1	0	0	0	1	1	0	0	0	0	-2	2	0	1	1	1	0	0	1	1	1	1	974	Reserved	
14	50	0	1	0	0	1	1	0	0	0	0	-2	2	1	0	1	1	0	0	1	1	1	1	973	Reserved	
15	52	0	0	1	0	1	1	0	0	0	0	-2	2	1	1	0	1	0	0	1	1	1	1	971	Control	7
16	56	0	0	0	1	1	1	0	0	0	0	-2	2	1	1	1	0	0	0	1	1	1	1	967	Control	8
17	67	1	1	0	0	0	0	1	0	0	0	-2	2	0	0	1	1	1	1	0	1	1	1	956	Reserved	
18	69	1	0	1	0	0	0	1	0	0	0	-2	2	0	1	0	1	1	1	0	1	1	1	954	Control	9
19	70	0	1	1	0	0	0	1	0	0	0	-2	2	1	0	0	1	1	1	0	1	1	1	953	Control	10
20	73	1	0	0	1	0	0	1	0	0	0	-2	2	0	1	1	0	1	1	0	1	1	1	950	Control	11
21	74	0	1	0	1	0	0	1	0	0	0	-2	2	1	0	1	0	1	1	0	1	1	1	949	Control	12
22	76	0	0	1	1	0	0	1	0	0	0	-2	2	1	1	0	0	1	1	0	1	1	1	947	Data	0
23	81	1	0	0	0	1	0	1	0	0	0	-2	2	0	1	1	1	0	1	0	1	1	1	942	Reserved	
24	82	0	1	0	0	1	0	1	0	0	0	-2	2	1	0	1	1	0	1	0	1	1	1	941	Reserved	
25	84	0	0	1	0	1	0	1	0	0	0	-2	2	1	1	0	1	0	1	0	1	1	1	939	Data	1
26	88	0	0	0	1	1	0	1	0	0	0	-2	2	1	1	1	0	0	1	0	1	1	1	935	Data	2
27	97	1	0	0	0	0	1	1	0	0	0	-2	2	0	1	1	1	1	0	0	1	1	1	926	Data	3
28	98	0	1	0	0	0	1	1	0	0	0	-2	2	1	0	1	1	1	0	0	1	1	1	925	Data	4
29	100	0	0	1	0	0	1	1	0	0	0	-2	2	1	1	0	1	1	0	0	1	1	1	923	Data	5

	Data Pattern												Complement of the Data Pattern													
		Place Value of Each Bit												Place Value of Each Bit												
Codepoint Number	Decimal Format	1	2	4	8	16	32	64	128	256	512	Negative Disparity	Positive Disparity	1	2	4	8	16	32	64	128	256	512	Decimal Format	Description	Value
30	104	0	0	0	1	0	1	1	0	0	0	-2	2	1	1	1	0	1	0	0	1	1	1	919	Data	6
31	112	0	0	0	0	1	1	1	0	0	0	-2	2	1	1	1	1	0	0	0	1	1	1	911	Data	7
32	131	1	1	0	0	0	0	0	1	0	0	-2	2	0	0	1	1	1	1	1	0	1	1	892	Reserved	
33	133	1	0	1	0	0	0	0	1	0	0	-2	2	0	1	0	1	1	1	1	0	1	1	890	Data	8
34	134	0	1	1	0	0	0	0	1	0	0	-2	2	1	0	0	1	1	1	1	0	1	1	889	Data	9
35	137	1	0	0	1	0	0	0	1	0	0	-2	2	0	1	1	0	1	1	1	0	1	1	886	Data	10
36	138	0	1	0	1	0	0	0	1	0	0	-2	2	1	0	1	0	1	1	1	0	1	1	885	Data	11
37	140	0	0	1	1	0	0	0	1	0	0	-2	2	1	1	0	0	1	1	1	0	1	1	883	Data	12
38	145	1	0	0	0	1	0	0	1	0	0	-2	2	0	1	1	1	0	1	1	0	1	1	878	Reserved	
39	146	0	1	0	0	1	0	0	1	0	0	-2	2	1	0	1	1	0	1	1	0	1	1	877	Reserved	
40	148	0	0	1	0	1	0	0	1	0	0	-2	2	1	1	0	1	0	1	1	0	1	1	875	Data	13
41	152	0	0	0	1	1	0	0	1	0	0	-2	2	1	1	1	0	0	1	1	0	1	1	871	Data	14
42	161	1	0	0	0	0	1	0	1	0	0	-2	2	0	1	1	1	1	0	1	0	1	1	862	Data	15
43	162	0	1	0	0	0	1	0	1	0	0	-2	2	1	0	1	1	1	0	1	0	1	1	861	Data	16
44	164	0	0	1	0	0	1	0	1	0	0	-2	2	1	1	0	1	1	0	1	0	1	1	859	Data	17
45	168	0	0	0	1	0	1	0	1	0	0	-2	2	1	1	1	0	1	0	1	0	1	1	855	Data	18
46	176	0	0	0	0	1	1	0	1	0	0	-2	2	1	1	1	1	0	0	1	0	1	1	847	Data	19
47	193	1	0	0	0	0	0	1	1	0	0	-2	2	0	1	1	1	1	1	0	0	1	1	830	Data	20
48	194	0	1	0	0	0	0	1	1	0	0	-2	2	1	0	1	1	1	1	0	0	1	1	829	Data	21
49	196	0	0	1	0	0	0	1	1	0	0	-2	2	1	1	0	1	1	1	0	0	1	1	827	Data	22
50	200	0	0	0	1	0	0	1	1	0	0	-2	2	1	1	1	0	1	1	0	0	1	1	823	Data	23
51	208	0	0	0	0	1	0	1	1	0	0	-2	2	1	1	1	1	0	1	0	0	1	1	815	Data	24
52	224	0	0	0	0	0	1	1	1	0	0	-2	2	1	1	1	1	1	0	0	0	1	1	799	Data	25
53	259	1	1	0	0	0	0	0	0	1	0	-2	2	0	0	1	1	1	1	1	1	0	1	764	Reserved	
54	261	1	0	1	0	0	0	0	0	1	0	-2	2	0	1	0	1	1	1	1	1	0	1	762	Data	26
55	262	0	1	1	0	0	0	0	0	1	0	-2	2	1	0	0	1	1	1	1	1	0	1	761	Data	27
56	265	1	0	0	1	0	0	0	0	1	0	-2	2	0	1	1	0	1	1	1	1	0	1	758	Data	28
57	266	0	1	0	1	0	0	0	0	1	0	-2	2	1	0	1	0	1	1	1	1	0	1	757	Data	29
58	268	0	0	1	1	0	0	0	0	1	0	-2	2	1	1	0	0	1	1	1	1	0	1	755	Data	30

	Data Pattern												Complement of the Data Pattern													
		Place Value of Each Bit												Place Value of Each Bit												
Codepoint Number	Decimal Format	1	2	4	8	16	32	64	128	256	512	Negative Disparity	Positive Disparity	1	2	4	8	16	32	64	128	256	512	Decimal Format	Description	Value
59	273	1	0	0	0	1	0	0	0	1	0	-2	2	0	1	1	1	0	1	1	1	0	1	750	Reserved	
60	274	0	1	0	0	1	0	0	0	1	0	-2	2	1	0	1	1	0	1	1	1	0	1	749	Reserved	
61	276	0	0	1	0	1	0	0	0	1	0	-2	2	1	1	0	1	0	1	1	1	0	1	747	Data	31
62	280	0	0	0	1	1	0	0	0	1	0	-2	2	1	1	1	0	0	1	1	1	0	1	743	Data	32
63	289	1	0	0	0	0	1	0	0	1	0	-2	2	0	1	1	1	1	0	1	1	0	1	734	Data	33
64	290	0	1	0	0	0	1	0	0	1	0	-2	2	1	0	1	1	1	0	1	1	0	1	733	Data	34
65	292	0	0	1	0	0	1	0	0	1	0	-2	2	1	1	0	1	1	0	1	1	0	1	731	Data	35
66	296	0	0	0	1	0	1	0	0	1	0	-2	2	1	1	1	0	1	0	1	1	0	1	727	Data	36
67	304	0	0	0	0	1	1	0	0	1	0	-2	2	1	1	1	1	0	0	1	1	0	1	719	Data	37
68	321	1	0	0	0	0	0	1	0	1	0	-2	2	0	1	1	1	1	1	0	1	0	1	702	Data	38
69	322	0	1	0	0	0	0	1	0	1	0	-2	2	1	0	1	1	1	1	0	1	0	1	701	Data	39
70	324	0	0	1	0	0	0	1	0	1	0	-2	2	1	1	0	1	1	1	0	1	0	1	699	Data	40
71	328	0	0	0	1	0	0	1	0	1	0	-2	2	1	1	1	0	1	1	0	1	0	1	695	Data	41
72	336	0	0	0	0	1	0	1	0	1	0	-2	2	1	1	1	1	0	1	0	1	0	1	687	Data	42
73	352	0	0	0	0	0	1	1	0	1	0	-2	2	1	1	1	1	1	0	0	1	0	1	671	Data	43
74	385	1	0	0	0	0	0	0	1	1	0	-2	2	0	1	1	1	1	1	1	0	0	1	638	Data	44
75	386	0	1	0	0	0	0	0	1	1	0	-2	2	1	0	1	1	1	1	1	0	0	1	637	Data	45
76	388	0	0	1	0	0	0	0	1	1	0	-2	2	1	1	0	1	1	1	1	0	0	1	635	Data	46
77	392	0	0	0	1	0	0	0	1	1	0	-2	2	1	1	1	0	1	1	1	0	0	1	631	Data	47
78	400	0	0	0	0	1	0	0	1	1	0	-2	2	1	1	1	1	0	1	1	0	0	1	623	Data	48
79	416	0	0	0	0	0	1	0	1	1	0	-2	2	1	1	1	1	1	0	1	0	0	1	607	Data	49
80	515	1	1	0	0	0	0	0	0	0	1	-2	2	0	0	1	1	1	1	1	1	1	0	508	Reserved	
81	517	1	0	1	0	0	0	0	0	0	1	-2	2	0	1	0	1	1	1	1	1	1	0	506	Data	50
82	518	0	1	1	0	0	0	0	0	0	1	-2	2	1	0	0	1	1	1	1	1	1	0	505	Data	51
83	521	1	0	0	1	0	0	0	0	0	1	-2	2	0	1	1	0	1	1	1	1	1	0	502	Data	52
84	522	0	1	0	1	0	0	0	0	0	1	-2	2	1	0	1	0	1	1	1	1	1	0	501	Data	53
85	524	0	0	1	1	0	0	0	0	0	1	-2	2	1	1	0	0	1	1	1	1	1	0	499	Data	54
86	529	1	0	0	0	1	0	0	0	0	1	-2	2	0	1	1	1	0	1	1	1	1	0	494	Reserved	
87	530	0	1	0	0	1	0	0	0	0	1	-2	2	1	0	1	1	0	1	1	1	1	0	493	Reserved	

	Data Pattern													Complement of the Data Pattern												
		Place Value of Each Bit												Place Value of Each Bit												
Codepoint Number	Decimal Format	1	2	4	8	16	32	64	128	256	512	Negative Disparity	Positive Disparity	1	2	4	8	16	32	64	128	256	512	Decimal Format	Description	Value
88	532	0	0	1	0	1	0	0	0	0	1	-2	2	1	1	0	1	0	1	1	1	1	0	491	Data	55
89	536	0	0	0	1	1	0	0	0	0	1	-2	2	1	1	1	0	0	1	1	1	1	0	487	Data	56
90	545	1	0	0	0	0	1	0	0	0	1	-2	2	0	1	1	1	1	0	1	1	1	0	478	Data	57
91	546	0	1	0	0	0	1	0	0	0	1	-2	2	1	0	1	1	1	0	1	1	1	0	477	Data	58
92	548	0	0	1	0	0	1	0	0	0	1	-2	2	1	1	0	1	1	0	1	1	1	0	475	Data	59
93	552	0	0	0	1	0	1	0	0	0	1	-2	2	1	1	1	0	1	0	1	1	1	0	471	Data	60
94	560	0	0	0	0	1	1	0	0	0	1	-2	2	1	1	1	1	0	0	1	1	1	0	463	Data	61
95	577	1	0	0	0	0	0	1	0	0	1	-2	2	0	1	1	1	1	1	0	1	1	0	446	Data	62
96	578	0	1	0	0	0	0	1	0	0	1	-2	2	1	0	1	1	1	1	0	1	1	0	445	Data	63
97	580	0	0	1	0	0	0	1	0	0	1	-2	2	1	1	0	1	1	1	0	1	1	0	443	Data	64
98	584	0	0	0	1	0	0	1	0	0	1	-2	2	1	1	1	0	1	1	0	1	1	0	439	Data	65
99	592	0	0	0	0	1	0	1	0	0	1	-2	2	1	1	1	1	0	1	0	1	1	0	431	Data	66
100	608	0	0	0	0	0	1	1	0	0	1	-2	2	1	1	1	1	1	0	0	1	1	0	415	Data	67
101	641	1	0	0	0	0	0	0	1	0	1	-2	2	0	1	1	1	1	1	1	0	1	0	382	Data	68
102	642	0	1	0	0	0	0	0	1	0	1	-2	2	1	0	1	1	1	1	1	0	1	0	381	Data	69
103	644	0	0	1	0	0	0	0	1	0	1	-2	2	1	1	0	1	1	1	1	0	1	0	379	Data	70
104	648	0	0	0	1	0	0	0	1	0	1	-2	2	1	1	1	0	1	1	1	0	1	0	375	Data	71
105	656	0	0	0	0	1	0	0	1	0	1	-2	2	1	1	1	1	0	1	1	0	1	0	367	Data	72
106	672	0	0	0	0	0	1	0	1	0	1	-2	2	1	1	1	1	1	0	1	0	1	0	351	Data	73
107	769	1	0	0	0	0	0	0	0	1	1	-2	2	0	1	1	1	1	1	1	1	0	0	254	Data	74
108	770	0	1	0	0	0	0	0	0	1	1	-2	2	1	0	1	1	1	1	1	1	0	0	253	Data	75
109	772	0	0	1	0	0	0	0	0	1	1	-2	2	1	1	0	1	1	1	1	1	0	0	251	Data	76
110	776	0	0	0	1	0	0	0	0	1	1	-2	2	1	1	1	0	1	1	1	1	0	0	247	Data	77
111	784	0	0	0	0	1	0	0	0	1	1	-2	2	1	1	1	1	0	1	1	1	0	0	239	Data	78
112	800	0	0	0	0	0	1	0	0	1	1	-2	2	1	1	1	1	1	0	1	1	0	0	223	Data	79
113	23	1	1	1	0	1	0	0	0	0	0	-1	1	0	0	0	1	0	1	1	1	1	1	1000	Reserved	
114	27	1	1	0	1	1	0	0	0	0	0	-1	1	0	0	1	0	0	1	1	1	1	1	996	Reserved	
115	29	1	0	1	1	1	0	0	0	0	0	-1	1	0	1	0	0	0	1	1	1	1	1	994	Data	80
116	30	0	1	1	1	1	0	0	0	0	0	-1	1	1	0	0	0	0	1	1	1	1	1	993	Data	81

	Data Pattern												Complement of the Data Pattern												
		Place Value of Each Bit											Place Value of Each Bit												
Codepoint Number	Decimal Format	1	2	4	8	16	32	64	128	256	512	Negative Disparity	Positive Disparity	1	2	4	8	16	32	64	128	256	512	Decimal Format	Description	Value
117	39	1	1	1	0	0	1	0	0	0	0	-1	1	0	0	0	1	1	0	1	1	1	1	984	Data	82
118	43	1	1	0	1	0	1	0	0	0	0	-1	1	0	0	1	0	1	0	1	1	1	1	980	Data	83
119	45	1	0	1	1	0	1	0	0	0	0	-1	1	0	1	0	0	1	0	1	1	1	1	978	Data	84
120	46	0	1	1	1	0	1	0	0	0	0	-1	1	1	0	0	0	1	0	1	1	1	1	977	Data	85
121	51	1	1	0	0	1	1	0	0	0	0	-1	1	0	0	1	1	0	0	1	1	1	1	972	Reserved	
122	53	1	0	1	0	1	1	0	0	0	0	-1	1	0	1	0	1	0	0	1	1	1	1	970	Data	86
123	54	0	1	1	0	1	1	0	0	0	0	-1	1	1	0	0	1	0	0	1	1	1	1	969	Data	87
124	57	1	0	0	1	1	1	0	0	0	0	-1	1	0	1	1	0	0	0	1	1	1	1	966	Data	88
125	58	0	1	0	1	1	1	0	0	0	0	-1	1	1	0	1	0	0	0	1	1	1	1	965	Data	89
126	60	0	0	1	1	1	1	0	0	0	0	-1	1	1	1	0	0	0	0	1	1	1	1	963	Data	90
127	71	1	1	1	0	0	0	1	0	0	0	-1	1	0	0	0	1	1	1	0	1	1	1	952	Data	91
128	75	1	1	0	1	0	0	1	0	0	0	-1	1	0	0	1	0	1	1	0	1	1	1	948	Data	92
129	77	1	0	1	1	0	0	1	0	0	0	-1	1	0	1	0	0	1	1	0	1	1	1	946	Data	93
130	78	0	1	1	1	0	0	1	0	0	0	-1	1	1	0	0	0	1	1	0	1	1	1	945	Data	94
131	83	1	1	0	0	1	0	1	0	0	0	-1	1	0	0	1	1	0	1	0	1	1	1	940	Reserved	
132	85	1	0	1	0	1	0	1	0	0	0	-1	1	0	1	0	1	0	1	0	1	1	1	938	Data	95
133	86	0	1	1	0	1	0	1	0	0	0	-1	1	1	0	0	1	0	1	0	1	1	1	937	Data	96
134	89	1	0	0	1	1	0	1	0	0	0	-1	1	0	1	1	0	0	1	0	1	1	1	934	Data	97
135	90	0	1	0	1	1	0	1	0	0	0	-1	1	1	0	1	0	0	1	0	1	1	1	933	Data	98
136	92	0	0	1	1	1	0	1	0	0	0	-1	1	1	1	0	0	0	1	0	1	1	1	931	Data	99
137	99	1	1	0	0	0	1	1	0	0	0	-1	1	0	0	1	1	1	0	0	1	1	1	924	Data	100
138	101	1	0	1	0	0	1	1	0	0	0	-1	1	0	1	0	1	1	0	0	1	1	1	922	Data	101
139	102	0	1	1	0	0	1	1	0	0	0	-1	1	1	0	0	1	1	0	0	1	1	1	921	Data	102
140	105	1	0	0	1	0	1	1	0	0	0	-1	1	0	1	1	0	1	0	0	1	1	1	918	Data	103
141	106	0	1	0	1	0	1	1	0	0	0	-1	1	1	0	1	0	1	0	0	1	1	1	917	Data	104
142	108	0	0	1	1	0	1	1	0	0	0	-1	1	1	1	0	0	1	0	0	1	1	1	915	Data	105
143	113	1	0	0	0	1	1	1	0	0	0	-1	1	0	1	1	1	0	0	0	1	1	1	910	Data	106
144	114	0	1	0	0	1	1	1	0	0	0	-1	1	1	0	1	1	0	0	0	1	1	1	909	Data	107
145	116	0	0	1	0	1	1	1	0	0	0	-1	1	1	1	0	1	0	0	0	1	1	1	907	Data	108

	Data Pattern												Complement of the Data Pattern													
		Place Value of Each Bit												Place Value of Each Bit												
Codepoint Number	Decimal Format	1	2	4	8	16	32	64	128	256	512	Negative Disparity	Positive Disparity	1	2	4	8	16	32	64	128	256	512	Decimal Format	Description	Value
146	120	0	0	0	1	1	1	1	0	0	0	-1	1	1	1	1	0	0	0	0	1	1	1	903	Data	109
147	135	1	1	1	0	0	0	0	1	0	0	-1	1	0	0	0	1	1	1	1	0	1	1	888	Data	110
148	139	1	1	0	1	0	0	0	1	0	0	-1	1	0	0	1	0	1	1	1	0	1	1	884	Data	111
149	141	1	0	1	1	0	0	0	1	0	0	-1	1	0	1	0	0	1	1	1	0	1	1	882	Data	112
150	142	0	1	1	1	0	0	0	1	0	0	-1	1	1	0	0	0	1	1	1	0	1	1	881	Data	113
151	147	1	1	0	0	1	0	0	1	0	0	-1	1	0	0	1	1	0	1	1	0	1	1	876	Reserved	
152	149	1	0	1	0	1	0	0	1	0	0	-1	1	0	1	0	1	0	1	1	0	1	1	874	Data	114
153	150	0	1	1	0	1	0	0	1	0	0	-1	1	1	0	0	1	0	1	1	0	1	1	873	Data	115
154	153	1	0	0	1	1	0	0	1	0	0	-1	1	0	1	1	0	0	1	1	0	1	1	870	Data	116
155	154	0	1	0	1	1	0	0	1	0	0	-1	1	1	0	1	0	0	1	1	0	1	1	869	Data	117
156	156	0	0	1	1	1	0	0	1	0	0	-1	1	1	1	0	0	0	1	1	0	1	1	867	Data	118
157	163	1	1	0	0	0	1	0	1	0	0	-1	1	0	0	1	1	1	0	1	0	1	1	860	Data	119
158	165	1	0	1	0	0	1	0	1	0	0	-1	1	0	1	0	1	1	0	1	0	1	1	858	Data	120
159	166	0	1	1	0	0	1	0	1	0	0	-1	1	1	0	0	1	1	0	1	0	1	1	857	Data	121
160	169	1	0	0	1	0	1	0	1	0	0	-1	1	0	1	1	0	1	0	1	0	1	1	854	Data	122
161	170	0	1	0	1	0	1	0	1	0	0	-1	1	1	0	1	0	1	0	1	0	1	1	853	Data	123
162	172	0	0	1	1	0	1	0	1	0	0	-1	1	1	1	0	0	1	0	1	0	1	1	851	Data	124
163	177	1	0	0	0	1	1	0	1	0	0	-1	1	0	1	1	1	0	0	1	0	1	1	846	Data	125
164	178	0	1	0	0	1	1	0	1	0	0	-1	1	1	0	1	1	0	0	1	0	1	1	845	Data	126
165	180	0	0	1	0	1	1	0	1	0	0	-1	1	1	1	0	1	0	0	1	0	1	1	843	Data	127
166	184	0	0	0	1	1	1	0	1	0	0	-1	1	1	1	1	0	0	0	1	0	1	1	839	Data	128
167	195	1	1	0	0	0	0	1	1	0	0	-1	1	0	0	1	1	1	1	0	0	1	1	828	Data	129
168	197	1	0	1	0	0	0	1	1	0	0	-1	1	0	1	0	1	1	1	0	0	1	1	826	Data	130
169	198	0	1	1	0	0	0	1	1	0	0	-1	1	1	0	0	1	1	1	0	0	1	1	825	Data	131
170	201	1	0	0	1	0	0	1	1	0	0	-1	1	0	1	1	0	1	1	0	0	1	1	822	Data	132
171	202	0	1	0	1	0	0	1	1	0	0	-1	1	1	0	1	0	1	1	0	0	1	1	821	Data	133
172	204	0	0	1	1	0	0	1	1	0	0	-1	1	1	1	0	0	1	1	0	0	1	1	819	Data	134
173	209	1	0	0	0	1	0	1	1	0	0	-1	1	0	1	1	1	0	1	0	0	1	1	814	Data	135
174	210	0	1	0	0	1	0	1	1	0	0	-1	1	1	0	1	1	0	1	0	0	1	1	813	Data	136

	Data Pattern												Complement of the Data Pattern													
		Place Value of Each Bit												Place Value of Each Bit												
Codepoint Number	**Decimal Format**	**1**	**2**	**4**	**8**	**16**	**32**	**64**	**128**	**256**	**512**	**Negative Disparity**	**Positive Disparity**	**1**	**2**	**4**	**8**	**16**	**32**	**64**	**128**	**256**	**512**	**Decimal Format**	**Description**	**Value**
175	212	0	0	1	0	1	0	1	1	0	0	-1	1	1	1	0	1	0	1	0	0	1	1	811	Data	137
176	216	0	0	0	1	1	0	1	1	0	0	-1	1	1	1	1	0	0	1	0	0	1	1	807	Data	138
177	225	1	0	0	0	0	1	1	1	0	0	-1	1	0	1	1	1	1	0	0	0	1	1	798	Data	139
178	226	0	1	0	0	0	1	1	1	0	0	-1	1	1	0	1	1	1	0	0	0	1	1	797	Data	140
179	228	0	0	1	0	0	1	1	1	0	0	-1	1	1	1	0	1	1	0	0	0	1	1	795	Data	141
180	232	0	0	0	1	0	1	1	1	0	0	-1	1	1	1	1	0	1	0	0	0	1	1	791	Data	142
181	240	0	0	0	0	1	1	1	1	0	0	-1	1	1	1	1	1	0	0	0	0	1	1	783	Data	143
182	263	1	1	1	0	0	0	0	0	1	0	-1	1	0	0	0	1	1	1	1	1	0	1	760	Data	144
183	267	1	1	0	1	0	0	0	0	1	0	-1	1	0	0	1	0	1	1	1	1	0	1	756	Data	145
184	269	1	0	1	1	0	0	0	0	1	0	-1	1	0	1	0	0	1	1	1	1	0	1	754	Data	146
185	270	0	1	1	1	0	0	0	0	1	0	-1	1	1	0	0	0	1	1	1	1	0	1	753	Data	147
186	275	1	1	0	0	1	0	0	0	1	0	-1	1	0	0	1	1	0	1	1	1	0	1	748	Reserved	
187	277	1	0	1	0	1	0	0	0	1	0	-1	1	0	1	0	1	0	1	1	1	0	1	746	Data	148
188	278	0	1	1	0	1	0	0	0	1	0	-1	1	1	0	0	1	0	1	1	1	0	1	745	Data	149
189	281	1	0	0	1	1	0	0	0	1	0	-1	1	0	1	1	0	0	1	1	1	0	1	742	Data	150
190	282	0	1	0	1	1	0	0	0	1	0	-1	1	1	0	1	0	0	1	1	1	0	1	741	Data	151
191	284	0	0	1	1	1	0	0	0	1	0	-1	1	1	1	0	0	0	1	1	1	0	1	739	Data	152
192	291	1	1	0	0	0	1	0	0	1	0	-1	1	0	0	1	1	1	0	1	1	0	1	732	Data	153
193	293	1	0	1	0	0	1	0	0	1	0	-1	1	0	1	0	1	1	0	1	1	0	1	730	Data	154
194	294	0	1	1	0	0	1	0	0	1	0	-1	1	1	0	0	1	1	0	1	1	0	1	729	Data	155
195	297	1	0	0	1	0	1	0	0	1	0	-1	1	0	1	1	0	1	0	1	1	0	1	726	Data	156
196	298	0	1	0	1	0	1	0	0	1	0	-1	1	1	0	1	0	1	0	1	1	0	1	725	Data	157
197	300	0	0	1	1	0	1	0	0	1	0	-1	1	1	1	0	0	1	0	1	1	0	1	723	Data	158
198	305	1	0	0	0	1	1	0	0	1	0	-1	1	0	1	1	1	0	0	1	1	0	1	718	Data	159
199	306	0	1	0	0	1	1	0	0	1	0	-1	1	1	0	1	1	0	0	1	1	0	1	717	Data	160
200	308	0	0	1	0	1	1	0	0	1	0	-1	1	1	1	0	1	0	0	1	1	0	1	715	Data	161
201	312	0	0	0	1	1	1	0	0	1	0	-1	1	1	1	1	0	0	0	1	1	0	1	711	Data	162
202	323	1	1	0	0	0	0	1	0	1	0	-1	1	0	0	1	1	1	1	0	1	0	1	700	Data	163
203	325	1	0	1	0	0	0	1	0	1	0	-1	1	0	1	0	1	1	1	0	1	0	1	698	Data	164
204	326	0	1	1	0	0	0	1	0	1	0	-1	1	1	0	0	1	1	1	0	1	0	1	697	Data	165

	Data Pattern												Complement of the Data Pattern												
		Place Value of Each Bit												Place Value of Each Bit											
Codepoint Number	Decimal Format	1	2	4	8	16	32	64	128	256	512	Negative Disparity	Positive Disparity	1	2	4	8	16	32	64	128	256	512	Decimal Format	Description	Value
205	329	1	0	0	1	0	0	1	0	1	0	-1	1	0	1	1	0	1	1	0	1	0	1	694	Data	166
206	330	0	1	0	1	0	0	1	0	1	0	-1	1	1	0	1	0	1	1	0	1	0	1	693	Data	167
207	332	0	0	1	1	0	0	1	0	1	0	-1	1	1	1	0	0	1	1	0	1	0	1	691	Data	168
208	337	1	0	0	0	1	0	1	0	1	0	-1	1	0	1	1	1	0	1	0	1	0	1	686	Data	169
209	338	0	1	0	0	1	0	1	0	1	0	-1	1	1	0	1	1	0	1	0	1	0	1	685	Data	170
210	340	0	0	1	0	1	0	1	0	1	0	-1	1	1	1	0	1	0	1	0	1	0	1	683	Data	171
211	344	0	0	0	1	1	0	1	0	1	0	-1	1	1	1	1	0	0	1	0	1	0	1	679	Data	172
212	353	1	0	0	0	0	1	1	0	1	0	-1	1	0	1	1	1	1	0	0	1	0	1	670	Data	173
213	354	0	1	0	0	0	1	1	0	1	0	-1	1	1	0	1	1	1	0	0	1	0	1	669	Data	174
214	356	0	0	1	0	0	1	1	0	1	0	-1	1	1	1	0	1	1	0	0	1	0	1	667	Data	175
215	360	0	0	0	1	0	1	1	0	1	0	-1	1	1	1	1	0	1	0	0	1	0	1	663	Data	176
216	368	0	0	0	0	1	1	1	0	1	0	-1	1	1	1	1	1	0	0	0	1	0	1	655	Data	177
217	387	1	1	0	0	0	0	0	1	1	0	-1	1	0	0	1	1	1	1	1	0	0	1	636	Data	178
218	389	1	0	1	0	0	0	0	1	1	0	-1	1	0	1	0	1	1	1	1	0	0	1	634	Data	179
219	390	0	1	1	0	0	0	0	1	1	0	-1	1	1	0	0	1	1	1	1	0	0	1	633	Data	180
220	393	1	0	0	1	0	0	0	1	1	0	-1	1	0	1	1	0	1	1	1	0	0	1	630	Data	181
221	394	0	1	0	1	0	0	0	1	1	0	-1	1	1	0	1	0	1	1	1	0	0	1	629	Data	182
222	396	0	0	1	1	0	0	0	1	1	0	-1	1	1	1	0	0	1	1	1	0	0	1	627	Data	183
223	401	1	0	0	0	1	0	0	1	1	0	-1	1	0	1	1	1	0	1	1	0	0	1	622	Data	184
224	402	0	1	0	0	1	0	0	1	1	0	-1	1	1	0	1	1	0	1	1	0	0	1	621	Data	185
225	404	0	0	1	0	1	0	0	1	1	0	-1	1	1	1	0	1	0	1	1	0	0	1	619	Data	186
226	408	0	0	0	1	1	0	0	1	1	0	-1	1	1	1	1	0	0	1	1	0	0	1	615	Data	187
227	417	1	0	0	0	0	1	0	1	1	0	-1	1	0	1	1	1	1	0	1	0	0	1	606	Data	188
228	418	0	1	0	0	0	1	0	1	1	0	-1	1	1	0	1	1	1	0	1	0	0	1	605	Data	189
229	420	0	0	1	0	0	1	0	1	1	0	-1	1	1	1	0	1	1	0	1	0	0	1	603	Data	190
230	424	0	0	0	1	0	1	0	1	1	0	-1	1	1	1	1	0	1	0	1	0	0	1	599	Data	191
231	432	0	0	0	0	1	1	0	1	1	0	-1	1	1	1	1	1	0	0	1	0	0	1	591	Data	192
232	449	1	0	0	0	0	0	1	1	1	0	-1	1	0	1	1	1	1	1	0	0	0	1	574	Data	193
233	450	0	1	0	0	0	0	1	1	1	0	-1	1	1	0	1	1	1	1	0	0	0	1	573	Data	194

	Data Pattern												Complement of the Data Pattern												
		Place Value of Each Bit												Place Value of Each Bit											
Codepoint Number	Decimal Format	1	2	4	8	16	32	64	128	256	512	Negative Disparity	Positive Disparity	1	2	4	8	16	32	64	128	256	512	Decimal Format	Description	Value
234	452	0	0	1	0	0	0	1	1	1	0	-1	1	1	1	0	1	1	1	0	0	0	1	571	Data	195
235	456	0	0	0	1	0	0	1	1	1	0	-1	1	1	1	1	0	1	1	0	0	0	1	567	Data	196
236	464	0	0	0	0	1	0	1	1	1	0	-1	1	1	1	1	1	0	1	0	0	0	1	559	Data	197
237	480	0	0	0	0	0	1	1	1	1	0	-1	1	1	1	1	1	1	0	0	0	0	1	543	Data	198
238	519	1	1	1	0	0	0	0	0	0	1	-1	1	0	0	0	1	1	1	1	1	1	0	504	Data	199
239	523	1	1	0	1	0	0	0	0	0	1	-1	1	0	0	1	0	1	1	1	1	1	0	500	Data	200
240	525	1	0	1	1	0	0	0	0	0	1	-1	1	0	1	0	0	1	1	1	1	1	0	498	Data	201
241	526	0	1	1	1	0	0	0	0	0	1	-1	1	1	0	0	0	1	1	1	1	1	0	497	Data	202
242	531	1	1	0	0	1	0	0	0	0	1	-1	1	0	0	1	1	0	1	1	1	1	0	492	Reserved	
243	533	1	0	1	0	1	0	0	0	0	1	-1	1	0	1	0	1	0	1	1	1	1	0	490	Data	203
244	534	0	1	1	0	1	0	0	0	0	1	-1	1	1	0	0	1	0	1	1	1	1	0	489	Data	204
245	537	1	0	0	1	1	0	0	0	0	1	-1	1	0	1	1	0	0	1	1	1	1	0	486	Data	205
246	538	0	1	0	1	1	0	0	0	0	1	-1	1	1	0	1	0	0	1	1	1	1	0	485	Data	206
247	540	0	0	1	1	1	0	0	0	0	1	-1	1	1	1	0	0	0	1	1	1	1	0	483	Data	207
248	547	1	1	0	0	0	1	0	0	0	1	-1	1	0	0	1	1	1	0	1	1	1	0	476	Data	208
249	549	1	0	1	0	0	1	0	0	0	1	-1	1	0	1	0	1	1	0	1	1	1	0	474	Data	209
250	550	0	1	1	0	0	1	0	0	0	1	-1	1	1	0	0	1	1	0	1	1	1	0	473	Data	210
251	553	1	0	0	1	0	1	0	0	0	1	-1	1	0	1	1	0	1	0	1	1	1	0	470	Data	211
252	554	0	1	0	1	0	1	0	0	0	1	-1	1	1	0	1	0	1	0	1	1	1	0	469	Data	212
253	556	0	0	1	1	0	1	0	0	0	1	-1	1	1	1	0	0	1	0	1	1	1	0	467	Data	213
254	561	1	0	0	0	1	1	0	0	0	1	-1	1	0	1	1	1	0	0	1	1	1	0	462	Data	214
255	562	0	1	0	0	1	1	0	0	0	1	-1	1	1	0	1	1	0	0	1	1	1	0	461	Data	215
256	564	0	0	1	0	1	1	0	0	0	1	-1	1	1	1	0	1	0	0	1	1	1	0	459	Data	216
257	568	0	0	0	1	1	1	0	0	0	1	-1	1	1	1	1	0	0	0	1	1	1	0	455	Data	217
258	579	1	1	0	0	0	0	1	0	0	1	-1	1	0	0	1	1	1	1	0	1	1	0	444	Data	218
259	581	1	0	1	0	0	0	1	0	0	1	-1	1	0	1	0	1	1	1	0	1	1	0	442	Data	219
260	582	0	1	1	0	0	0	1	0	0	1	-1	1	1	0	0	1	1	1	0	1	1	0	441	Data	220
261	585	1	0	0	1	0	0	1	0	0	1	-1	1	0	1	1	0	1	1	0	1	1	0	438	Data	221
262	586	0	1	0	1	0	0	1	0	0	1	-1	1	1	0	1	0	1	1	0	1	1	0	437	Data	222
263	588	0	0	1	1	0	0	1	0	0	1	-1	1	1	1	0	0	1	1	0	1	1	0	435	Data	223

	Data Pattern													Complement of the Data Pattern													
		Place Value of Each Bit													Place Value of Each Bit												
Codepoint Number	Decimal Format	1	2	4	8	16	32	64	128	256	512	Negative Disparity	Positive Disparity	1	2	4	8	16	32	64	128	256	512	Decimal Format	Description	Value
264	593	1	0	0	0	1	0	1	0	0	1	-1	1	0	1	1	1	0	1	0	1	1	0	430	Data	224
265	594	0	1	0	0	1	0	1	0	0	1	-1	1	1	0	1	1	0	1	0	1	1	0	429	Data	225
266	596	0	0	1	0	1	0	1	0	0	1	-1	1	1	1	0	1	0	1	0	1	1	0	427	Data	226
267	600	0	0	0	1	1	0	1	0	0	1	-1	1	1	1	1	0	0	1	0	1	1	0	423	Data	227
268	609	1	0	0	0	0	1	1	0	0	1	-1	1	0	1	1	1	1	0	0	1	1	0	414	Data	228
269	610	0	1	0	0	0	1	1	0	0	1	-1	1	1	0	1	1	1	0	0	1	1	0	413	Data	229
270	612	0	0	1	0	0	1	1	0	0	1	-1	1	1	1	0	1	1	0	0	1	1	0	411	Data	230
271	616	0	0	0	1	0	1	1	0	0	1	-1	1	1	1	1	0	1	0	0	1	1	0	407	Data	231
272	624	0	0	0	0	1	1	1	0	0	1	-1	1	1	1	1	1	0	0	0	1	1	0	399	Data	232
273	643	1	1	0	0	0	0	0	1	0	1	-1	1	0	0	1	1	1	1	1	0	1	0	380	Data	233
274	645	1	0	1	0	0	0	0	1	0	1	-1	1	0	1	0	1	1	1	1	0	1	0	378	Data	234
275	646	0	1	1	0	0	0	0	1	0	1	-1	1	1	0	0	1	1	1	1	0	1	0	377	Data	235
276	649	1	0	0	1	0	0	0	1	0	1	-1	1	0	1	1	0	1	1	1	0	1	0	374	Data	236
277	650	0	1	0	1	0	0	0	1	0	1	-1	1	1	0	1	0	1	1	1	0	1	0	373	Data	237
278	652	0	0	1	1	0	0	0	1	0	1	-1	1	1	1	0	0	1	1	1	0	1	0	371	Data	238
279	657	1	0	0	0	1	0	0	1	0	1	-1	1	0	1	1	1	0	1	1	0	1	0	366	Data	239
280	658	0	1	0	0	1	0	0	1	0	1	-1	1	1	0	1	1	0	1	1	0	1	0	365	Data	240
281	660	0	0	1	0	1	0	0	1	0	1	-1	1	1	1	0	1	0	1	1	0	1	0	363	Data	241
282	664	0	0	0	1	1	0	0	1	0	1	-1	1	1	1	1	0	0	1	1	0	1	0	359	Data	242
283	673	1	0	0	0	0	1	0	1	0	1	-1	1	0	1	1	1	1	0	1	0	1	0	350	Data	243
284	674	0	1	0	0	0	1	0	1	0	1	-1	1	1	0	1	1	1	0	1	0	1	0	349	Data	244
285	676	0	0	1	0	0	1	0	1	0	1	-1	1	1	1	0	1	1	0	1	0	1	0	347	Data	245
286	680	0	0	0	1	0	1	0	1	0	1	-1	1	1	1	1	0	1	0	1	0	1	0	343	Data	246
287	688	0	0	0	0	1	1	0	1	0	1	-1	1	1	1	1	1	0	0	1	0	1	0	335	Data	247
288	705	1	0	0	0	0	0	1	1	0	1	-1	1	0	1	1	1	1	1	0	0	1	0	318	Data	248
289	706	0	1	0	0	0	0	1	1	0	1	-1	1	1	0	1	1	1	1	0	0	1	0	317	Data	249
290	708	0	0	1	0	0	0	1	1	0	1	-1	1	1	1	0	1	1	1	0	0	1	0	315	Data	250
291	712	0	0	0	1	0	0	1	1	0	1	-1	1	1	1	1	0	1	1	0	0	1	0	311	Data	251
292	720	0	0	0	0	1	0	1	1	0	1	-1	1	1	1	1	1	0	1	0	0	1	0	303	Data	252
293	736	0	0	0	0	0	1	1	1	0	1	-1	1	1	1	1	1	1	0	0	0	1	0	287	Data	253

	Data Pattern												Complement of the Data Pattern													
		Place Value of Each Bit												Place Value of Each Bit												
Codepoint Number	Decimal Format	1	2	4	8	16	32	64	128	256	512	Negative Disparity	Positive Disparity	1	2	4	8	16	32	64	128	256	512	Decimal Format	Description	Value
294	771	1	1	0	0	0	0	0	0	1	1	-1	1	0	0	1	1	1	1	1	1	0	0	252	Data	254
295	773	1	0	1	0	0	0	0	0	1	1	-1	1	0	1	0	1	1	1	1	1	0	0	250	Data	255
296	774	0	1	1	0	0	0	0	0	1	1	-1	1	1	0	0	1	1	1	1	1	0	0	249	Data	256
297	777	1	0	0	1	0	0	0	0	1	1	-1	1	0	1	1	0	1	1	1	1	0	0	246	Data	257
298	778	0	1	0	1	0	0	0	0	1	1	-1	1	1	0	1	0	1	1	1	1	0	0	245	Data	258
299	780	0	0	1	1	0	0	0	0	1	1	-1	1	1	1	0	0	1	1	1	1	0	0	243	Data	259
300	785	1	0	0	0	1	0	0	0	1	1	-1	1	0	1	1	1	0	1	1	1	0	0	238	Data	260
301	786	0	1	0	0	1	0	0	0	1	1	-1	1	1	0	1	1	0	1	1	1	0	0	237	Data	261
302	788	0	0	1	0	1	0	0	0	1	1	-1	1	1	1	0	1	0	1	1	1	0	0	235	Data	262
303	792	0	0	0	1	1	0	0	0	1	1	-1	1	1	1	1	0	0	1	1	1	0	0	231	Data	263
304	801	1	0	0	0	0	1	0	0	1	1	-1	1	0	1	1	1	1	0	1	1	0	0	222	Data	264
305	802	0	1	0	0	0	1	0	0	1	1	-1	1	1	0	1	1	1	0	1	1	0	0	221	Data	265
306	804	0	0	1	0	0	1	0	0	1	1	-1	1	1	1	0	1	1	0	1	1	0	0	219	Data	266
307	808	0	0	0	1	0	1	0	0	1	1	-1	1	1	1	1	0	1	0	1	1	0	0	215	Data	267
308	816	0	0	0	0	1	1	0	0	1	1	-1	1	1	1	1	1	0	0	1	1	0	0	207	Data	268
309	833	1	0	0	0	0	0	1	0	1	1	-1	1	0	1	1	1	1	1	0	1	0	0	190	Data	269
310	834	0	1	0	0	0	0	1	0	1	1	-1	1	1	0	1	1	1	1	0	1	0	0	189	Data	270
311	836	0	0	1	0	0	0	1	0	1	1	-1	1	1	1	0	1	1	1	0	1	0	0	187	Data	271
312	840	0	0	0	1	0	0	1	0	1	1	-1	1	1	1	1	0	1	1	0	1	0	0	183	Data	272
313	848	0	0	0	0	1	0	1	0	1	1	-1	1	1	1	1	1	0	1	0	1	0	0	175	Data	273
314	864	0	0	0	0	0	1	1	0	1	1	-1	1	1	1	1	1	1	0	0	1	0	0	159	Data	274
315	897	1	0	0	0	0	0	0	1	1	1	-1	1	0	1	1	1	1	1	1	0	0	0	126	Data	275
316	898	0	1	0	0	0	0	0	1	1	1	-1	1	1	0	1	1	1	1	1	0	0	0	125	Data	276
317	900	0	0	1	0	0	0	0	1	1	1	-1	1	1	1	0	1	1	1	1	0	0	0	123	Data	277
318	904	0	0	0	1	0	0	0	1	1	1	-1	1	1	1	1	0	1	1	1	0	0	0	119	Data	278
319	912	0	0	0	0	1	0	0	1	1	1	-1	1	1	1	1	1	0	1	1	0	0	0	111	Data	279
320	928	0	0	0	0	0	1	0	1	1	1	-1	1	1	1	1	1	1	0	1	0	0	0	95	Data	280
321	31	1	1	1	1	1	0	0	0	0	0	0	N/A												Reserved	
322	47	1	1	1	1	0	1	0	0	0	0	0	N/A												Data	281
323	55	1	1	1	0	1	1	0	0	0	0	0	N/A												Reserved	

	Data Pattern												Complement of the Data Pattern													
		Place Value of Each Bit												Place Value of Each Bit												
Codepoint Number	Decimal Format	1	2	4	8	16	32	64	128	256	512	Negative Disparity	Positive Disparity	1	2	4	8	16	32	64	128	256	512	Decimal Format	Description	Value
324	59	1	1	0	1	1	1	0	0	0	0	0	N/A												Reserved	
325	61	1	0	1	1	1	1	0	0	0	0	0	N/A												Data	282
326	62	0	1	1	1	1	1	0	0	0	0	0	N/A												Data	283
327	79	1	1	1	1	0	0	1	0	0	0	0	N/A												Data	284
328	87	1	1	1	0	1	0	1	0	0	0	0	N/A												Reserved	
329	91	1	1	0	1	1	0	1	0	0	0	0	N/A												Reserved	
330	93	1	0	1	1	1	0	1	0	0	0	0	N/A												Data	285
331	94	0	1	1	1	1	0	1	0	0	0	0	N/A												Data	286
332	103	1	1	1	0	0	1	1	0	0	0	0	N/A												Data	287
333	107	1	1	0	1	0	1	1	0	0	0	0	N/A												Data	288
334	109	1	0	1	1	0	1	1	0	0	0	0	N/A												Data	289
335	110	0	1	1	1	0	1	1	0	0	0	0	N/A												Data	290
336	115	1	1	0	0	1	1	1	0	0	0	0	N/A												Reserved	
337	117	1	0	1	0	1	1	1	0	0	0	0	N/A												Data	291
338	118	0	1	1	0	1	1	1	0	0	0	0	N/A												Data	292
339	121	1	0	0	1	1	1	1	0	0	0	0	N/A												Data	293
340	122	0	1	0	1	1	1	1	0	0	0	0	N/A												Data	294
341	124	0	0	1	1	1	1	1	0	0	0	0	N/A												Data	295
342	143	1	1	1	1	0	0	0	1	0	0	0	N/A												Data	296
343	151	1	1	1	0	1	0	0	1	0	0	0	N/A												Reserved	
344	155	1	1	0	1	1	0	0	1	0	0	0	N/A												Reserved	
345	157	1	0	1	1	1	0	0	1	0	0	0	N/A												Data	297
346	158	0	1	1	1	1	0	0	1	0	0	0	N/A												Data	298
347	167	1	1	1	0	0	1	0	1	0	0	0	N/A												Data	299
348	171	1	1	0	1	0	1	0	1	0	0	0	N/A												Data	300
349	173	1	0	1	1	0	1	0	1	0	0	0	N/A												Data	301
350	174	0	1	1	1	0	1	0	1	0	0	0	N/A												Data	302
351	179	1	1	0	0	1	1	0	1	0	0	0	N/A												Reserved	
352	181	1	0	1	0	1	1	0	1	0	0	0	N/A												Data	303
353	182	0	1	1	0	1	1	0	1	0	0	0	N/A												Data	304

	Data Pattern												Complement of the Data Pattern													
		Place Value of Each Bit												Place Value of Each Bit												
Codepoint Number	Decimal Format	1	2	4	8	16	32	64	128	256	512	Negative Disparity	Positive Disparity	1	2	4	8	16	32	64	128	256	512	Decimal Format	Description	Value
354	185	1	0	0	1	1	1	0	1	0	0	0	N/A												Data	305
355	186	0	1	0	1	1	1	0	1	0	0	0	N/A												Data	306
356	188	0	0	1	1	1	1	0	1	0	0	0	N/A												Data	307
357	199	1	1	1	0	0	0	1	1	0	0	0	N/A												Data	308
358	203	1	1	0	1	0	0	1	1	0	0	0	N/A												Data	309
359	205	1	0	1	1	0	0	1	1	0	0	0	N/A												Data	310
360	206	0	1	1	1	0	0	1	1	0	0	0	N/A												Data	311
361	211	1	1	0	0	1	0	1	1	0	0	0	N/A												Reserved	
362	213	1	0	1	0	1	0	1	1	0	0	0	N/A												Data	312
363	214	0	1	1	0	1	0	1	1	0	0	0	N/A												Data	313
364	217	1	0	0	1	1	0	1	1	0	0	0	N/A												Data	314
365	218	0	1	0	1	1	0	1	1	0	0	0	N/A												Data	315
366	220	0	0	1	1	1	0	1	1	0	0	0	N/A												Data	316
367	227	1	1	0	0	0	1	1	1	0	0	0	N/A												Data	317
368	229	1	0	1	0	0	1	1	1	0	0	0	N/A												Data	318
369	230	0	1	1	0	0	1	1	1	0	0	0	N/A												Data	319
370	233	1	0	0	1	0	1	1	1	0	0	0	N/A												Data	320
465	590	0	1	1	1	0	0	1	0	0	1	0	N/A												Data	407
466	595	1	1	0	0	1	0	1	0	0	1	0	N/A												Reserved	
467	597	1	0	1	0	1	0	1	0	0	1	0	N/A												Data	408
468	598	0	1	1	0	1	0	1	0	0	1	0	N/A												Data	409
469	601	1	0	0	1	1	0	1	0	0	1	0	N/A												Data	410
470	602	0	1	0	1	1	0	1	0	0	1	0	N/A												Data	411
471	604	0	0	1	1	1	0	1	0	0	1	0	N/A												Data	412
472	611	1	1	0	0	0	1	1	0	0	1	0	N/A												Data	413
473	613	1	0	1	0	0	1	1	0	0	1	0	N/A												Data	414
474	614	0	1	1	0	0	1	1	0	0	1	0	N/A												Data	415
475	617	1	0	0	1	0	1	1	0	0	1	0	N/A												Data	416
476	618	0	1	0	1	0	1	1	0	0	1	0	N/A												Data	417
477	620	0	0	1	1	0	1	1	0	0	1	0	N/A												Data	418

	Data Pattern												Complement of the Data Pattern													
		Place Value of Each Bit												Place Value of Each Bit												
Codepoint Number	Decimal Format	1	2	4	8	16	32	64	128	256	512	Negative Disparity	Positive Disparity	1	2	4	8	16	32	64	128	256	512	Decimal Format	Description	Value
478	625	1	0	0	0	1	1	1	0	0	1	0	N/A												Data	419
479	626	0	1	0	0	1	1	1	0	0	1	0	N/A												Data	420
480	628	0	0	1	0	1	1	1	0	0	1	0	N/A												Data	421
481	632	0	0	0	1	1	1	1	0	0	1	0	N/A												Data	422
482	647	1	1	1	0	0	0	0	1	0	1	0	N/A												Data	423
483	651	1	1	0	1	0	0	0	1	0	1	0	N/A												Data	424
484	653	1	0	1	1	0	0	0	1	0	1	0	N/A												Data	425
485	654	0	1	1	1	0	0	0	1	0	1	0	N/A												Data	426
486	659	1	1	0	0	1	0	0	1	0	1	0	N/A												Reserved	
487	661	1	0	1	0	1	0	0	1	0	1	0	N/A												Data	427
488	662	0	1	1	0	1	0	0	1	0	1	0	N/A												Data	428
489	665	1	0	0	1	1	0	0	1	0	1	0	N/A												Data	429
490	666	0	1	0	1	1	0	0	1	0	1	0	N/A												Data	430
491	668	0	0	1	1	1	0	0	1	0	1	0	N/A												Data	431
492	675	1	1	0	0	0	1	0	1	0	1	0	N/A												Data	432
493	677	1	0	1	0	0	1	0	1	0	1	0	N/A												Data	433
494	678	0	1	1	0	0	1	0	1	0	1	0	N/A												Data	434
495	681	1	0	0	1	0	1	0	1	0	1	0	N/A												Data	435
496	682	0	1	0	1	0	1	0	1	0	1	0	N/A												Data	436
497	684	0	0	1	1	0	1	0	1	0	1	0	N/A												Data	437
498	689	1	0	0	0	1	1	0	1	0	1	0	N/A												Data	438
499	690	0	1	0	0	1	1	0	1	0	1	0	N/A												Data	439
500	692	0	0	1	0	1	1	0	1	0	1	0	N/A												Data	440
501	696	0	0	0	1	1	1	0	1	0	1	0	N/A												Data	441
502	707	1	1	0	0	0	0	1	1	0	1	0	N/A												Data	442
503	709	1	0	1	0	0	0	1	1	0	1	0	N/A												Data	443
504	710	0	1	1	0	0	0	1	1	0	1	0	N/A												Data	444
505	713	1	0	0	1	0	0	1	1	0	1	0	N/A												Data	445
506	714	0	1	0	1	0	0	1	1	0	1	0	N/A												Data	446
507	716	0	0	1	1	0	0	1	1	0	1	0	N/A												Data	447

	Data Pattern												Complement of the Data Pattern													
		Place Value of Each Bit												Place Value of Each Bit												
Codepoint Number	Decimal Format	1	2	4	8	16	32	64	128	256	512	Negative Disparity	Positive Disparity	1	2	4	8	16	32	64	128	256	512	Decimal Format	Description	Value
508	721	1	0	0	0	1	0	1	1	0	1	0	N/A												Data	448
509	722	0	1	0	0	1	0	1	1	0	1	0	N/A												Data	449
510	724	0	0	1	0	1	0	1	1	0	1	0	N/A												Data	450
511	728	0	0	0	1	1	0	1	1	0	1	0	N/A												Data	451
512	737	1	0	0	0	0	1	1	1	0	1	0	N/A												Data	452
513	738	0	1	0	0	0	1	1	1	0	1	0	N/A												Data	453
514	740	0	0	1	0	0	1	1	1	0	1	0	N/A												Data	454
515	744	0	0	0	1	0	1	1	1	0	1	0	N/A												Data	455
516	752	0	0	0	0	1	1	1	1	0	1	0	N/A												Data	456
517	775	1	1	1	0	0	0	0	0	1	1	0	N/A												Data	457
518	779	1	1	0	1	0	0	0	0	1	1	0	N/A												Data	458
519	781	1	0	1	1	0	0	0	0	1	1	0	N/A												Data	459
520	782	0	1	1	1	0	0	0	0	1	1	0	N/A												Data	460
521	787	1	1	0	0	1	0	0	0	1	1	0	N/A												Reserved	
522	789	1	0	1	0	1	0	0	0	1	1	0	N/A												Data	461
523	790	0	1	1	0	1	0	0	0	1	1	0	N/A												Data	462
524	793	1	0	0	1	1	0	0	0	1	1	0	N/A												Data	463
525	794	0	1	0	1	1	0	0	0	1	1	0	N/A												Data	464
526	796	0	0	1	1	1	0	0	0	1	1	0	N/A												Data	465
527	803	1	1	0	0	0	1	0	0	1	1	0	N/A												Data	466
528	805	1	0	1	0	0	1	0	0	1	1	0	N/A												Data	467
529	806	0	1	1	0	0	1	0	0	1	1	0	N/A												Data	468
530	809	1	0	0	1	0	1	0	0	1	1	0	N/A												Data	469
531	810	0	1	0	1	0	1	0	0	1	1	0	N/A												Data	470
532	812	0	0	1	1	0	1	0	0	1	1	0	N/A												Data	471
533	817	1	0	0	0	1	1	0	0	1	1	0	N/A												Data	472
534	818	0	1	0	0	1	1	0	0	1	1	0	N/A												Data	473
535	820	0	0	1	0	1	1	0	0	1	1	0	N/A												Data	474
536	824	0	0	0	1	1	1	0	0	1	1	0	N/A												Data	475
537	835	1	1	0	0	0	0	1	0	1	1	0	N/A												Data	476

	Data Pattern												Complement of the Data Pattern													
		Place Value of Each Bit												Place Value of Each Bit												
Codepoint Number	Decimal Format	1	2	4	8	16	32	64	128	256	512	Negative Disparity	Positive Disparity	1	2	4	8	16	32	64	128	256	512	Decimal Format	Description	Value
538	837	1	0	1	0	0	0	1	0	1	1	0	N/A												Data	477
539	838	0	1	1	0	0	0	1	0	1	1	0	N/A												Data	478
540	841	1	0	0	1	0	0	1	0	1	1	0	N/A												Data	479
541	842	0	1	0	1	0	0	1	0	1	1	0	N/A												Data	480
542	844	0	0	1	1	0	0	1	0	1	1	0	N/A												Data	481
543	849	1	0	0	0	1	0	1	0	1	1	0	N/A												Data	482
544	850	0	1	0	0	1	0	1	0	1	1	0	N/A												Data	483
545	852	0	0	1	0	1	0	1	0	1	1	0	N/A												Data	484
546	856	0	0	0	1	1	0	1	0	1	1	0	N/A												Data	485
547	865	1	0	0	0	0	1	1	0	1	1	0	N/A												Data	486
548	866	0	1	0	0	0	1	1	0	1	1	0	N/A												Data	487
549	868	0	0	1	0	0	1	1	0	1	1	0	N/A												Data	488
550	872	0	0	0	1	0	1	1	0	1	1	0	N/A												Data	489
551	880	0	0	0	0	1	1	1	0	1	1	0	N/A												Data	490
552	899	1	1	0	0	0	0	0	1	1	1	0	N/A												Data	491
553	901	1	0	1	0	0	0	0	1	1	1	0	N/A												Data	492
554	902	0	1	1	0	0	0	0	1	1	1	0	N/A												Data	493
555	905	1	0	0	1	0	0	0	1	1	1	0	N/A												Data	494
556	906	0	1	0	1	0	0	0	1	1	1	0	N/A												Data	495
557	908	0	0	1	1	0	0	0	1	1	1	0	N/A												Data	496
558	913	1	0	0	0	1	0	0	1	1	1	0	N/A												Data	497
559	914	0	1	0	0	1	0	0	1	1	1	0	N/A												Data	498
560	916	0	0	1	0	1	0	0	1	1	1	0	N/A												Data	499
561	920	0	0	0	1	1	0	0	1	1	1	0	N/A												Data	500
562	929	1	0	0	0	0	1	0	1	1	1	0	N/A												Data	501
563	930	0	1	0	0	0	1	0	1	1	1	0	N/A												Data	502
564	932	0	0	1	0	0	1	0	1	1	1	0	N/A												Data	503
565	936	0	0	0	1	0	1	0	1	1	1	0	N/A												Data	504
566	944	0	0	0	0	1	1	0	1	1	1	0	N/A												Data	505
567	961	1	0	0	0	0	0	1	1	1	1	0	N/A												Data	506

	Data Pattern												Complement of the Data Pattern												
		Place Value of Each Bit												Place Value of Each Bit											
Codepoint Number	Decimal Format	1	2	4	8	16	32	64	128	256	512	Negative Disparity	Positive Disparity	1	2	4	8	16	32	64	128	256	512	Decimal Format	Description	Value
568	962	0	1	0	0	0	0	1	1	1	1	0	N/A												Data	507
569	964	0	0	1	0	0	0	1	1	1	1	0	N/A												Data	508
570	968	0	0	0	1	0	0	1	1	1	1	0	N/A												Data	509
571	976	0	0	0	0	1	0	1	1	1	1	0	N/A												Data	510
572	992	0	0	0	0	0	1	1	1	1	1	0	N/A												Data	511

Bibliography

[1] P. W. France, *Local Access Network Technologies*, UK: Institution of Engineering and Technology, 2004.

[2] J. Zheng and H. T. Mouftah, "Media access control for Ethernet passive optical networks: an overview," *IEEE Commun. Magazine,* vol. 43, no. 2, pp. 145-150, 2005.

[3] I. Papagiannakis, G. Bosco, D. Fonseca, D. Klonidis, P. Poggiolini, W. Rosenkranz, A. Teixeira, I. Tomkos, and C. Xia, "Electronic channel equalization techniques," *Towards Digital Optical Networks: COST Action 291 Final Report*, Springer, 2009.

[4] I. P. Kaminow and T. Li, *Optical Fiber Telecommunications IV A: Components*, USA: Academic Press, 2002.

[5] T. E. Stern, G. Ellinas, and K. Bala, *Multiwavelength Optical Networks: Architectures, Design, and Control*, UK: Cambridge University Press, 2009.

[6] G. P. Agrawal, *Fiber-Optic Communication Systems*, USA: John Wiley & Sons, 2002.

[7] X. Zhao, "Optical injection locking on vertical-cavity surface-emitting lasers (VCSELs): physics and applications," PhD Thesis, University of California, Berkeley, 2003.

[8] H. S. Chung, Y. G. Jang, and Y. C. Chung, "Directly modulated 10-Gb/s signal transmission over 320 km of negative dispersion fiber for regional metro network," *IEEE Photon. Technol. Lett.,* vol. 15, no. 9, pp. 1306-1308, 2003.

[9] I. Papagiannakis, C. Xia, D. Klonidis, W. Rosenkranz, A. N. Birbas, and I. Tomkos, “Electronic distortion equalisation by using decision-feedback/feed-forward equaliser for transient and adiabatic chirped directly modulated lasers at 2.5 and 10 Gb/s,” *IET Optoelectronics,* vol. 3, no. 1, pp. 18-29, 2009.

[10] M. D. Feuer, S.-Y. Huang, S. L. Woodward, O. Coskun, and M. Boroditsky, “Electronic dispersion compensation for a 10-Gb/s link using a directly modulated laser,” *IEEE Photon. Technol. Lett.,* vol. 15, no. 12, pp. 1788-1790, 2003.

[11] S. Warm, C. A. Bunge, T. Wuth, and K. Petermann, “Electronic dispersion precompensation with a 10-Gb/s directly modulated laser,” *IEEE Photon. Technol. Lett.,* vol. 21, no. 15, pp. 1090-1092, 2009.

[12] P. J. Winzer, F. Fidler, M. J. Matthews, L. E. Nelson, H. J. Thiele, J. H. Sinsky, S. Chandrasekhar, M. Winter, D. Castagnozzi, L. W. Stulz, and L. L. Buhl, “10-Gb/s upgrade of bidirectional CWDM systems using electronic equalization and FEC,” *J. Lightw. Technol.,* vol. 23, no. 1, pp. 203-210, 2005.

[13] M. Du, L. G. Nielsen, C. G. Jorgensen, and D. DiGiovanni, “Dispersion compensated 10-Gb/s directly modulated lasers for 6×80km, DWDM metro network applications,” in *Proc. ECOC 2006*, pp. 1-2.

[14] A. Filios, B. Hallock, T. Kennedy, I. Tomkos, M. Vodhanel, and R. Vodhanel, “16 channel, 10 Gb/s DWDM transmission of directly modulated lasers with 100 GHz channel spacing over 100 km of negative dispersion fiber,” in *Proc. LEOS 2001*, vol. 2, pp. 742-743.

[15] C.-C. Wang, I. Roudas, I. Tomkos, M. Sharma and R. S. Vodhanel, "Negative dispersion fibers for uncompensated metropolitan networks," in *Proc. ECOC 2000*.

[16] I. Tomkos, B. Hallock, I. Roudas, R. Hesse, A. Boskovic, J. Nakano, and R. Vodhanel, "10-Gb/s transmission of 1.55-μm directly modulated signal over 100 km of negative dispersion fibre," *IEEE Photon. Technol. Lett.,* vol. 13, no. 7, pp. 735-737, 2001.

[17] K. Uomi, S. Sasaki, T. Tsuchiya, H. Nakano, and N. Chinone, "Ultralow chirp and high-speed 1.55 μm multiquantum well λ/4-shifted DFB lasers," *IEEE Photon. Technol. Lett.,* vol. 2, no. 4, pp. 229-230, 1990.

[18] M. Blez, D. Mathoorasing, C. Kazmierski, M Quillec, M. Gilleron, J. Landreau, and H. Nakajima, "Very low chirping of InGaAs-InGaAlAs MQW DFB BRS lasers under 10 Gbit/s modulation," *IEEE J. Quantum Electron.,* vol. 29, no. 6, pp. 1676-1681, 1993.

[19] S. Kakimoto, K. Takagi, H. Watanabe, and H. Higuchi, "Threshold currents of 1.55-μm InGaAs/InGaAsP multiple quantum well laser diodes," *J. Appl. Phys.,* vol. 84, no. 4, pp. 1820-1824, 1998.

[20] S. Kobayashi, Y. Yamamoto, M. Ito, and T. Kimura, "Direct frequency modulation in AlGaAs semiconductor lasers," *IEEE J. Quantum Electron.,* vol. 18, no. 4, pp. 582-595, 1982.

[21] P. Baroni, V. Miot, A. Carena, and P. Poggiolini, "8B10B line coding to mitigate the non-uniform FM laser response of direct modulated CPFSK transmitter," *Opt. Express,* vol. 16, no. 10, pp. 7279-7284, 2008.

[22] R. S. Vodhanel, A. F. Elrefaie, M. Z. Iqbal, R. E. Wagner, J. L. Gimlett, and S. Tsuji, “Performance of directly modulated DFB lasers in 10-Gb/s ASK, FSK, and DPSK lightwave systems,” *J. Lightw. Technol.,* vol. 8, no. 9, pp. 1379-1386, 1990.

[23] S. Ogita, Y. Kotaki, M. Matsuda, Y. Kuwahara, H. Onaka, H. Miyata, and H. Ishikawa, “FM response of narrow-linewidth, multielectrode lambda/4 shift DFB laser,” *IEEE Photon. Technol. Lett.,* vol. 2, no. 3, pp. 165-166, 1990.

[24] A. E. Willner, M. Kuznetsov, I. P. Kaminow, J. Stone, L. W. Stulz, and C. A. Burrus, “FM and FSK response of tunable two-electrode DFB lasers and their performance with noncoherent detection,” *IEEE Photon. Technol. Lett.,* vol. 1, no. 12, pp. 412-415, 1989.

[25] Y. Yoshikuni and G. Motosugi, “Multielectrode distributed feedback laser for pure frequency modulation and chirping suppressed amplitude modulation,” *J. Lightw. Technol.,* vol. 5, no. 4, pp. 516-522, 1987.

[26] S. Saito, Y. Yamamoto, and T. Kimura, “S/N and error rate evaluation for an optical FSK-heterodyne detection system using semiconductor lasers,” *IEEE J. Quantum Electron.,* vol. 19, no. 2, pp. 180-193, 1983.

[27] S. Saito, O. Nilsson, and Y. Yamamoto, “Coherent FSK transmitter using a negative feedback stabilised semiconductor laser,” *Electron. Lett.,* vol. 20, no. 17, pp. 703-704, 1984.

[28] S. B. Alexander and D. Welford, “Equalisation of semiconductor diode laser frequency modulation with a passive network,” *Electron. Lett.,* vol. 21, no. 9, pp. 361-362, 1985.

[29] L.-S. Yan, Y. Wang, B. Zhang, C. Yu, J. McGeehan, L. Paraschis, and A. E. Willner, “Reach extension in 10-Gb/s directly modulated transmission systems using asymmetric and narrowband optical filtering,” *Opt. Express,* vol. 13, no. 13, pp. 5106-5115, 2005.

[30] R. Noe, M. W. Maeda, S. G. Menocal, and C. E. Zah, “AMI signal format for pattern-independent FSK heterodyne transmission and two channel crosstalk measurements,” in *Proc. ECOC 1988*, pp. 175-178.

[31] R. C. Steele and M. Creaner, “565 Mbit/s AMI FSK coherent system using commercial DFB lasers,” *Electron. Lett.,* vol. 25, no. 11, pp. 732-734, 1989.

[32] H. Tsushima, S. Sasaki, R. Takeyari, and K. Uomi, “Alternate-mark-inversion optical continuous phase FSK heterodyne transmission using delay-line demodulation,” *J. Lightw. Technol.,* vol. 9, no. 5, pp. 666-674, 1991.

[33] P. W. Hooijmans, M. T. Tomesen, and A. Grijp, “Penalty free biphase linecoding for pattern independent FSK coherent transmission systems,” *J. Lightw. Technol.,* vol. 8, no. 3, pp. 323-328, 1990.

[34] R. Ramaswami, K. N. Sivarajan, and G. H. Sasaki, *Optical Networks: A Practical Perspective*, USA: Morgan Kaufmann Publishers, 2010.

[35] W. S. Chang, *RF Photonic Technology in Optical Fiber Links*, UK: Cambridge University Press, 2002.

[36] F. Koyama and Y. Suematsu, “Analysis of dynamic spectral width of dynamic-single-mode (DSM) lasers and related transmission bandwidth of single-mode fibers,” *IEEE J. Quantum Electron.,* vol. 21, no. 4, pp. 292-297, 1985.

[37] X. Zhao, D. Parekh, E. K. Lau, H-.K. Sung, M. C. Wu, W. Hofmann, M. C. Amann, and C. J. Chang-Hasnain, “Novel cascaded injection-locked 1.55-µm VCSELs with 66 GHz modulation bandwidth,” *Opt. Express,* vol. 15, no. 22, pp. 14810-14816, 2007.

[38] T. L. Koch and R. A. Linke, “Effect of nonlinear gain reduction on semiconductor laser wavelength chirping,” *App. Phys. Lett.,* vol. 48, no. 10, pp. 613-615, 1986.

[39] G. P. Agrawal and N. K. Dutta, *Long-Wavelength Semiconductor Lasers*, USA: Van Nostrand Reinhold, 1993.

[40] G. E. Shtengel, R. F. Kazarinov, G. L. Belenky, and C. L. Reynolds, “Wavelength chirp and dependence of carrier temperature on current in MQW InGaAsP-InP lasers,” *IEEE J. Quantum Electron.,* vol. 33, no. 8, pp. 1396-1402, 1997.

[41] I. Tomkos, I. Roudas, R. Hesse, N. Antoniades, A. Boskovic, and R. Vodhanel, “Extraction of laser rate equations parameters for representative simulations of metropolitan-area transmission systems and networks,” *Opt. Commun.,* vol. 194, no. 1-3, pp. 109-129, 2001.

[42] M. S. Stix, M. P. Kesler, and E. P. Ippen, “Observations of subpicosecond dynamics in GaAlAs laser diodes,” *App. Phys. Lett.,* vol. 48, no. 25, pp. 1722-1724, 1986.

[43] K. L. Hall, J. Mark, E. P. Ippen, and G. Eisenstein, “Femtosecond gain dynamics in InGaAsP optical amplifiers,” *App. Phys. Lett.,* vol. 56, no. 18, pp. 1740-1742, 1990.

[44] R. F. Kazarinov, C. H. Henry, and R. A. Logan, “Longitudinal mode self-stabilization in semiconductor lasers,” *J. Appl. Phys.,* vol. 53, no. 7, pp. 4631-4644, 1982.

[45] P. Krehlik, “Characterization of semiconductor laser frequency chirp based on signal distortion in dispersive optical fiber,” *Opto-Electron. Rev.,* vol. 14, no. 2, pp. 123-128, 2006.

[46] H. D. Summers and I. H. White, “Measurement of the static and dynamic linewidth enhancement factor in strained 1.55 μm InGaAsP lasers,” *Electron. Lett.,* vol. 30, no. 14, pp. 1140-1141, 1994.

[47] R. I. Killey, P. M. Watts, V. Mikhailov, M. Glick, and P. Bayvel, “Electronic dispersion compensation by signal predistortion using a dual-drive Mach-Zehnder modulator,” in *Proc. OFC/NFOEC 2005*, vol. 4.

[48] J. McNicol, M. O'Sullivan, K. Roberts, A. Comeau, D. McGhan, and L. Strawczynski, “Electrical domain compensation of optical dispersion [optical fibre communication applications],” in *Proc. OFC/NFOEC 2005*, vol. 4.

[49] I. Tomkos, D. Chowdhury, J. Conradi, D. Culverhouse, K. Ennser, C. Giroux, B. Hallock, T. Kennedy, A. Kruse, S. Kumar, N. Lascar, I. Roudas, M. Sharma, R. S. Vodhanel, and C. C. Wang, “Demonstration of negative dispersion fibers for DWDM metropolitan area networks,” *IEEE J. Select. Topics Quantum Electron.,* vol. 7, no. 3, pp. 439-460, 2001.

[50] T. Saito, N. Henmi, S. Fujita, M. Yamaguchi, and M. Shikada, “Prechirp technique for dispersion compensation for a high-speed long-span transmission,” *IEEE Photon. Technol. Lett.,* vol. 3, no. 1, pp. 74-76, 1991.

[51] B. Jopson and A. Gnauck, “Dispersion compensation for optical fiber systems,” *IEEE Commun. Magazine,* vol. 33, no. 6, pp. 96-102, 1995.

[52] P. M. Watts, V. Mikhailov, S. Savory, P. Bayvel, M. Glick, M. Lobel, B. Christensen, P. Kirkpatrick, S. Song, and R. I. Killey, “Performance of single-mode fiber links using electronic feed-forward and decision feedback equalizers,” *IEEE Photon. Technol. Lett.,* vol. 17, no. 10, pp. 2206-2208, 2005.

[53] R. I. Killey, P. M. Watts, V. Mikhailov, M. Glick, and P. Bayvel, “Electronic dispersion compensation by signal predistortion using digital Processing and a dual-drive Mach-Zehnder Modulator,” *IEEE Photon. Technol. Lett.,* vol. 17, no. 3, pp. 714-716, 2005.

[54] S. Warm, “Electronic predistortion strategies for directly modulated laser systems,” Berlin Institute of Technology, Germany, 2009.

[55] A. Ghatak, *Optics*, 3 ed., USA: McGraw-Hill, 2005.

[56] J. Ryan, “Fiber considerations for metropolitan networks,” *Alcatel Telekommun. Rev., 1st quarter*, pp. 52-56, 2002.

[57] C. D. Poole, J. M. Wiesenfeld, and D. J. DiGiovanni, “Elliptical-core dual-mode fiber dispersion compensator,” *IEEE Photon. Technol. Lett.,* vol. 5, no. 2, pp. 194-197, 1993.

[58] J. Antos, D. W. Hall, and D. K. Smith, “Dispersion-compensating fiber for upgrading existing 1310-nm-optimized systems to 1550-nm operation,” in *Proc. OFC 1993*, pp. 204-205.

[59] A. Urano, H. Kanamorl, M. Nishimura, M. Shigematsu, K. Nakazato, and T. Kashiwada, “Characteristics of extremely high Δn singlemode fiber,” in *Proc. OEC 1992*, Chiba, Japan, 1992, pp. 44-45.

[60] L. Gruner-Nielsen, M. Wandel, P. Kristensen, C. Jorgensen, L. V. Jorgensen, B. Edvold, B. Palsdottir, and D. Jakobsen, “Dispersion-compensating fibers,” *J. Lightw. Technol.,* vol. 23, no. 11, pp. 3566-3579, 2005.

[61] J. Osterwalder and B. Rickett, “Frequency modulation of GaAlAs injection lasers at microwave frequency rates,” *IEEE J. Quantum Electron.,* vol. 16, no. 3, pp. 250-252, 1980.

[62] W. Idler, A. Klekamp, R. Dischler, and B. Wedding, “Advantages of frequency shift keying in 10 Gb/s systems,” in *Proc. IEEE/LEOS 2004*, pp. 51-52.

[63] Z. Al-Qazwini and H. Kim, “Line coding to enhance the performance of 10-Gb/s CPFSK-ASK directly modulated signals,” *Opt. Express,* vol. 18, no. 8, pp. 8360-8366, 2010.

[64] E. Forestieri and G. Prati, “Analysis of delay-and-multiply optical FSK receivers with line-coding and non-flat laser FM response,” *IEEE J. Select. Areas in Commun.,* vol. 13, no. 3, pp. 543-556, 1995.

[65] K. C. Sum and N. J. Gomes, “Modulation circuit design for chirp-suppressed IM and intensity fluctuation-suppressed FM with multi-electrode DFB lasers,” in *Proc. IEEE/LEOS 1996*, pp. 176-177.

[66] B. Hoffmann, N. G. Jensen, E. Bodtker, S. K. Nielsen, and B. Broberg, “Comparison of NRZ and AMI coding schemes using three-electrode and conventional DFB laser transmitters in a 636 Mbit/s SF-FSK coherent system,” *Electron. Lett.,* vol. 26, no. 22, pp. 1903-1904, 1990.

[67] A. Agarwal, S. Banerjee, D. F. Grosz, A. P. Kung, D. N. Maywar, A. Gurevich, and T. H. Wood, “Ultra-high-capacity long-haul 40-Gb/s WDM

transmission with 0.8-b/s/Hz spectral efficiency by means of strong optical filtering," *IEEE Photon. Technol. Lett.,* vol. 15, no. 3, pp. 470-472, 2003.

[68] N. Yoshikane and I. Morita, "160% spectrally-efficient 5.12-Tb/s (64×85.4 Gb/s RZ DQPSK) transmission without polarization demultiplexing," in *Proc. ECOC 2004*, Stockholm, Sweden, 2004.

[69] M. McAdams, E. Peral, D. Provenzano, W. K. Marshall, and A. Yariv, "Improved laser modulation response by frequency modulation to amplitude modulation conversion in transmission through a fiber grating," *App. Phys. Lett.,* vol. 71, no. 7, pp. 879-881, 1997.

[70] Y. Matsui, D. Mahgerefteh, X. Zheng, C. Liao, Z. F. Fan, K. McCallion, and P. Tayebati, "Chirp-managed directly modulated laser (CML)," *IEEE Photon. Technol. Lett.,* vol. 18, no. 2, pp. 385-387, 2006.

[71] D. Mahgerefteh, C. Liao, X. Zheng, Y. Matsui, B. Johnson, D. Walker, Z. F. Fan, K. McCallion, and P. Tayebati, "Error-free 250 km transmission in standard fibre using compact 10 Gbit/s chirp-managed directly modulated lasers (CML) at 1550 nm," *Electron. Lett.,* vol. 41, no. 9, pp. 543-544, 2005.

[72] R. S. Vodhanel, B. Enning, and A. F. Elrefaie, "Bipolar optical FSK transmission experiments at 150 Mbit/s and 1 Gbit/s," *Journal of Lightwave Technology,* vol. 6, no. 10, pp. 1549-1553, 1988.

[73] A. X. Widmer and P. A. Franaszek, "A DC-balanced, partitioned-block, 8B/10B transmission code," *IBM J. Research and Develop.,* vol. 27, no. 5, pp. 440-451, 1983.

[74] F. Effenberger, Y. Fan, Z. Wang, and J. Gao, "A 9b10b line code for 2.5Gb/s upstream PONs," in *Proc. OFC/NFOEC 2009*, San Diego, California, pp. 1-3.

[75] X. Widmer, DC balanced 7B/8B, 9B/10B, and partitioned DC balanced 12B/14B, 17B/20B, and 16B/18B transmission codes, U.S. Patent 6614369 B1, 2003.

[76] R. Walker and R. Dugan, "64B/66B low-overhead coding proposal for serial links," *IEEE 802.3ah (10 GE) Task Force*, 2000.

[77] H. Kim, S. K. Kim, H. Lee, S. Hwang, and Y. Oh, "A novel way to improve the dispersion-limited transmission distance of electroabsorption modulated lasers," *IEEE Photon. Technol. Lett.,* vol. 18, no. 8, pp. 947-949, 2006.

[78] K. J. Park, S. K. Shin, and Y. C. Chung, "A simple monitoring technique for WDM networks," in *Proc. OFC 1999*, vol.4, pp. 152-154.

[79] Z. Al-Qazwini and H. Kim, "Directly modulated laser driven by low-bandwidth duobinary signals," *IEEE Photon. Technol. Lett.,* vol. 22, no. 17, pp. 1306-1308, 2010.

[80] E. K. Lau, H.-K. Sung, and M. C. Wu, "Ultra-high, 72 GHz resonance frequency and 44 GHz bandwidth of injection-locked 1.55-µm DFB lasers," in *Proc. OFC 2006*.

[81] T. B. Simpson, J. M. Liu, and A. Gavrielides, "Bandwidth enhancement and broadband noise reduction in injection-locked semiconductor lasers," *IEEE Photon. Technol. Lett.,* vol. 7, no. 7, pp. 709-711, 1995.

[82] M. X. Jun, T. Jung, C. Tai, and M. C. Wu, "Gain and bandwidth enhancement of directly modulated analog fiber optic links using injection-locked gain-coupled DFB lasers," in *Proc. MWP 1999*, pp. 141-144.

[83] A. Tan and E. Pincemin, “Performance comparison of duobinary formats for 40-Gb/s and mixed 10/40-Gb/s long-haul WDM transmission on SSMF and LEAF fibers,” *J. Lightw. Technol.,* vol. 27, no. 4, pp. 396-408, 2009.

[84] J. Prat and J. M. Gene, “Reduction of laser modulation bandwidth requirement in FSK systems using duobinary coding and differential detection,” *Electron. Lett.,* vol. 42, no. 10, pp. 591-592, 2006.

[85] D. R. Smith, *Digital Transmission Systems*, USA: Kluwer Academic Publishers, 2004.

[86] Y. C. Lu, C. C. Wei, J. Chen, K. M. Feng, P. C. Yeh, T. Y. Huang, C. C. Chang, C. Tsao, and S. Chi, “Effects of filter bandwidth and driving voltage on optical duobinary transmission systems,” *Optical Fiber Technol.,* vol. 13, no. 3, pp. 231-235, 2007.

[87] S. Walklin and J. Conradi, “On the relationship between chromatic dispersion and transmitter filter response in duobinary optical communication systems,” *IEEE Photon. Technol. Lett.,* vol. 9, no. 7, pp. 1005-1007, 1997.

[88] H. Lee, H. Kim, J. Lee, S. K. Kim, G. Lee, S. Hwang, Y. Oh, J. Jeong, and C. Shim, “Cost-effective optical chirped duobinary transmitter using an electroabsorption modulated laser,” *IEEE Photon. Technol. Lett.,* vol. 17, no. 4, pp. 905-907, 2005.

[89] K. Morito, R. Sahara, K. Sato, and Y. Kotaki, “Penalty-free 10 Gb/s NRZ transmission over 100 km of standard fiber at 1.55-μm with a blue-chirp modulator integrated DFB laser,” *IEEE Photon. Technol. Lett.,* vol. 8, no. 3, pp. 431-433, 1996.

[90] I. Kim, B.-K. Kang, Y.-D. Bae, B. Park, S.-M. Lee, Y. H. Kim, and D.-H. Jang, “Design of amplifier- and modulator-integrated laser diode for 10-Gb/s 80-km transmission,” *IEEE J. Select. Topics Quantum Electron.,* vol. 11, no. 2, pp. 323-328, 2005.

[91] Z. Al-Qazwini and H. Kim, “DC-balanced line coding for dual modulation-based electro-absorption modulated lasers,” in *Proc. OECC 2011*, Taiwan, pp. 63-64.

[92] K. Hasebe, S. Matsuo, H. Sanjoh, A. Ohki, T. Kakitsuka, and Y. Shibata, “Directly frequency modulated DFB laser integrated with EA modulator for extended transmission reach,” in *Proc. ECOC 2010*, pp. 1-3.

[93] J. Petit, D. Erasme, C. Kazmierski, C. Jany, J. Decobert, F. Alexandre, N. Dupuis, and R. Gabet, “Enhanced 10-Gb/s NRZ transmission distance using dual modulation of an integrated electro-absoprtion modulated laser transmitter,” in *Proc. OFC 2009*, pp. 1-3.

[94] F. Devaux, Y. Sorel, and J. F. Kerdiles, “Simple measurement of fiber dispersion and of chirp parameter of intensity modulated light emitter,” *J. Lightw. Technol.,* vol. 11, no. 12, pp. 1937-1940, 1993.

[95] U. Hilbk, T. Hermes, J. Saniter, and F. J. Westphal, “High capacity WDM overlay on a passive optical network,” *Electron. Lett.,* vol. 32, no. 23, pp. 2162-2163, 1996.

[96] P. Healey, P. Townsend, C. Ford, L. Johnston, P. Townley, I. Lealman, L. Rivers, S. Perrin, and R. Moore, “Spectral slicing WDM-PON using wavelength-seeded reflective SOAs,” *Electron. Lett.,* vol. 37, no. 19, pp. 1181-1182, 2001.

[97] E. Wong, K. L. Lee, and T. B. Anderson, "Directly modulated self-seeding reflective semiconductor optical amplifiers as colorless transmitters in wavelength division multiplexed passive optical networks," *J. Lightw. Technol.,* vol. 25, no. 1, pp. 67-74, 2007.

[98] H. D. Kim, S.-G. Kang, and C.-H. Lee, "A low-cost WDM source with an ASE injected Fabry-Perot semiconductor laser," *IEEE Photon. Technol. Lett.,* vol. 12, no. 8, pp. 1067-1069, 2000.

[99] J. J. Koponen and M. J. Soderlund, "A duplex WDM passive optical network with 1:16 power split using reflective SOA remodulator at ONU," in *Proc. OFC 2004*, vol. 1.

[100] K. Grobe and J. P. Elbers, "PON in adolescence: from TDMA to WDM-PON," *IEEE Commun. Magazine,* vol. 46, no. 1, pp. 26-34, 2008.

[101] W. Lee, M. Y. Park, S. H. Cho, J. Lee, C. Kim, G. Jeong, and B. W. Kim, "Bidirectional WDM-PON based on gain-saturated reflective semiconductor optical amplifiers," *IEEE Photon. Technol. Lett.,* vol. 17, no. 11, pp. 2460-2462, 2005.

[102] T.-Y. Kim and S.-K. Han, "Reflective SOA-based bidirectional WDM-PON sharing optical source for up/downlink data and broadcasting transmission," *IEEE Photon. Technol. Lett.,* vol. 18, no. 22, pp. 2350-2352, 2006.

[103] Y.-Y. Won, H.-C. Kwon, and S.-K. Han, "1.25-Gb/s wavelength-division multiplexed single-wavelength colorless radio-on-fiber systems using reflective semiconductor optical amplifier," *J. Lightw. Technol.,* vol. 25, no. 11, pp. 3472-3478, 2007.

[104] J. J. Martinez, J. I. G. Gregorio, A. L. Lucia, A. V. Velasco, J. C. Aguado, and M. A. L. Binue, "Novel WDM-PON architecture based on a spectrally efficient IM-FSK scheme using DMLs and RSOA," *J. Lightw. Technol.,* vol. 26, no. 3, pp. 350-356, 2008.

[105] Z. Al-Qazwini and H. Kim, "DC-balanced line coding for downlink modulation in bidirectional WDM PONs using remodulation," *IEEE Photon. Technol. Lett.,* vol. 23, no. 18, pp. 1331-1333, 2011.

[106] H. Takesue and T. Sugie, "Wavelength channel data rewrite using saturated SOA modulator for WDM networks with centralized light sources," *J. Lightw. Technol.,* vol. 21, no. 11, pp. 2546-2556, 2003.

[107] H. Wai, C.-K. Chan, L.-K. Chen, and F. Tong, "An optical network unit for WDM access networks with downstream DPSK and upstream remodulated OOK data using injection-locked FP laser," *IEEE Photon. Technol. Lett.,* vol. 15, no. 10, pp. 1476-1478, 2003.

[108] K. Y. Cho, S. P. Jung, A. Murakami, A. Agata, Y. Takushima, and Y. C. Chung, "Recent progresses in RSOA-based WDM PON," in *Proc. ICTON 2009*, pp. 1-4.

[109] I. Garces, J. C. Aguado, J. J. Martinez, A. Lopez, A. Villafranca, and M. A. Losada, "Analysis of narrow-FSK downstream modulation in colourless WDM PONs," *Electron. Lett.,* vol. 43, no. 8, pp. 471-472, 2007.

[110] M. Presi, R. Proietti, K. Prince, G. Contestabile, and E. Ciaramella, "A novel line coding pair for fully passive long reach WDM-PONs," in *Proc. ECOC 2008*, pp. 1-2.

[111] S. Y. Kim, S. B. Jun, Y. Takushima, E. S. Son, and Y. C. Chung, “Enhanced performance of RSOA-based WDM PON by using Manchester coding,” *J. Optical Networks,* vol. 6, no. 6, pp. 624-630, 2007.

[112] G.-W. Lu, N. Deng, C.-K. Chan, and L.-K. Chen, “Use of downstream inverse-RZ signal for upstream data re-modulation in a WDM passive optical network,” in *Proc. OFC/NFOEC 2005*.

[113] B. Fondeur and D. J. Dougherty, Asymmetric Mach-Zehnder interferometer having a reduced drive voltage coupled to a compact low-loss arrayed waveguide grating, U.S. Patent 2008/0044122, 2008.

[114] M. Fujiwara, K. Jun-ichi, H. Suzuki, and K. Iwatsuki, “Impact of backreflection on upstream transmission in WDM single-fiber loopback access networks,” *J. Lightw. Technol.,* vol. 24, no. 2, pp. 740-746, 2006.

[115] S. Chong, S. Li, Z. Al-Qazwini, S. Takahashi, T. Okamura, A. Tajima, and H. Kim, “Directly modulated laser transmitter using scramble-and-select-based line coding with Low Overhead,” in *Proc. OECC 2011*, Taiwan, pp. 834-835.

List of Publications

The following is a list of my publications.

Books

[1] Zaineb Al-Qazwini, "Nonlinear Stimulated Raman Scattering in Optical CDMA Systems," LAP LAMBERT Academic Publishing, Germany, Mar. 2012.

Journal Papers

[1] Zaineb Al-Qazwini, Madhan Thollabandi, and Hoon Kim, "Colorless optical transmitter for upstream WDM PON based on wavelength conversion," *J. Lightw. Technol.*, submitted.

[2] Zaineb Al-Qazwini and Hoon Kim, "Ultra-narrow spectrum-sliced incoherent light source for 10-Gb/s WDM PON," *J. Lightw. Technol.*, vol. 30 , no. 19, pp. 3157-3163, Oct. 2012.

[3] Zaineb Al-Qazwini and Hoon Kim, "Symmetric 10-Gb/s WDM-PON using directly modulated lasers for downlink and RSOAs for uplink," *J. Lightw. Technol.*, vol. 30, no. 12, pp. 1891-1899, Jun. 2012.

[4] Zaineb Al-Qazwini and Hoon Kim, "DC-balanced line coding for downlink modulation in bidirectional WDM PONS using remodulation," *IEEE Photon. Technol. Lett.*, vol. 23, no. 18, pp. 1331-1333, Aug. 2011.

[5] Zaineb Al-Qazwini and Hoon Kim, "Directly modulated laser driven by low-bandwidth duobinary signals," *IEEE Photon. Technol. Lett.*, vol. 22, no. 17, pp. 1306-1308, Sep. 2010.

[6] Zaineb Al-Qazwini and Hoon Kim, “Line coding to enhance the performance of 10-Gb/s CPFSK-ASK directly modulated signals,” *Optics Express*, vol. 18, no. 8, pp. 8360-8366, Apr. 2010.

[7] Zaineb A. T. Al-Qazwini, Mohd. K. Abdullah, and Makhfudzah Mokhtar, “Measurements of stimulated Raman scattering-induced tilt in spectral-amplitude-coding optical code-division multiple-access systems", *Optical Engineering*, vol. 48, no. 1, Jan. 2009.

Conference Papers

[1] Zaineb Al-Qazwini and Hoon Kim, “Photonic frequency up-conversion using directly modulated RSOA and delay interferometer,” in *Proc. OECC 2012*, Busan, Korea, paper 6F3-6, Jul. 2012.

[2] Zaineb Al-Qazwini and Hoon Kim, “Transmission of 10-Gb/s Incoherent Light over 20-km SSMF without Dispersion Compensation,” in *Proc. OECC 2012*, Busan, Korea, paper 3A1-4, Jul. 2012.

[3] Zaineb Al-Qazwini and Hoon Kim, “10-Gbps single-feeder, full-duplex WDM-PON using directly modulated laser and RSOA,” in *Proc. OFC/NFOEC 2012*, Los Angeles, USA, paper OTh1F.5, Mar. 2012.

[4] Medi Nazar, Manu Ignatius, Prabandana Listyanto, and Zaineb Al-Qazwini, “Modified CHOKe: Analysis and improvement of a stateless queue management scheme for fair bandwidth allocation,” in *Proc. ICUMT 2011*, Budapest, Hungary, pp. 1-8, Oct. 2011.

[5] Zaineb Al-Qazwini and Hoon Kim, “DC-balanced line coding for dual modulation-based electro-absorption modulated lasers,” in *Proc. OECC 2011*, Taiwan, paper 5D3-4, Jul. 2011.

[6] Samuel Chong, Shuo Li, Zaineb Al-Qazwini, Seigo Takahashi, Toshihiko Okamura, Akio Tajima, and Hoon Kim, “Directly modulated laser transmitter using scramble-and-select-based line coding with low overhead,” in *Proc. OECC 2011*, Taiwan, paper 8E1-5, Jul. 2011.

[7] Zaineb Al-Qazwini and Hoon Kim, “Line coding for downlink DML modulation in λ-shared, RSOA-based asymmetric bidirectional WDM PONs,” in *Proc. OFC/NFOEC 2011*, Los Angeles, USA, paper OMP5, Mar. 2011.

[8] Zaineb Al-Qazwini and Hoon Kim, “Bidirectional WDM PON using directly modulated lasers for downlink and RSOAs for uplink,” in *Proc. PGC 2010*, Singapore, paper 1-3F-3, Dec. 2010.

[9] Zaineb Al-Qazwini and Hoon Kim, “10-Gb/s directly-modulated lasers driven by 3.5-GHz-bandwidth duobinary signals,” in *Proc. OECC 2010*, Japan, paper 8B1-5, Jul. 2010.

[10] Zaineb Al-Qazwini and Hoon Kim, “Optical RZ transmitter using directly modulated laser driven by NRZ signals,” in *Proc. OECC 2010*, Japan, paper 7P-12, Jul. 2010.

[11] Zaineb Al-Qazwini and Hoon Kim, “Line coding for 10-Gb/s directly modulated lasers,” in *Proc. OFC/NFOEC 2010*, San Diego, USA, paper OThW8, Mar. 2010.

[12] Zaineb A. T. Al-Qazwini, Mohd. K. Abdullah, and Makhfudzah Mokhtar, “Optical power limitations in spectral-amplitude-coding optical code-division multiple-access systems due to stimulated Raman scattering,” in *Proc. NCTT-MCP 2008*, Putrajaya, Malaysia, pp: 42-44, Aug. 2008.

[13] Zaineb A. T. Al-Qazwini and Firas Al-Attar, "Quality improvement of fingerprint images using weight median filtering scheme," *E-Technology and E-Environments Conference*, Sohar University, Oman, Apr. 2008.

[14] Zaineb A. T. Al-Qazwini, Mohd. K. Abdullah, and Makhfudzah Mokhtar, "Signal distortion due to stimulated Raman scattering in optical CDMA transmission systems," in *Proc. ICIAS 2007*, Kuala Lumpur, Malaysia, pp: 335-337, Nov. 2007.

[15] Mohd. K. Abdullah, Zaineb A. T. Al-Qazwini, M. D. A. Samad, and Makhfudzah Mokhtar, "Optimum transmit power for optical CDMA transmission systems considering stimulated Raman scattering (SRS) effects," in *Proc. WOCN 2007*, Singapore, pp: 1-4, Jul. 2007.

[16] Zaineb Al-Qazwini and Hussein Al-Maghbob, "Applying the electronic management in the Faculty of Engineering of Al-Fatah University," *The 1st Conference of Quality*, Libyan National Center for Standardization Metrology, Tripoli, Libya, May 2005.